USGS
science for a changing world

A Field Trip Guide to the Petrology of Quaternary Volcanism on the Yellowstone Plateau

Scientific Investigations Report 2017–5022–Q

U.S. Department of the Interior
U.S. Geological Survey

COVER

Watercolor artwork "Yellowstone Canyon" by Thomas Moran, 1871. Yellowstone National Park collection, YELL 8539. During the summer of 1871, Moran accompanied the Hayden Survey of the U.S. Geological Survey of the Territories to document the Yellowstone landscape. Moran's paintings helped convince Congress to establish Yellowstone as our Nation's first National Park.

A Field Trip Guide to the Petrology of Quaternary Volcanism on the Yellowstone Plateau

By Jorge Vazquez, Mark Stelten, Ilya Bindeman, and Kari Cooper

Scientific Investigations Report 2017–5022–Q

U.S. Department of the Interior
U.S. Geological Survey

U.S. Department of the Interior
RYAN K. ZINKE, Secretary

U.S. Geological Survey
William H. Werkheiser, Acting Director

U.S. Geological Survey, Reston, Virginia: 2017

Suggested citation:
Vazquez, J., Stelten, M., Bindeman, I., and Cooper, K., 2017, A field trip guide to the petrology of Quaternary volcanism on the Yellowstone Plateau: U.S. Geological Survey Scientific Investigations Report 2017–5022–Q, 68 p., https://doi.org/10.3133/sir20175022q.

ISSN 2328-0328 (online)

Preface

The North American Cordillera is home to a greater diversity of volcanic provinces than any comparably sized region in the world. The interplay between changing plate-margin interactions, tectonic complexity, intra-crustal magma differentiation, and mantle melting have resulted in a wealth of volcanic landscapes. Field trips in this series visit many of these landscapes, including (1) active subduction-related arc volcanoes in the Cascade Range; (2) flood basalts of the Columbia Plateau; (3) bimodal volcanism of the Snake River Plain-Yellowstone volcanic system; (4) some of the world's largest known ignimbrites from southern Utah, central Colorado, and northern Nevada; (5) extension-related volcanism in the Rio Grande Rift and Basin and Range Province; and (6) the spectacular eastern Sierra Nevada featuring Long Valley Caldera and the iconic Bishop Tuff. Some of the field trips focus on volcanic eruptive and emplacement processes, calling attention to the fact that the western United States provides opportunities to examine a wide range of volcanological phenomena at many scales.

The 2017 Scientific Assembly of the International Association of Volcanology and Chemistry of the Earth's Interior (IAVCEI) in Portland, Oregon, marks the first time that the U.S. volcanological community has hosted this quadrennial meeting since 1989, when it was held in Santa Fe, New Mexico. The 1989 field-trip guides are still widely used by students and professionals alike. This new set of field guides is similarly a legacy collection that summarizes decades of advances in our understanding of magmatic and tectonic processes of volcanic western North America.

The field of volcanology has flourished since the 1989 IAVCEI meeting, and it has profited from detailed field investigations coupled with emerging new analytical methods. Mapping has been enhanced by plentiful major- and trace-element whole-rock and mineral data, technical advances in radiometric dating and collection of isotopic data, GPS (Global Positioning System) advances, and the availability of lidar (light detection and ranging) imagery. Spectacularly effective microbeam instruments, geodetic and geophysical data collection and processing, paleomagnetic determinations, and modeling capabilities have combined with mapping to provide new information and insights over the past 30 years. The collective works of the international community have made it possible to prepare wholly new guides to areas across the western United States. These comprehensive field guides are available, in large part, because of enormous contributions from many experienced geologists who have devoted entire careers to their field areas. Early career scientists are carrying forward and refining their foundational work with impressive results.

Our hope is that future generations of scientists as well as the general public will use these field guides as introductions to these fascinating areas and will be enticed toward further exploration and field-based research.

Michael Dungan, University of Oregon
Judy Fierstein, U.S. Geological Survey
Cynthia Gardner, U.S. Geological Survey
Dennis Geist, National Science Foundation
Anita Grunder, Oregon State University
John Wolff, Washington State University
Field-trip committee, IAVCEI 2017

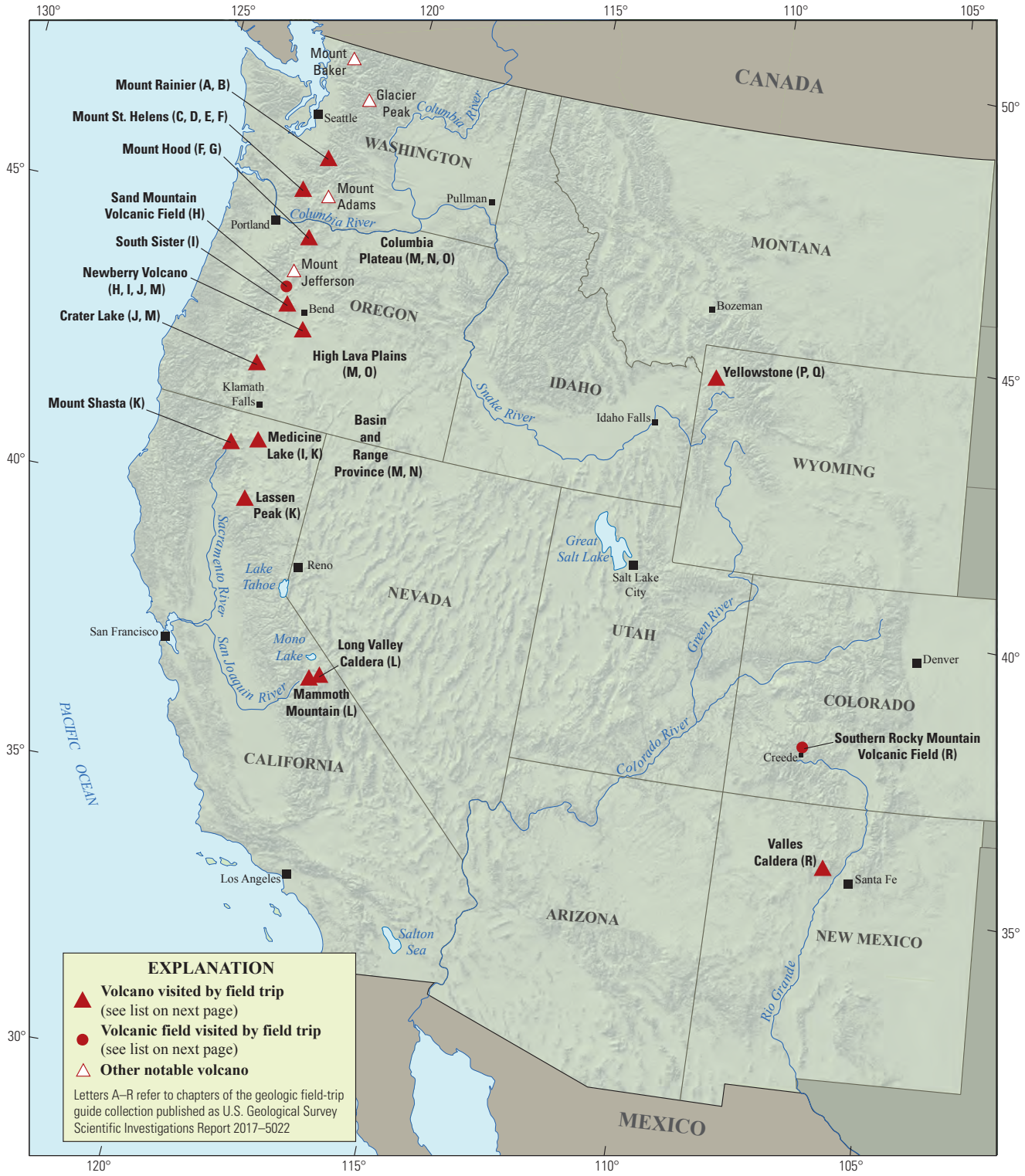

Map of the western United States showing volcanoes and volcanic fields visited by geologic field trips scheduled in conjunction with the 2017 meeting of the International Association of Volcanology and Chemistry of the Earth's Interior (IAVCEI) in Portland, Oregon, and available as chapters in U.S. Geological Survey Scientific Investigations Report 2017–5022. Shaded-relief base from U.S. Geological Survey National Elevation Dataset 30-meter digital elevation model data.

Contributing Authors

Boise State University
Brittany D. Brand
Nicholas Pollock

Colgate University
Karen Harpp
Alison Koleszar

Durham University
Richard J. Brown

Eastern Oregon University
Mark L. Ferns

ETH Zurich
Olivier Bachmann

Georgia Institute of Technology
Josef Dufek

GNS Science, New Zealand
Natalia I. Deligne

Hamilton College
Richard M. Conrey

Massachusetts Institute of Technology
Timothy Grove

National Science Foundation
Dennis Geist (also with Colgate University and University of Idaho)

New Mexico Bureau of Geology and Mineral Resources
Paul W. Bauer
William C. McIntosh
Matthew J. Zimmerer

New Mexico State University
Emily R. Johnson

Northeastern University
Martin E. Ross

Oregon Department of Geology and Mineral Industries
William J. Burns
Lina Ma
Ian P. Madin
Jason D. McClaughry

Oregon State University
Adam J.R. Kent
Benjamin J. Drenth
William C. Evans
Judy Fierstein
Cynthia A. Gardner
V.J.S. Grauch
Christopher J. Harpel
Wes Hildreth
Richard P. Hoblitt
Peter W. Lipman
Jacob B. Lowenstern
Jon J. Major
Seth C. Moran
Lisa A. Morgan
Leah E. Morgan
L.J. Patrick Muffler
James E. O'Connor
John S. Pallister
Thomas C. Pierson
Joel E. Robinson
Juliet Ryan-Davis
Kevin M. Scott
William E. Scott
Wayne (Pat) Shanks
David R. Sherrod
Thomas W. Sisson
Mark Evan Stelten
Weston Thelen
Ren A. Thompson
Kenzie J. Turner
James W. Vallance
Alexa R. Van Eaton
Jorge A. Vazquez
Richard B. Waitt
Heather M. Wright

Portland State University
Jonathan H. Fink (also with University of British Columbia)
Martin J. Streck
Ashley R. Streig

San Diego State University
Victor E. Camp

Smithsonian Institution
Lee Siebert

Universidad Nacional Autónoma de San Luis Potosi
Damiano Sarocchi

University of California, Davis
Kari M. Cooper

University of Liverpool
Peter B. Kokelaar

University of Northern Colorado
Steven W. Anderson

University of Oregon
Ilya N. Binderman
Michael A. Dungan
Daniele McKay (also with Oregon State University and Oregon State University, Cascades)

University of Portland
Kristin Sweeney

University of Tasmania
Martin Jutzeler
Jocelyn McPhie

University of Utah
Jamie Farrell

U.S. Army Corps of Engineers
Keith I. Kelson

U.S. Forest Service
Gordon E. Grant (also with Oregon State University
Robert A. Jensen

U.S. Geological Survey
Charles R. Bacon
Andrew T. Calvert
Christine F. Chan
Robert L. Christiansen
Michael A. Clynne
Michael A. Cosca
Julie M. Donnelly-Nolan

U.S. Nuclear Regulatory Commission
Stephen Self (also with University of California, Berkeley)

Washington State University
Joseph R. Boro
Owen K. Neill
Stephen P. Reidel
John A. Wolff

Acknowledgments
Juliet Ryan-Davis and Kate Sullivan created the overview map, and Vivian Nguyen created the cover design for this collection of field-trip guide books. The field trip committee is grateful for their contributions.

Contents

Figures

Table

A Field Trip Guide to the Petrology of Quaternary Volcanism on the Yellowstone Plateau

By Jorge Vazquez[1], Mark Stelten[1], Ilya Bindeman[2], and Kari Cooper[3]

Introduction

Overview

The Yellowstone Plateau is one of the largest manifestations of silicic volcanism on Earth, and marks the youngest focus of magmatism associated with the Yellowstone Hot Spot (Christiansen and others, 2002). The earliest products of Yellowstone Hot Spot volcanism are from ~17 million years ago (Ma), but may be as old as ~32 Ma (Seligman and others, 2014), and include contemporaneous eruption of voluminous mafic and silicic magmas, which are mostly located in the region of northwestern Nevada and southeastern Oregon (fig. 1) (Camp, 1995; Coble and Mahood, 2012). Since 17 Ma, the main locus of Yellowstone Hot Spot volcanism has migrated northeastward producing numerous silicic caldera complexes that generally remain active for ~2–4 million years (m.y.), with the present-day focus being the Yellowstone Plateau (figs. 1, 2). Northeastward migration of volcanism associated with the Yellowstone Hot Spot resulted in the formation of the Snake River Plain (SRP), a low relief physiographic feature extending ~750 kilometers (km) from northern Nevada to eastern Idaho (fig. 1). Most of the silicic volcanic centers along the SRP have been inundated by younger basalt volcanism, but many of their ignimbrites and lava flows are exposed in the extended regions at the margins of the SRP.

Contrasting tectonic and physiographic elements of the western United States surround the Yellowstone Plateau and SRP. Over at least 20 m.y., basin-and-range extension has occurred at different rates in the regions to the north and south of the SRP, suggesting that the Neogene magmatism of the SRP and Yellowstone Hot Spot may have tracked along an accommodation zone between these regions (Konstantinou and Miller, 2015). Earthquakes around the Yellowstone Plateau are largely confined to a "seismic parabola", which appears to reflect the lithospheric response to heating at the leading edge of the hot spot (fig. 2; Anders and others, 1989). Older portions of the hot spot along the SRP are seismically quiescent, possibly reflecting time-integrated strengthening of the lithosphere by magmatic inputs into the lower and middle crust (Anders and others, 1989). The Yellowstone Hot Spot has been ascribed to a deep-sourced and fixed mantle plume, with the eastward migration of volcanism reflecting the westward movement of the North American Plate (for example, Anders and others, 1989, 2014; Pierce and Morgan, 1992; Smith and others, 2009). High $^{3}He/^{4}He$ ratios in Yellowstone-related basalts have been interpreted as geochemical evidence for a deep mantle source (Graham and others, 2009). Alternatively, the hot spot has been ascribed to a shallow sourced plume or upper mantle upwelling (for example, Humphreys and others, 2000; Christiansen and others, 2002; James and others, 2011).

Since 2.1 Ma, silicic volcanism associated with the Yellowstone Hot Spot has been centered at Yellowstone Plateau. Approximately 6,500 cubic kilometers (km^3) of magma has erupted on the Yellowstone Plateau during three caldera cycles. During these three caldera cycles the Huckleberry Ridge (HRT), Mesa Falls (MFT), and Lava Creek (LCT) Tuffs were deposited (Christiansen, 1984, 2001). Volcanism at Yellowstone is the surface expression of a batholithic-scale accumulation of intrusions estimated to be 3 to 10 times greater in volume than what has been erupted (Christiansen, 2001; White and others, 2006). Seismic tomography indicates that the Yellowstone Plateau, specifically under the third cycle Yellowstone caldera (fig. 3), is underlain by a 90-km-long low velocity zone between 5–17 km deep, which correlates with the location of a large negative gravity anomaly (Farrell and others, 2014). This low velocity zone is interpreted to represent the Yellowstone's current upper-crustal magma reservoir with ~5 to 15 percent partial melt, or 200–600 km^3 of melt (Farrell and others, 2014), although seismic data do not indicate the particular distribution of melt (spread uniformly throughout versus accumulated in smaller pods of larger-melt fraction). At least 30 percent of the CO_2 from the active geothermal system appears to be derived from basaltic magma, suggesting the upper crustal reservoir is underlain by mafic intrusions (Werner and Brantley, 2003; Hurwitz and Lowenstern, 2014). Furthermore, using a joint local and teleseismic earthquake *P*-waves seismic inversion, Huang and others (2015) suggests that a basaltic magma body with a volume of 46,000 km^3 and a melt fraction of ~2 percent resides in the lower crust beneath Yellowstone.

[1]U.S. Geological Survey.

[2]University of Oregon.

[3]University of California–Davis.

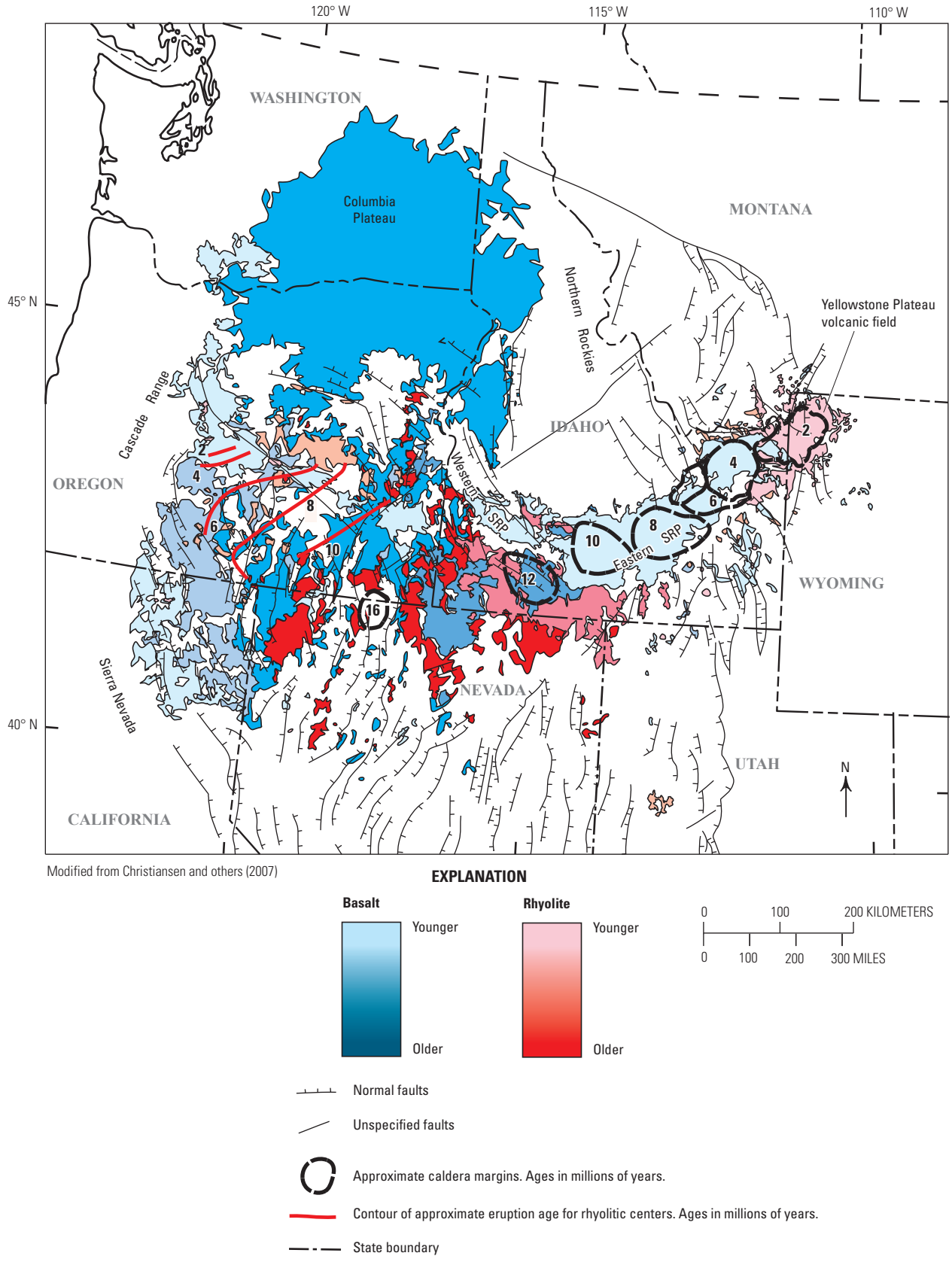

Figure 1. Map of the northwestern United States showing major tectonic and volcanic features 17 Ma and younger. Rhyolitic volcanic centers of the eastern Snake River Plain (SRP) are indicated by heavy black dashed lines marking locations of calderas with their approximate ages of initiation annotated (after Pierce and Morgan, 1992). A trend of westward propagating rhyolitic centers in eastern Oregon is shown by red age contour lines (after MacLeod and others, 1976). Modified from Christiansen and others (2007).

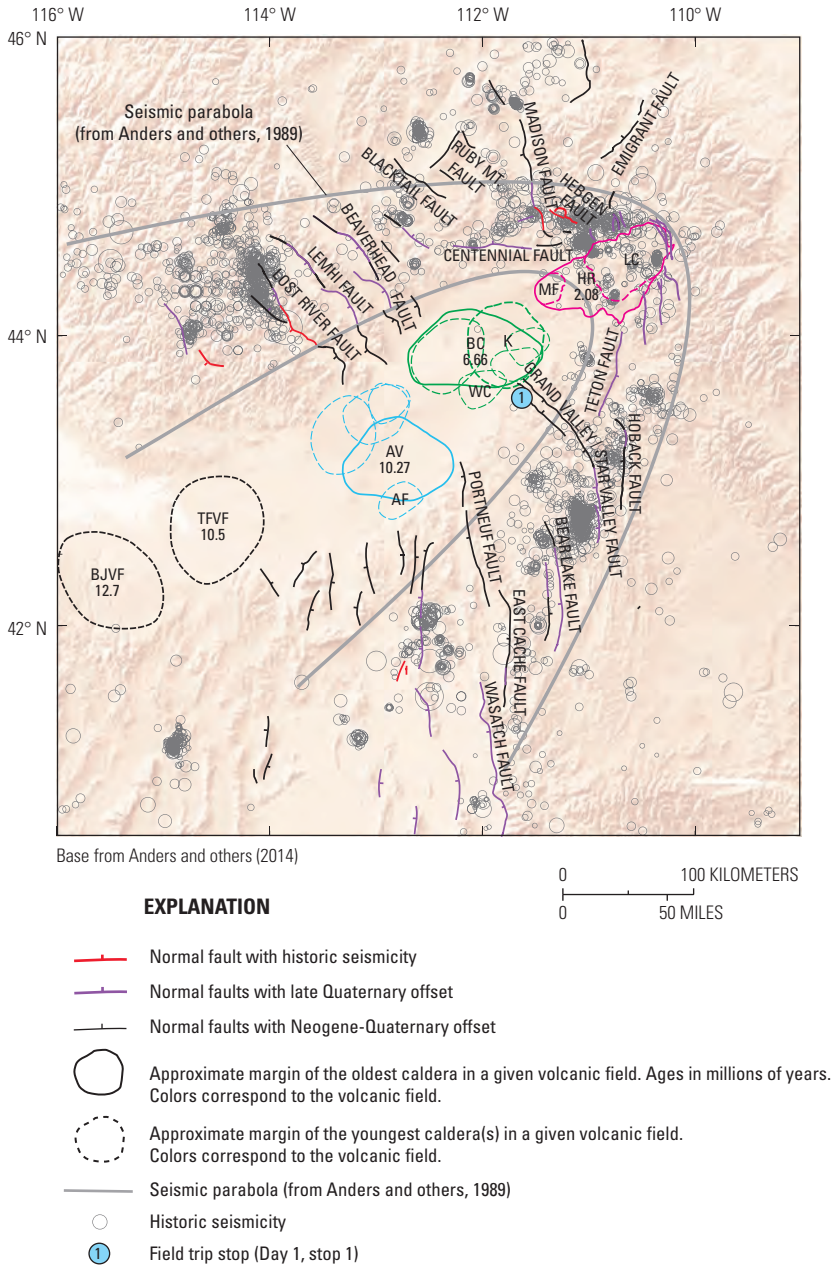

Figure 2. Map showing locations of volcanic fields and silicic caldera sources for major pyroclastic units along the central and eastern Snake River Plain as estimated from erupted volumes and proximal/distal characteristics (Anders and others, 2014). The oldest caldera, and its age in millions of years ago (Ma), in each volcanic field is marked by a solid colored line, the younger calderas in each field are marked by dashed lines of the same color and labeled (Anders and others, 2014). Day 1, Stop 1 is shown by the blue numbered circle. Historic seismicity (gray circles) defines a seismic parabola (gray lines), which reflects lithospheric response to the passing Yellowstone Hot Spot (Anders and others, 1989, 2014). Faults with historical seismicity are in red, faults with late Quaternary offset are in purple, and Neogene to Quaternary faults are in black. Yellowstone Plateau volcanic field (red) includes: LC, Lava Creek Tuff; MF, Mesa Falls Tuff; and HR, Huckleberry Ridge Tuff. Heise volcanic center (green) includes: K, tuff of Kilgore; WC, tuff of Wolverine Creek; and BC, tuff of Blacktail Creek. Picabo volcanic center (light blue) includes: AF, tuff of American Falls; and AV, Arbon Valley Tuff. Approximate locations of the Twin Falls volcanic field (TFVF) and Bruneau-Jarbidge volcanic field (BJVF) are noted by dashed black lines (from Bonnichsen and others, 2008). The Yellowstone Plateau volcanic field is from Christiansen (2001). Dates are from Anders and others (2014), Singer and others (2014), Rivera and others (2016), and Matthews and others (2015). Map modified from Anders and others (2014).

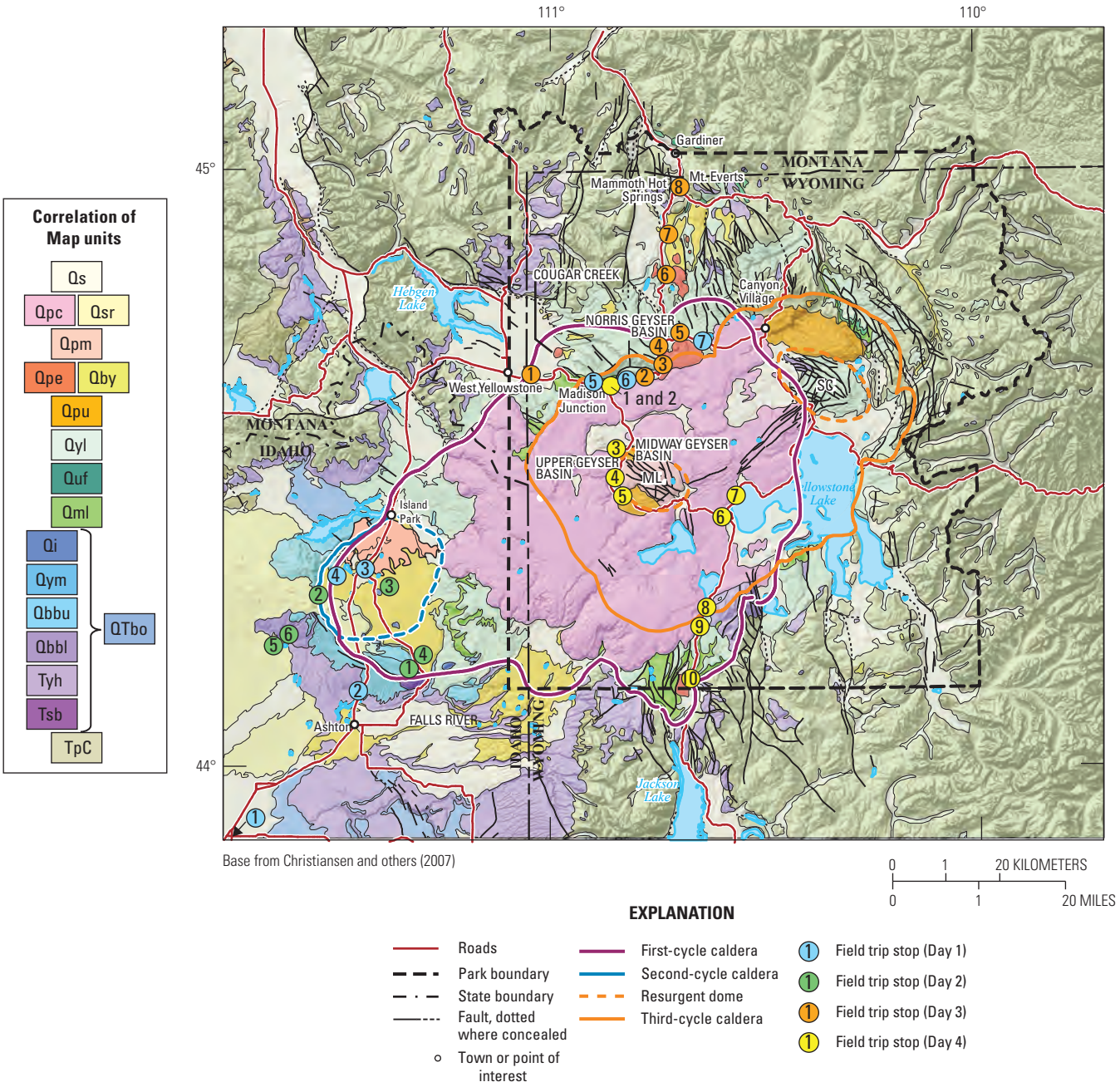

Figure 3. Geologic map of the Yellowstone Plateau volcanic field and vicinity. Field trip stops are labeled with colored circles. ML, Mallard Lake resurgent dome; SC, Sour Creek resurgent dome. Unit symbols: Qs, surficial deposits; Qpc, Plateau Rhyolite, Central Plateau Member; Qsr, basalts of Snake River Group; Qpm, Plateau Rhyolite, Mallard Lake Member; Qpe, extracaldera rhyolites; Qby, young extracaldera basalts; Qpu, Plateau Rhyolite, Upper Basin Member; Qyl, Lava Creek Tuff; Quf, Undine Falls Basalt; Qml, Mount Jackson and Lewis Canyon Rhyolites; Qi, Island Park Rhyolite; Qym, Mesa Falls Tuff; Qbbu, upper lavas of Big Bend Ridge Rhyolite; Qbbl, lower lavas of Big Bend Ridge Rhyolite; Tyh, Huckleberry Ridge Tuff; Tsb, rhyolite of Snake River Butte; QTbo, older basalts; TpC, rocks predating the Yellowstone Plateau volcanic field. Modified from Christiansen and others (2007).

This field guide examines the volcanic products of the Yellowstone Plateau, with emphasis on units that have been important for establishing the geochronology and understanding the petrologic evolution of the Pliocene–Quaternary rhyolites and basalts in and around Yellowstone. The figures and table provided are intended to provide relevant background information for this field trip. Major geologic features in the western United States and Snake River Plain are shown in figures 1 and 2, respectively. Major geologic features at and around the Yellowstone Plateau volcanic field and the location of the field trip stops for each day are shown in figure 3. Table 1 includes all of the published geochronology data that are referred to throughout this field trip guide. Unless noted, the radioisotopic dates presented in this guide are as published in

the scientific literature, and have not been normalized to any common set of calibration factors.

A number of excellent field guides have been published on Yellowstone, including those that focus on petrology and volcanology (Christiansen and Embree, 1987; Christiansen and Hutchinson, 1987; Bonnichsen and others, 1989; Embree and Hoggan, 1999; Morgan and others, 2008), as well as the hydrothermal system and glacial geology (Fournier and others, 1994). We refer the reader to these publications for more general information on the regional geology, tectonics, glacial history, and hydrothermal system at Yellowstone Plateau. *Please keep in mind that collecting any kind of sample in a United States National Park is prohibited by law except when done by permission and under a specific collecting permit issued by the United States National Park Service. Field trip participants are asked to leave their geologic hammers in their luggage while in Yellowstone National Park.*

The Petrologic Evolution of Yellowstone Plateau

In order to provide a framework for the petrologic evolution of Yellowstone's magmatic system and to highlight the current research questions being addressed at Yellowstone, we provide a brief description of the volcanic history of Yellowstone Plateau from 2.1 Ma to the present day. We focus on recent studies that examine the eruption and crystallization ages and geochemistry of volcanic products at Yellowstone. A simplified stratigraphy of volcanic deposits at the Yellowstone Plateau volcanic field is available in figure 4. Published geochronology data that are referred to throughout the text can be found in table 1.

First Cycle Rhyolitic Volcanism

The Yellowstone Plateau volcanic field is the youngest expression of the Yellowstone-SRP Hot Spot. An approximately 2.3 m.y. hiatus occurred between the last significant caldera-forming events, the 4.5 Ma Kilgore eruption (Wotzlaw and others, 2014) in the Heise volcanic field to the southwest (Morgan and McIntosh, 2005; Ellis and others, 2017a) and the initiation of volcanism at Yellowstone Plateau around 2.1 Ma. The first known eruption at Yellowstone Plateau produced the Snake River Butte, which is a small rhyolite dome located at the southeast margin of the Big Bend Ridge caldera (the caldera produced during the first caldera-forming eruption at Yellowstone). The Snake River Butte is the only preserved eruption that occurred before the first caldera-forming eruption at Yellowstone. The eruption age of the Snake River Butte has been constrained by a sanidine potassium-argon (K-Ar) date of 1.99±0.02 Ma (Obradovich, 1992), but recent uranium-lead dating reveals that most Snake River Butte zircons crystallized 2.1506±0.0052 Ma, which may indicate an older eruption age than indicated by the K-Ar dating (Wotzlaw and others, 2015).

Following eruption of the Snake River Butte rhyolite, the voluminous Huckleberry Ridge Tuff was erupted at 2.079±0.005 Ma (Rivera and others, 2014) and formed the Big Bend Ridge caldera (fig. 3). The Huckleberry Ridge Tuff has been the focus of numerous recent geochronologic and petrologic studies. For example, Rivera and others (2014) measured uranium-lead dates and trace-element compositions for zircons from Huckleberry Ridge Tuff member B and concluded that the Huckleberry Ridge magma differentiated over a 10 thousand year period prior to eruption about 2.08 Ma. Additionally,

Epoch	Volcanic Cycle	Precaldera rhyolite	Caldera-forming ash flow tuff	Postcaldera rhyolite	Contemporaneous plateau-marginal basalts
Pleistocene	Third			Plateau rhyolite: Central Plateau Member; Upper Basin Member	Osprey basalt Madison River basalt basalt of Geode Creek Swan Lake Flat basalt Gerrit basalt Falls River basalt Basalt of Mariposa Lake
			Lava Creek tuff		
		Mount Jackson rhyolite Lewis Canyon rhyolite			Undine Falls basalt basalt of Warm River basalt of Shotgun Valley
	Second			Island Park rhyolite	Basalt of the Narrows
			Mesa Falls tuff		
		Big Bend Ridge rhyolite			
				Big Bend Ridge rhyolite	
Pliocene	First		Huckleberry Ridge tuff		
		Rhyolite of Snake River Butte			Junction Butte basalt

Figure 4. Simplified volcanic stratigraphy for the Yellowstone Plateau volcanic field. Modified from Christiansen (2001).

Table 1. Summary of selected K-Ar or $^{40}Ar/^{39}Ar$ eruption ages for units discussed in the field trip guide.

Unit	Source	Lithology	Age (Ma)	± Age (Ma)	Uncertainty confidence level[1]	Method
Pinehaven basalt	George and others (2015)	Basalt	0.029	0.009	1 sigma	Ar/Ar
Pitchstone Plateau flow	Stelten and others (2015)	Rhyolite	0.0749	0.0034	1 sigma	Ar/Ar
Moose Falls flow	Christiansen and others (2007)	Rhyolite	0.0806	0.0046	1 sigma	Ar/Ar
Hayden Valley flow	Obradovich (1992)	Rhyolite	0.102	0.004	1 sigma	K/Ar
Solfatara Plateau flow	Christiansen and others (2007)	Rhyolite	0.1028	0.0076	1 sigma	Ar/Ar
Obsidian Cliff flow	Nastanski (2005)	Rhyolite	0.1056	0.0010	1 sigma	Ar/Ar
Gibbon River flow	Dallegge (2008)	Rhyolite	0.1076	0.0071	1 sigma	Ar/Ar
West Yellowstone flow	Christiansen and others (2007)	Rhyolite	0.1140	0.0012	1 sigma	Ar/Ar
Summit Lake flow	Christiansen and others (2007)	Rhyolite	0.124	0.010	1 sigma	Ar/Ar
Gibbon Hill dome	Nastanski (2005)	Rhyolite	0.1343	0.0026	1 sigma	Ar/Ar
Tuff of Cold Mountain Creek	Christiansen and others (2007)	Rhyolite	0.143	0.005	1 sigma	Ar/Ar
Nez Perce Creek flow	Christiansen and others (2007)	Rhyolite	0.1483	0.0051	1 sigma	Ar/Ar
Elephant Back flow	Obradovich (1992)	Rhyolite	0.153	0.002	1 sigma	K-Ar
Aster Creek flow	Obradovich (1992)	Rhyolite	0.155	0.003	1 sigma	K-Ar
Dry Creek Flow	Christiansen (2007)	Rhyolite	0.166	0.009	1 sigma	Ar/Ar
Tuff of Bluff Point	Christiansen and others (2007)	Rhyolite	0.1731	0.0049	1 sigma	Ar/Ar
Swan Lake Flat Basalt (Panther Creek vent)	Bennett (2006)	Basalt	0.174	0.046	1 sigma	Ar/Ar
Paintpot Hill dome	Nastanski (2005)	Rhyolite	0.2081	0.0049	1 sigma	Ar/Ar
Scaup Lake flow	Christiansen and others (2007)	Rhyolite	0.257	0.013	1 sigma	Ar/Ar
South Biscuit Basin flow	Watts and others (2012)	Rhyolite	0.261	0.017	1 sigma	Ar/Ar
Gardner River complex	Nastanski (2005)	Rhyolite	0.3005	0.0028	1 sigma	Ar/Ar
Tuff of Sulphur Creek	Gansecki and others (1996)	Rhyolite	0.479	0.020	2 sigma	Ar/Ar
Middle Biscuit Basin flow	Gansecki and others (1996)	Rhyolite	0.516	0.014	2 sigma	Ar/Ar
Riverside flow	Nastanski (2005)	Rhyolite	0.526	0.003	1 sigma	Ar/Ar
Madison River Basalt	Bennett (2006)	Basalt	0.530	0.060	1 sigma	Ar/Ar
Swan Lake Flat Basalt (Tower Road vent)	Bennett (2006)	Basalt	0.590	0.065	1 sigma	Ar/Ar
Lava Creek Tuff	Matthews and others (2015)	Rhyolite	0.6313	0.0043	95% conf.	Ar/Ar
Mount Haynes flow	Troch and others (2017)	Rhyolite	0.7016	0.0016	2 sigma	Ar/Ar
Harlequin Lake flow	Troch and others (2017)	Rhyolite	0.8300	0.0074	2 sigma	Ar/Ar
Wapiti Lake flow	Troch and others (2017)	Rhyolite	1.2187	0.0160	2 sigma	Ar/Ar
Lookout Butte	Troch and others (2017)	Rhyolite	1.2190	0.0146	2 sigma	Ar/Ar
Osborne Butte	Troch and others (2017)	Rhyolite	1.2784	0.0054	2 sigma	Ar/Ar
Warm River Butte	Troch and others (2017)	Rhyolite	1.2943	0.0026	2 sigma	Ar/Ar
Mesa Falls Tuff	Rivera and others (2016)	Rhyolite	1.300	0.001	95% conf.	Ar/Ar
Tuff of Lyle Spring	Obradovich (1992)	Rhyolite	1.32	0.02	1 sigma	K-Ar
Headquarters flow	Rivera and others (2017)	Rhyolite	1.9476	0.0037	2 sigma	Ar/Ar
Blue Creek flow	Rivera and others (2017)	Rhyolite	1.9811	0.0035	2 sigma	Ar/Ar
Snake River Butte	Obradovich (1992)	Rhyolite	1.99	0.02	1 sigma	K-Ar
Huckleberry Ridge Tuff	Singer and others (2014)	Rhyolite	2.077	0.003	2 sigma	Ar/Ar
Tuff of Kilgore	Wotzlaw and others (2014)	Rhyolite	4.510	0.047	2 sigma	Ar/Ar
Tuff of Wolverine Creek	Anders and others (2014)	Rhyolite	5.72	0.03	1 sigma	Ar/Ar
Blacktail Creek tuff	Anders and others (2014)	Rhyolite	6.66	0.01	1 sigma	Ar/Ar
Tuff of American Falls	Anders and others (2014)	Rhyolite	7.58	0.01	1 sigma	Ar/Ar
Arbon Valley Tuff	Anders and others (2014)	Rhyolite	10.27	0.01	1 sigma	Ar/Ar

[1]Uncertainties and confidence intervals are those reported in the original literature.

Wotzlaw and others (2015) performed uranium-lead dating, oxygen isotope, and hafnium isotope analysis of zircons from Huckleberry Ridge Tuff members B and C, and suggested the Huckleberry Ridge Tuff was rapidly assembled from multiple, chemically heterogeneous magma bodies stored within Yellowstone's magmatic system.

Second Cycle Rhyolitic Volcanism

The second volcanic cycle is the smallest—in terms of volume of erupted material—of the caldera cycles on the Yellowstone Plateau (Christiansen, 2001). The Mesa Falls Tuff reflects the caldera-forming eruption of the second cycle at 1.30 Ma (Rivera and others, 2016; Wotzlaw and other, 2015; Ellis and others, 2017b), and is primarily distributed around the Island Park area (Christiansen, 2001). The Mesa Falls eruption generated the Henrys Fork caldera, which is centered in the Island Park area of the Yellowstone Plateau (fig. 3). Pre-Mesa Falls Tuff eruptions associated with the second cycle are represented by several domes and tuffs that crop out along the western portion of the Island Park area (Christiansen, 2001). K-Ar dating and field relations suggest these rhyolites erupted shortly before the Mesa Falls eruption (Christiansen, 2001). Post-Mesa Falls Tuff domes of crystal-rich rhyolite are exposed on the floor of the Henrys Fork caldera (fig. 3), and are collectively known as the Island Park Rhyolite (Christiansen, 2001). $^{40}Ar/^{39}Ar$ dating indicates the Island Park Rhyolite domes erupted during an ~80 k.y. interval after the Mesa Falls eruption (Troch and others, 2017). These second cycle rhyolites are distinct because of their relatively high abundance of hydrous minerals such biotite and amphibole (Christiansen and others, 2001; Troch and others, 2017). Coeval with the eruption of the youngest (~1.22 Ma) Island Park Rhyolite domes, the Wapiti Lake rhyolite, with compositional similarities to the rhyolites of the third cycle, erupted near the eastern margin of the later-formed Yellowstone caldera, suggesting the presence of widely distributed and compositionally distinct bodies of magma at the end of the second caldera cycle (Troch and others, 2017).

Third Cycle Rhyolitic Volcanism

The onset of the third volcanic cycle was marked by the eruption of the large silicic lavas of the Mount Jackson and Lewis Canyon Rhyolites (Christiansen, 2001), which together yield $^{40}Ar/^{39}Ar$ dates from about 1.22 Ma to 702 ka (Troch and others, 2017). These lavas are exposed along the western walls of Yellowstone caldera, and may have erupted along incipient ring faults (Christiansen, 2001). The enormous (>1,000 km^3) explosive eruption that resulted in the Lava Creek Tuff and Yellowstone caldera is dated to approximately 630 ka based on $^{40}Ar/^{39}Ar$ dating (Matthews and others, 2015; Jicha and others, 2016; Mark and others, 2017) and reflects the evacuation of a shallow rhyolitic magma body with gradients in geochemistry, mineralogy, temperature (Hildreth, 1981; Hildreth and others, 1991; Christiansen, 2001; Matthews and others, 2015), and isotopic composition (Wotzlaw and others, 2015). As with the Huckleberry Ridge Tuff and Mesa Falls Tuff rhyolites, uranium-lead dating of Lava Creek zircons suggests the voluminous Lava Creek magma chamber evolved relatively rapidly over a few tens of thousand of years before eruption (Matthews and others, 2015; Wotzlaw and others, 2015). The Lava Creek eruption generated extensive tephra, which covered much of the western United States and has served as an important chronostratigraphic marker for diverse Quaternary studies (Sarna-Wojcicki and others, 1984). The extremely widespread dispersal of Lava Creek tephra suggests ash transport in a continent-scale umbrella cloud, which was little affected by ambient winds (Mastin and others, 2014).

Since the Lava Creek eruption at 631.3±4.3 ka (Matthews and others, 2015) the magmatic system at Yellowstone Plateau has been characterized by dominantly effusive intracaldera eruptions and a few explosive eruptions. Intracaldera rhyolitic eruptions at Yellowstone have volumes ranging from <0.5 km^3 to as much as 70 km^3 (Christiansen, 2001). Post-Lava Creek Tuff intracaldera volcanism has been divided into two general groups that make up the Upper Basin and Central Plateau Members of the Plateau Rhyolite, both of which have distinctive petrologic characteristics (Christiansen and Blank, 1972). The first post-Lava Creek eruptive episode produced the Upper Basin Member rhyolites, which are characterized by a mineral assemblage of plagioclase, quartz, sanidine, pyroxene, iron-titanium oxides, and trace zircon. The Upper Basin Member rhyolites can be divided into the early Upper Basin Member rhyolites and the late Upper Basin Member rhyolites. The early Upper Basin Member rhyolites, which erupted between 516±14 ka and 479±20 ka (Gansecki and others, 1996) near the Mallard Lake and Sour Creek resurgent domes (fig. 5) are characterized by large depletions of ^{18}O in the melt ($\delta^{18}O$ as low as ~1‰ [per mil, or part per thousand]; Hildreth and others, 1984; Bindeman and Valley, 2001; Bindeman and others, 2008; Pritchard and Larson, 2012) and zircon populations with heterogeneous $\delta^{18}O$ values (Bindeman and Valley, 2001; Bindeman and others, 2008). Additionally, each Upper Basin Member rhyolite has a distinct trace-element composition relative to the other Upper Basin Member rhyolites (Girard and Stix, 2009). Based on these observations (and zircons as old as 2.1 Ma) the early Upper Basin Member rhyolites have been interpreted to represent independent parcels of melt generated by remelting of hydrothermally altered intracaldera rocks composed of Huckleberry Ridge Tuff and pre-Lava Creek Tuff Yellowstone rhyolites (or their unerupted equivalents). The heat source driving this remelting has been attributed to mafic magmas ponding beneath the silicic magma reservoir and potentially silicic recharge magmas injected into the reservoir (Bindeman and others, 2008; Girard and Stix, 2009).

After an ~220 k.y. hiatus the late Upper Basin Member rhyolites, which include the South Biscuit Basin flow ($^{40}Ar/^{39}Ar$ date of 261±17 ka; Watts and others, 2012) and Scaup Lake flow ($^{40}Ar/^{39}Ar$ date of 257±13 ka; Christiansen and others, 2007), erupted near the Mallard Lake resurgent

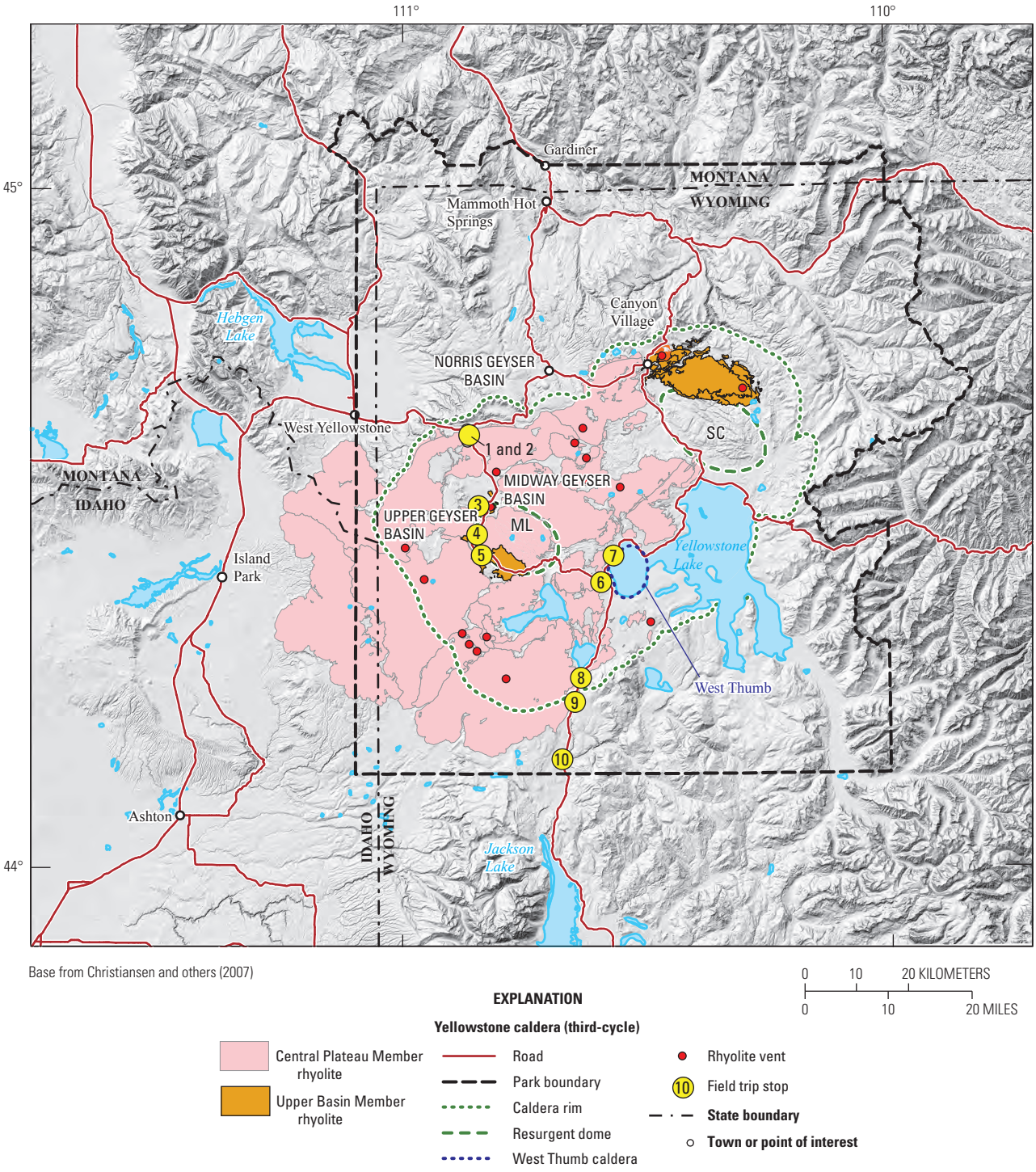

Figure 5. Map of Yellowstone National Park showing the Yellowstone caldera, resurgent domes, and post-Lava Creek Tuff intracaldera rhyolitic lavas. Vents for the lava flows from the younger Central Plateau Member rhyolites form two linear northwest trending vent zones across the caldera. ML, Mallard Lake resurgent dome; SC, Sour Creek resurgent dome. Modified from Christiansen and others (2007).

dome. Similar to the early Upper Basin Member rhyolites, the late Upper Basin Member rhyolites have less chemically evolved mineral and whole-rock compositions relative to the younger Central Plateau Member (CPM) rhyolites (Vazquez and others, 2009; Girard and Stix, 2009, 2010). The late Upper Basin Member rhyolites also have a similar mineralogy to the early Upper Basin Member (UBM) rhyolites. However, the late Upper Basin Member rhyolites have neodymium, lead, and oxygen isotopic compositions that are more similar to the Central Plateau Member rhyolites than the early Upper Basin Member rhyolites (Bindeman and others, 2008; Pritchard and Larson, 2012; Till and others, 2013; Vazquez and Reid, 2002; Vazquez and others, 2009). These observations have been interpreted to suggest that the late Upper Basin Member rhyolites represent a transitional period between early Upper Basin Member and the subsequent Central Plateau Member magmatism (Girard and Stix, 2009, 2010; Vazquez and Reid, 2002; Watts and others, 2012). In fact, Loewen and Bindeman (2015) refer to the late Upper Basin Member rhyolites as the beginning of the Central Plateau Member eruptive episode rather than the end of the Upper Basin Member eruptive episode.

Approximately 80 k.y. after eruption of the late Upper Basin Member rhyolites, the second major post-Lava Creek Tuff eruptive episode generated the voluminous Central Plateau Member rhyolites, which consist of at least 18 lava flows and two ignimbrites, which were erupted intermittently from ~170 ka to ~70 ka (fig. 3; Christiansen, 2001; Christiansen and others, 2007). The Central Plateau Member rhyolites are petrographically distinct from the Upper Basin Member rhyolites because they typically lack plagioclase and are dominated by sanidine and quartz. The Central Plateau Member rhyolites were likely erupted episodically in four or five pulses separated by 15 to 30 k.y. (Christiansen and others, 2007). However, the number of pulses reported for the Central Plateau Member eruptive episode ranges from three to five, depending on the author (Christiansen and others, 2007; Girard and Stix, 2010; Loewen and Bindeman, 2015). Additionally, the timing between eruptions within a given eruptive pulse remains geochronologically unconstrained and is currently limited by the precision of the K-Ar and $^{40}Ar/^{39}Ar$ dates reported for Yellowstone. Understanding the potentially episodic nature of volcanism at Yellowstone is critical for improving probabilistic estimates of future volcanic hazards (Christiansen and others, 2007). Higher precision $^{40}Ar/^{39}Ar$ dates would further constrain the number and duration of eruption pulses at Yellowstone.

The Central Plateau Member rhyolites have low $\delta^{18}O$ compositions of ~4.5‰ and therefore their source region is composed, at least partly, of remelted hydrothermally altered material (Loewen and Bindeman, 2015). However, their $\delta^{18}O$ values are significantly higher than the preceding Upper Basin Member rhyolites, suggesting less hydrothermally altered material in the source region for the Central Plateau Member rhyolites. Unlike the Upper Basin Member rhyolites, the Central Plateau Member rhyolites erupted along two north-northwest trending vent lineaments, which align with major extracaldera faults (Christiansen, 2001; Christiansen and others, 2007). The tectonically controlled vent locations of the Central Plateau Member rhyolites have been interpreted to reflect the reestablishment of major extracaldera faults through the top of a crystallizing magma chamber (Christiansen, 2001; Girard and Stix, 2010).

Several studies have suggested that the Central Plateau Member rhyolites were derived from a common mushy magma reservoir (not a single large tank of magmatic liquid), which evolved over time to more fractionated compositions, cooler temperatures, and more juvenile isotopic compositions thorough a combination of crystallization, assimilation, and magma recharge. This model is based on secular trends in:

- Glass and whole-rock trace-element and isotopic compositions (compatible elements like Sr, Eu, and Ba decrease through time and incompatible elements such as Nb and Y increase through time),
- Compositions of major mineral phases,
- Zircon trace-element compositions, and
- Various geothermometry estimates for Central Plateau Member rhyolites (Hildreth and others, 1984, 1991; Christiansen, 2001; Vazquez and Reid, 2002; Vazquez and others, 2009; Girard and Stix, 2010, 2012; Watts and others, 2012; Stelten and others, 2015).

However, Loewen and Bindeman (2015) propose a different model for the generation of the Central Plateau Member rhyolites where the observed chemical trends through time are the result of repeated batch melting events at the base of a homogenized low-$\delta^{18}O$ intracaldera fill. This produces liquidus rhyolites and a refractory residue that is rich in feldspar.

A key difference between the models for the temporal evolution of the Central Plateau Member rhyolites centers on the thermal evolution of the magmatic system. In the crystallization model, the temperature of the system is decreasing though time, which is supported by temporal decreases in titanium-in-quartz temperatures, pyroxene-fayalite temperatures, titanium-in-zircon temperatures, and iron-titanium oxide temperatures (Vazquez and others, 2009; Girard and Stix, 2010; Stelten and others, 2015). The temperatures implied by the progressive crystallization model are also supported by recent experimental work performed on natural Central Plateau Member rhyolites by Befus and Gardner (2016), which suggest minerals in the rhyolites crystallized at 750±25 °C, in excellent agreement with titanium-in-zircon crystallization temperatures of Stelten and others (2015). Conversely, Loewen and Bindeman (2015) present a model where the rhyolites are generated by equilibrium melting of a shallow refractory feldspar-rich source, which can be in a mushy or subsolidus state. In this model the temperature of the rhyolites would increase though time as the source becomes more refractory and difficult to melt. Evidence for this temperature increase comes largely from oxygen isotopic measurements of pyroxene-quartz and glass $\delta^{18}O$ thermometry and increasing (or constant) zircon saturation temperatures observed in glass

of the Central Plateau Member rhyolites. Loewen and Bindeman (2015) suggest that the source for the Central Plateau Member rhyolites is melted to form zircon-undersaturated supersolidus rhyolites that then cool and crystallize sanidine, pyroxene, quartz, and zircon prior to eruption.

Some degree of open system behavior is required during the Central Plateau Member eruptive episode as demonstrated by systematic temporal changes in lead isotopic composition observed in the rhyolite glasses and their phenocrysts (Vazquez and others, 2009; Watts and others, 2012; Stelten and others, 2015). However, the source(s) responsible for the isotopic changes in the Central Plateau Member rhyolites and the amount of material required to generate these changes is currently debated. Based on temporal lead isotope trends in the Central Plateau Member rhyolites, it is likely that injection of silicic derivatives of Yellowstone basalts into the shallow magmatic system is driving the isotopic changes though time (Vazquez and others, 2009). This concept is supported by zircon crystallization age and hafnium isotope data reported by Stelten and others (2013), which document the presence of young zircons with near mantle-like hafnium isotope compositions in some Central Plateau Member rhyolites. However, the amount of recharge material required to generate these temporal isotopic changes though time is likely small (~5 percent).

Basalts

In addition to producing large rhyolitic ignimbrites and lava flows, Yellowstone has been the site of numerous eruptions of tholeiitic basaltic magma over its ~2.1 m.y. history. Although basaltic eruptions are volumetrically minor compared to rhyolitic eruptions, basaltic magmas are interpreted as fundamental to volcanism at Yellowstone because they provide the heat necessary to develop and maintain Yellowstone's silicic magmatic system (Hildreth and others, 1991). Even though no basaltic eruption has occurred at Yellowstone in the last ~30 k.y., evidence from modern day CO_2 emissions and heat flux estimates at Yellowstone suggest high intrusion rates of basaltic magma (~0.3 cubic kilometers per year [km^3/y] assuming 1 weight percent CO_2 in mantle-derived basalt, which is comparable to the Hawaiian hot spot; Lowenstern and Hurwitz [2008]) persist to this day.

Unlike the majority of rhyolite flows at Yellowstone, which erupt within the margins of the preceding caldera-forming eruption, basaltic magmas erupt peripherally to the caldera margins (fig. 3). Most Yellowstone basalts are assigned to nine units, which correspond to eruptive groups based largely on the location of their eruption and their stratigraphic relation to deposits from the caldera-forming eruptions at Yellowstone (fig. 4; Christiansen, 2001). Each of these eruptive groups consists of as many as 50 lava flows, with total volumes ranging from <1 to ~25 km^3, erupted from a dozen or more separate vents. Basalts from a given eruptive group are not necessarily associated in time and often have eruption ages that differ by tens to hundreds of thousands of years. In this field trip we will examine the youngest, post-Lava Creek Tuff basalts, which erupted in three principal locations (fig. 3):

- North of the Yellowstone caldera along the zone of recurrent faulting that extends north from Norris Geyser Basin to Mammoth Hot Springs (the Norris-Mammoth corridor),
- North-northwest of Yellowstone caldera along a vent zone trending northeast from Madison Valley into the Norris-Mammoth corridor, and
- Southwest of Yellowstone caldera.

The pattern of basaltic volcanism that has been exclusively erupted outside of its contemporaneous caldera margin on the Yellowstone Plateau is interpreted to reflect the existence of a silicic magmatic system over the past ~2.1 m.y. that provides a low-density barrier through which ascending basaltic magmas cannot penetrate (Smith, 1979; Christiansen, 1984, 2001). It is worth noting that no basaltic magmas have erupted within the present day Yellowstone caldera, but many post-Lava Creek Tuff basaltic eruptions have occurred within the first and second cycle caldera margins (fig. 3). Additionally, some SRP-type basalts (which are compositionally distinct from Yellowstone basalts; Doe and others, 1982; Hildreth and others, 1991) have erupted within the western margin of the first and second cycle calderas. This observation is interpreted to mean that the silicic reservoirs feeding the first and second cycles of magmatism at Yellowstone have cooled and crystallized to the point where basaltic magmas are now able to ascend through this portion of the crust.

In addition to providing the heat necessary to generate silicic magmas at Yellowstone, chemical and isotopic data suggest that basaltic magmas contribute a significant amount of mass to the silicic system. Isotopic data rule out the possibility that Yellowstone rhyolites are pure differentiates of Yellowstone basalts (Hildreth and others, 1991; Nash and others, 2006; Watts and others, 2010). However, isotopic data also demonstrate that erupted Yellowstone rhyolites have isotopic compositions intermediate between Yellowstone basalts and the potential crustal sources (fig. 6). These observations require that some mass fraction of the rhyolites at Yellowstone come from mantle-derived basalts and both mafic and silicic crustal sources (Hildreth and others, 1991; Nash and others, 2006; McCurry and Rodgers, 2009). This observation is typically explained by hybridization of basaltic magmas with crustal melts (Hildreth and others, 1991; Christiansen, 2001; Watts and others, 2010; Wotzlaw and others, 2015). In this model the source for intracaldera rhyolites and caldera-forming eruptions at Yellowstone is a hybridized crust that consists of mantle derived magmas mixed with partial melts of various crustal components (fig. 7). This hybridized source, with isotopic compositions intermediate to that of Yellowstone basalts and the surrounding crust, is then melted to form silicic magmas with isotopic compositions similar to the erupted intracaldera rhyolites and caldera-forming eruptions (Hildreth and others, 1991). These silicic magmas may undergo further

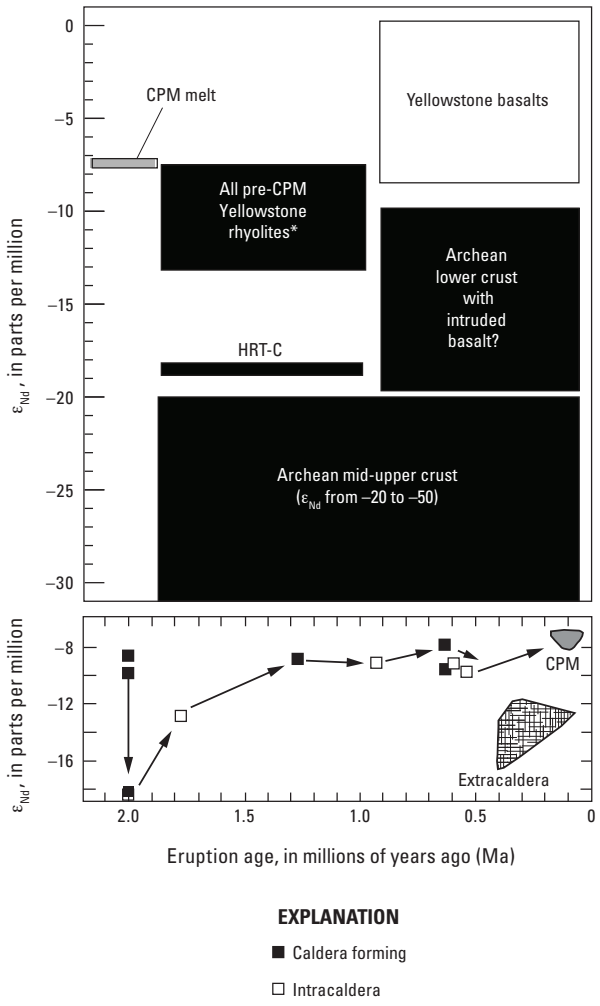

Figure 6. Summary of neodymium isotopic data for Yellowstone rhyolites, basalts, and local crust. The Nd isotopic compositions are reported in epsilon units, calculated as [($^{143}Nd/^{144}Nd$ Sample)/ $^{143}Nd/^{144}Nd$ CHUR(0)) -1]*10,000, where $^{143}Nd/^{144}Nd$ $CHUR_{(0)}$ = 0.512638. $CHUR_{(0)}$ = Chondritic Uniform Reservoir at time zero. Potential crustal sources for the generation of the Central Plateau Member (CPM) rhyolites are shown in black. The mantle input into the system (the Yellowstone basalt) is shown in white. The CPM rhyolites are shown in gray. The extracaldera rhyolites are shown with a hatched fill. Note that Yellowstone rhyolites (the caldera-forming eruptions and intracaldera rhyolites) have ε_{Nd} values intermediate to potential local crustal source and Yellowstone basalts. The field labeled "All pre-CPM Yellowstone rhyolites*" includes the range of data for all Yellowstone rhyolites except for Huckleberry Ridge Tuff member C, which shows evidence for large amounts of crustal assimilation and is plotted separately (see Hildreth and others, 1991). Neodymium isotopic data are from Hildreth and others (1991), Vazquez and Reid (2002), Bennett (2006), Nash and others (2006), and Pritchard and Larson (2012). Figure modified from Stelten and others (2017).

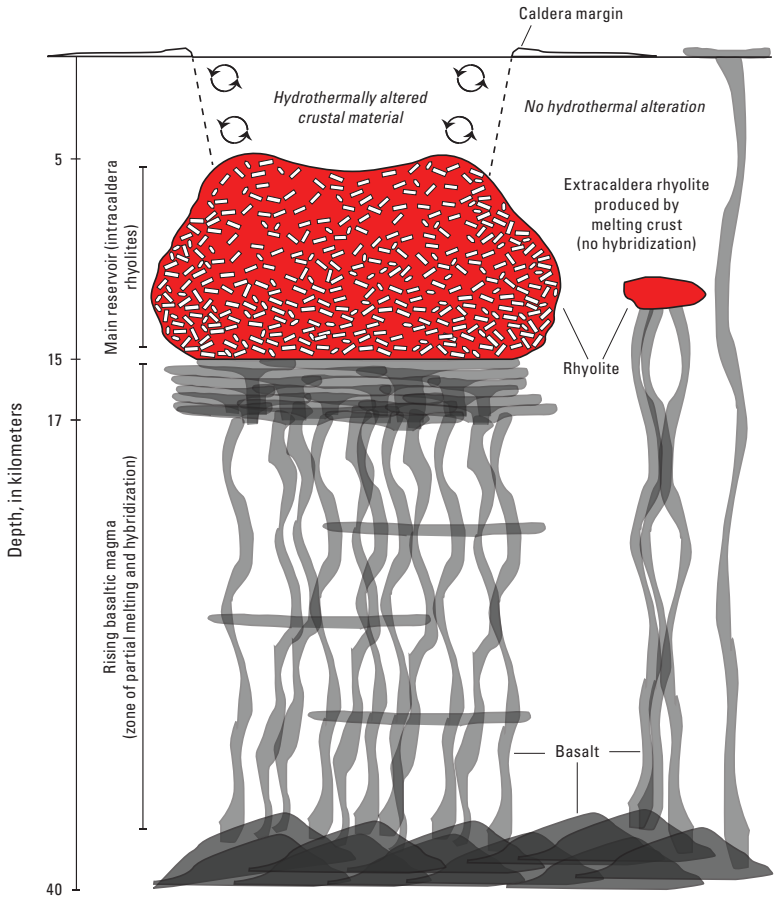

Figure 7. Schematic diagram showing the relation between basaltic magmas, intracaldera rhyolites (including caldera forming tuffs, pre-, and post-caldera rhyolites), and extracaldera rhyolites. Depths are based on Farrell and others (2014).

melting and assimilation of upper crustal rocks before being erupted (fig. 7; Wotzlaw and others, 2015).

Extracaldera Rhyolites

Following eruption of the caldera-forming Lava Creek Tuff at 631.3±4.3 ka (Matthews and others, 2015), numerous small volume rhyolites have erupted outside of Yellowstone (fig. 3). These extracaldera rhyolites erupted from ~530 to ~80 ka and span the same range of time as post-Lava Creek Tuff intracaldera rhyolite eruptions (Christiansen and others, 2007), but are distinct from intracaldera rhyolites in several ways. In general, extracaldera rhyolites have distinct isotopic compositions relative to intracaldera rhyolite flows. Compared to intracaldera rhyolites, extracaldera rhyolites have lower $^{143}Nd/^{144}Nd$, which suggests a stronger crustal influence during their formation (fig. 6; Hildreth and others, 1991; Pritchard and Larson, 2012; Pritchard and others, 2013). Modeling by Pritchard and Larson (2012) suggests that the isotopic composition of the extracaldera rhyolites can be explained by injection of basaltic magmas into the crust, followed by assimilation of Archean crust and extensive fractional crystallization. In addition to lower $^{143}Nd/^{144}Nd$, the extracaldera rhyolites have higher $\delta^{18}O$ relative to intracaldera eruptions at Yellowstone and are similar to the earliest Huckleberry Ridge Tuff magmas (Hildreth and others, 1984). This suggests that the extracaldera rhyolites did not interact with hydrothermally altered crust prior to eruption, and this in turn implies that the crust outside of the caldera has not been hydrothermally altered. The compositional distinction between extracaldera and intracaldera rhyolites provides an opportunity to assess the structure of the magmatic system at Yellowstone.

Extracaldera rhyolitic lavas at Yellowstone are divided into two groups based on their petrography. The Obsidian Creek Member rhyolites are porphyritic with quartz, sanidine, and plagioclase phenocrysts, and the Roaring Mountain Member rhyolites are sparsely porphyritic to aphyric. The aphyric nature of the Roaring Mountain rhyolites suggests these magmas were emplaced at, or above their liquidus temperature (Christiansen, 2001; Christiansen and others, 2007). Both the Obsidian Creek and Roaring Mountain rhyolites occur almost exclusively to the north of Yellowstone caldera in the Norris-Mammoth corridor (the same area as the majority of post-Lava Creek Tuff basaltic volcanism; fig. 3). In several cases extracaldera rhyolites are intimately associated with basalt, which occurs as quenched magmatic inclusions or large masses within the rhyolites (for example, the Gardner River and Grizzly Lake complexes). So although volumetrically minor, extracaldera rhyolites provide important information about the interaction of basalt and rhyolite at Yellowstone. Examples of Obsidian Creek rhyolites, Roaring Mountain rhyolites, and a mixed basalt-rhyolite complex can be seen on this field trip.

Hydrothermal Features

Yellowstone Plateau is host to a vast hydrothermal system and is world famous for its spectacular hydrothermal features. A detailed discussion of the hydrothermal system at Yellowstone is beyond the scope of this field trip guide; readers interested in detailed descriptions should see Fournier and others (1994), Hurwitz and Lowenstern (2014), or Morgan and others (2009). On this field trip we will briefly examine a number of hydrothermal features located outside of Yellowstone caldera that lie along a network of faults in the zone extending from Norris Geyser basin through Mammoth Hot Spring (the Norris-Mammoth Corridor). Hydrothermal activity in this region is intimately related to extracaldera basaltic and rhyolitic magmatism and is the result of several factors:

- An abundant supply of meteoric recharge water that largely originates from snow on the surrounding mountains,
- The abundant heat supply from the magmatic system underlying Yellowstone Plateau, and
- Frequent seismic activity at Yellowstone, which opens fractures in the crust, creating pathways for fluid flow (Fournier and others, 1994).

In general, hydrothermal activity is located near zones with abundant fractures in the crust such as the outer edge of the main ring fracture zone, near the Mallard Lake and Sour Creek resurgent domes within the caldera, and outside of the caldera in the Norris-Mammoth Corridor.

Day 1

Overview

The first day will concentrate on the calderas and ignimbrites produced by the three caldera cycles of the Yellowstone Plateau volcanic field, and discussing their petrology and geochronology (see fig. 4 for general stratigraphic relationships at Yellowstone). Stops include examining exposures of the Huckleberry Ridge, Mesa Falls, and Lava Creek Tuffs; and viewing the caldera structures associated with each explosive eruption. In addition, we will examine the tuff of Kilgore a voluminous low $\delta^{18}O$ rhyolite, which represents the youngest ignimbrite-forming eruption from the pre-Yellowstone Heise volcanic center (figs. 1, 2). Post-caldera basalt that marks the end of the second caldera cycle, which produced the MFT, will also be examined. The trip will begin in the city of Idaho Falls, Idaho, drive to the edge of the Snake River Plain (SRP),

proceed through the Island Park basin, and end in the northern portion of Yellowstone caldera within Yellowstone National Park. *It is important to note that traffic as well as wildlife, such as rattlesnakes, bison, and bears, are potential hazards in the Yellowstone area.*

Day 1 Road Log

Mileage (in miles)

0.0 Reset trip odometer at Idaho Falls airport terminal, and exit the airport along Skyline Drive.

0.9 Turn left (east) onto Grandview Drive. Grandview Drive turns into U.S. Route 20, which is America's longest road, extending 3,365 miles from Newport, Oregon, to Boston, Massachusetts.

4.7 Exit Route 20 at St. Leon Road (Exit 311). Turn right (south) onto St. Leon Road.

5.3 Turn left onto East 49th Street after crossing railroad tracks.

7.1 Turn left (east) onto U.S. Highway 26.

19.8 Turn right onto Meadow Creek Road.

23.0 Pass entrance to Ririe Recreation Area. Continue on gravel road.

26.1 Stop 1.1 Tuff of Kilgore and Huckleberry Ridge Tuff near Ririe Reservoir, Idaho. Park at intersection of Meadow Creek and Mud Springs Roads, and walk downhill along Meadow Creek Road. Here a stratigraphic section including ignimbrites and fallout erupted from the Heise volcanic field then capped by HRT is nicely exposed in a roadcut. *Watch out for rattlesnakes*. The Heise volcanic field is significant for understanding Yellowstone magmatism because it is the youngest complex that has completely endured the compositional, isotopic, and volcanic evolution associated with the development of a nested caldera cluster along the Yellowstone Hot Spot, including the generation of voluminous low $\delta^{18}O$ rhyolite at the end of its lifespan (figs. 1, 2). Four Miocene–Pliocene caldera-forming eruptions occurred at the Heise center since ~6.7 Ma, resulting in a ~10,000 square kilometer (km^2) area of nested calderas, although much of the volcanic center is now buried by sediments and Pleistocene–Holocene basalts of the SRP (Morgan and McIntosh, 2005). The youngest Heise units, sampled by drill cores, are dated at ~3.9 Ma (Watts and others, 2011; Ellis and others, 2017a).

The volcanic sequence includes pyroclastic units from the Heise and Yellowstone Plateau centers (Morgan and others, 2008; Watts and others, 2011). At the base of the sequence is the gray-colored tuff of Wolverine Creek containing glassy pyroclasts of obsidian and pumice. Sanidines from the tuff of Wolverine Creek have yielded $^{40}Ar/^{39}Ar$ dates of 5.72±0.03 Ma (Anders and others, 2014) and 5.59±0.05 Ma (Morgan and McIntosh, 2005). The latter date recalculates to 5.67 Ma if the calibration factors of the former are used (Anders and others, 2014). $^{206}Pb/^{238}U$ dating of zircons yields a slightly younger date of 5.5941±0.0097 Ma (Szymanowski and others, 2016). The sense of this discordance is reversed from what would be expected for eruption quench ages (Ar/Ar) and pre-eruptive crystallization (U-Pb) ages. The reason for this difference is unclear, but may reflect imperfect intercalibration of the Ar/Ar and U/Pb geochronometers (Renne and others, 2010) or problems related to crystal recycling and (or) excess argon, which could result in Ar/Ar dates that are too old (Ellis and others, 2017b). The tuff of Wolverine Creek is noteworthy because it contains a subpopulation of zoned low-Mg# (~60–90) clinopyroxenes that contain melt inclusions with intermediate, 57–67 weight percent SiO_2, compositions (Szymanowski and others, 2015). These intermediate composition melt inclusions appear to record the compositional signature of fractional crystallization that is partly responsible for the evolved compositions of Yellowstone Hot Spot-related rhyolites (Szymanowski and others, 2015).

Figure 8. Photograph showing roadcut exposures along Meadow Creek Road near Ririe Reservoir, Idaho. Section includes the gray-colored and obsidian-rich tuff of Wolverine Creek (WCT), which is unconformably overlain by a pre-Kilgore sequence (PKS), composed of gravels, paleosols, reworked pyroclastic material and bedded fallout. This sequence is overlain by the dark vitrophyric tuff of Kilgore (KT). The entire exposed sequence is capped by Huckleberry Ridge Tuff (HRT).

The pre-Kilgore sequence, an approximately 11-meter (m) package of gravels, paleosols, and sandy tuffaceous sediments unconformably overlies the tuff of Wolverine Creek ignimbrite (fig. 8). Gravel and resedimented volcanic clasts locally occupy channels that crosscut and scour the ignimbrite. This sequence of sediments includes a primary fallout bed about 1.1 m above the tuff of Wolverine Creek (Watts and others, 2011). Zircons from this fallout bed yield a $^{206}Pb/^{238}U$ date of 4.8896±0.0066 Ma (Wotzlaw and others, 2014). The top of the package is capped by a coarse lithic breccia, which contains abundant sandstone clasts (Watts and others, 2011).

Dark-colored tuff of Kilgore, an approximately 4-m-thick resistant unit of crystal-poor densely welded tuff, directly overlies the pre-Kilgore package of sediments (fig. 8; Watts and others, 2011). The lower ~1 m of the tuff is somewhat less welded and less dark than its overlying portion. Lithic fragments of sandstone and volcanic rock are scattered through the tuff (Watts and others, 2011). The tuff of Kilgore was the youngest of the large explosive eruptions from Heise volcanic center, it covered an area of at least 20,000 km^2 across Idaho, Montana, and Wyoming (Morgan and McIntosh, 2005), and has yielded a $^{40}Ar/^{39}Ar$ sanidine date of 4.510±0.047 Ma (Wotzlaw and others, 2014). At least 1,100 km^3 (Anders and others, 2014) and possibly as much as 4,000 km^3 of low $\delta^{18}O$ rhyolite ($\delta^{18}O$ = +3.4‰) was released during the Kilgore eruption (Bindeman and others, 2007; Watts and others, 2011). This volume is comparable to the largest supereruptions from the Yellowstone Plateau. Similar to many other Yellowstone Hot Spot-related rhyolites, the tuff of Kilgore has low crystal concentrations and yields relatively high magmatic temperatures. The tuff of Kilgore contains 1–10 percent phenocrysts of plagioclase, sanidine, clinopyroxene, and orthopyroxene, along with iron-titanium oxides that yield eruption temperature estimates of ~860 °C (Watts and others, 2011). Kilgore zircons yield a limited range of $^{206}Pb/^{238}U$ dates, which are indistinguishable from the apparent eruption age from $^{40}Ar/^{39}Ar$ dating (fig. 9A). The Kilgore zircons show a range of $\delta^{18}O$ values (fig. 9B,C) with most between –1 to +3‰ (within and between individual crystals), indicating that the Kilgore rhyolite is a low $\delta^{18}O$ magma derived by near-eruption assembly of isotopically distinct batches of magma, which were at least partly derived from remelting of shallow hydrothermally altered subcaldera rocks (Watts and others, 2011; Wotzlaw and others, 2014). These isotopic data constrain the magma generation and assembly timescale to within the uncertainties of the geochronology, over a timescale of 1–10 k.y. (Wotzlaw and others, 2014). Heise center rhyolites show decreasing $\delta^{18}O$ values over time, which resembles the isotopic evolution of Yellowstone Plateau rhyolites, and indicates a shallow hydrothermal rather than a deeper crustal or mantle

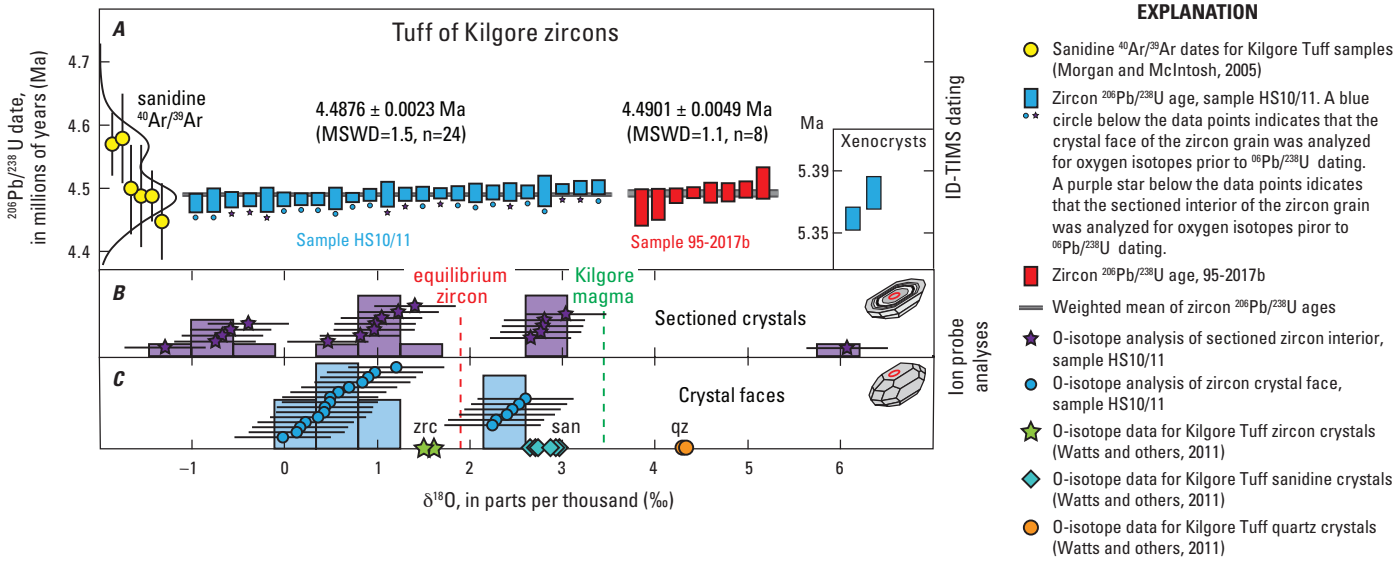

Figure 9. Chart showing Pb/U dates and oxygen isotope compositions of zircon crystals from the tuff of Kilgore. *A*, High precision $^{206}Pb/^{238}U$ dates for single zircons determined by isotope dilution thermal ionization mass spectrometry (ID-TIMS) for two samples (blue and red rectangles) from geographically separated localities of the tuff of Kilgore. The length of the data rectangles represents 2 sigma uncertainties. Sanidine $^{40}Ar/^{39}Ar$ dates (yellow circles) are from Morgan and McIntosh (2005) but recalculated by Wotzlaw and others (2014). *B*, Oxygen isotope compositions for sectioned zircon crystals and *C*, the faces of nonsectioned crystals both measured by ion microprobe. The correspondence of the $^{206}Pb/^{238}U$ dates to the ion probe analyses of sectioned or crystal faces is shown by stars or circles beneath each number-ranked date in *A*. For reference, the equilibrium values of Kilgore melt and zircon in $^{18}O/^{16}O$ equilibrium with quartz (orange circles) and sanidine (blue diamonds) are shown by dashed lines. The $\delta^{18}O$ values of bulk zircons are shown for reference (green stars). MSWD, mean square of weighted deviates; n, number of dated crystals. Figure modified from Wotzlaw and others (2014).

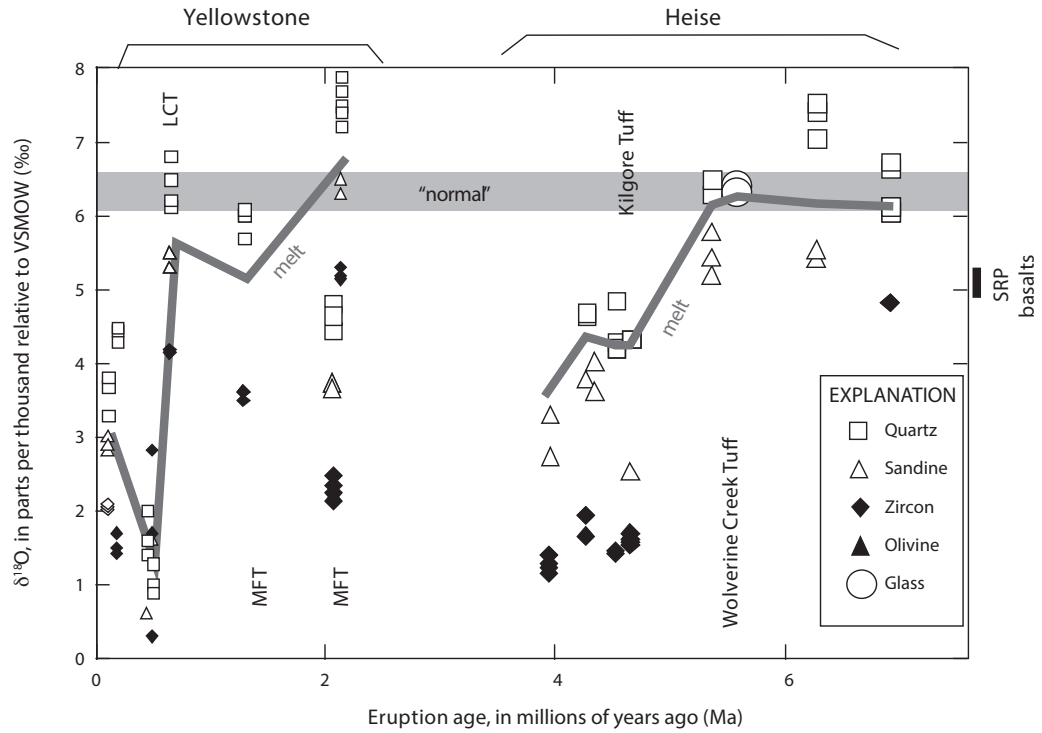

Figure 10. Graph showing temporal variation of oxygen isotope compositions for volcanic rocks from the Yellowstone Plateau and Heise eruptive centers. Calculated melt compositions are shown by the gray lines. LCT, Lava Creek Tuff; MFT, Mesa Falls Tuff; HRT, Huckleberry Ridge Tuff; SRP, Snake River Plain; VSMOW, Vienna Standard Mean Ocean Water. Figure modified from Bindeman and others (2007).

source for the low $\delta^{18}O$ values (fig. 10, Bindeman and others, 2007). Bindeman and others (2007) noted that magmatic $\delta^{18}O$ values for Heise and Yellowstone Plateau rhyolites appear to be positively correlated with eruptive volume, suggesting that rhyolites formed by larger degrees of shallow crustal remelting have a larger contribution of source material that is relatively unaffected by hydrothermal alteration and low $\delta^{18}O$ values. However, the time integrated effects of remelting, mixing, and hydrothermal alteration in the subcaldera system result in an inverse relation of ~1‰ decrease for every ~1,000 km^3 of cumulative erupted rhyolite (Watts and others, 2011).

HRT ignimbrite overlies the dark-colored tuff of Kilgore (figs. 8, 11), with an ~0.5 m bed of calcrete paleosol separating the two tuff units (Watts and others, 2011). At more than 2,500 km^3, the HRT is the largest of the Quaternary ignimbrites erupted from Yellowstone Plateau and covers an area of more than 15,000 km^2 (fig. 12, Christiansen, 1982, 2001). The HRT is divided into three informal members; A, B, and C (Christiansen and Blank, 1972). Based on isopach thicknesses, these informal members appear to have vented from different parts of the Yellowstone Plateau (figs. 12, 13). The HRT exposed here is from member B (Christiansen, 2001), and shows a vertical change in color from tan to pink related to degree of devitrification (fig. 6). The HRT rhyolite contains phenocrysts of sanidine, quartz, plagioclase, hedenbergitic clinopyroxene, fayalite, magnetite, and accessory zircon and chevkinite (Hildreth, 1981; Christiansen, 2001). Abundant lithic fragments occur in the HRT ignimbrite at this location (Watts and others, 2011).

Recent $^{40}Ar/^{39}Ar$ dating studies using single sanidines from HRT member B by Singer and others (2014) and Rivera and others (2014) have derived similar ages for the Huckleberry Ridge eruption of 2.077±0.003 Ma and 2.079±0.005 Ma, respectively, (figs. 14, 15). Ellis and others (2012) determined indistinguishable $^{40}Ar/^{39}Ar$ dates for HRT members A and B, but determined that member C sanidines may have erupted at least 6 k.y. later from a different magma body. However, high precision $^{206}Pb/^{238}U$ dating of zircons from HRT members A, B, and C has yielded indistinguishable dates (fig. 15), suggesting that the three members indeed reflect a single eruption at 2.08 Ma (Wotzlaw and others, 2015). $^{40}Ar/^{39}Ar$ dating studies using single crystals (Gansecki and others, 1998; Ellis and others, 2012; Singer and others, 2014; Rivera and others, 2014) have revealed the pervasive presence of sanidines that yield "old" dates, owing to excess argon derived from melt inclusions, near-eruption recycling of antecrystic sanidines that did not have sufficient time to re-equilibrate and release their radiogenic argon, or both. This characteristic has been noted in other Yellowstone rhyolites (Stelten and others, 2015; Matthews and others, 2015; Troch and others, 2017). The $^{206}Pb/^{238}U$ datasets (fig. 15) have been interpreted to indicate that the majority of HRT zircons crystallized within 1–10 k.y. of the eruption age (Rivera and others, 2014b; Wotzlaw and others, 2015); similar crystallization duration has been

Figure 11. Photograph showing Huckleberry Ridge Tuff exposed along Meadow Creek Road, showing a change in color and character of parting. From Morgan and Bonnichsen, (1989).

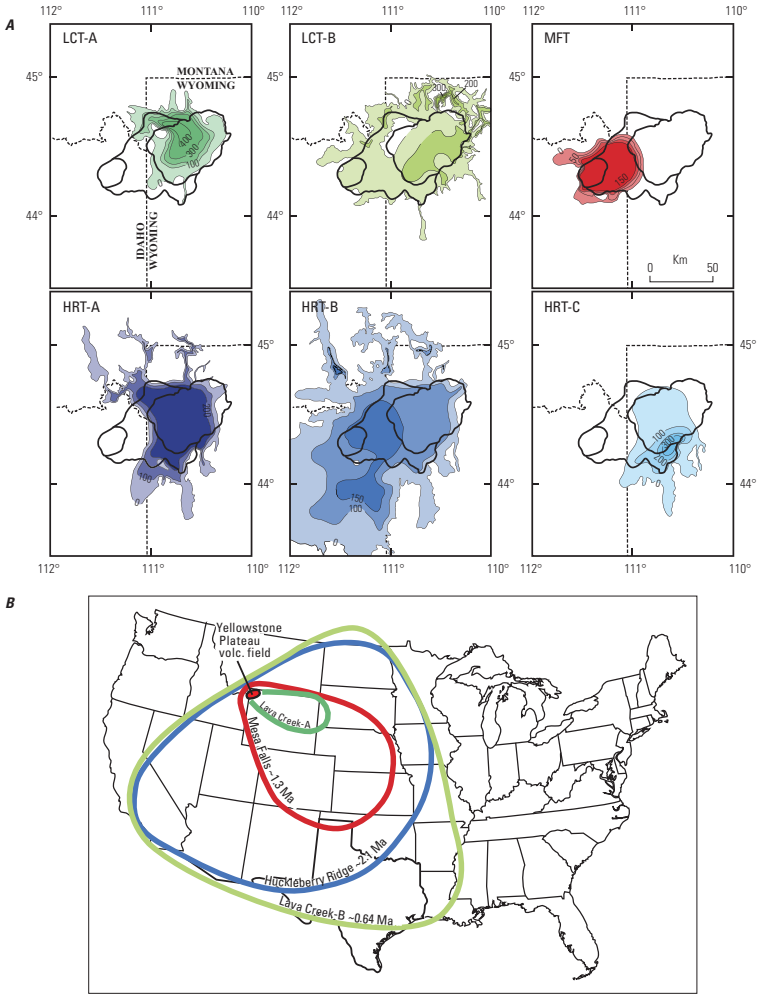

Figure 12. Maps of (*A*) Huckleberry Ridge Tuff (HRT), Mesa Falls Tuff (MFT), and Lava Creek Tuff (LCT) members occurrences on and around the Yellowstone Plateau; and (*B*) tephra distributions around the continental United States. (*A*) modified from Wotzlaw and others (2015), and (*B*) from Christiansen and others (2007).

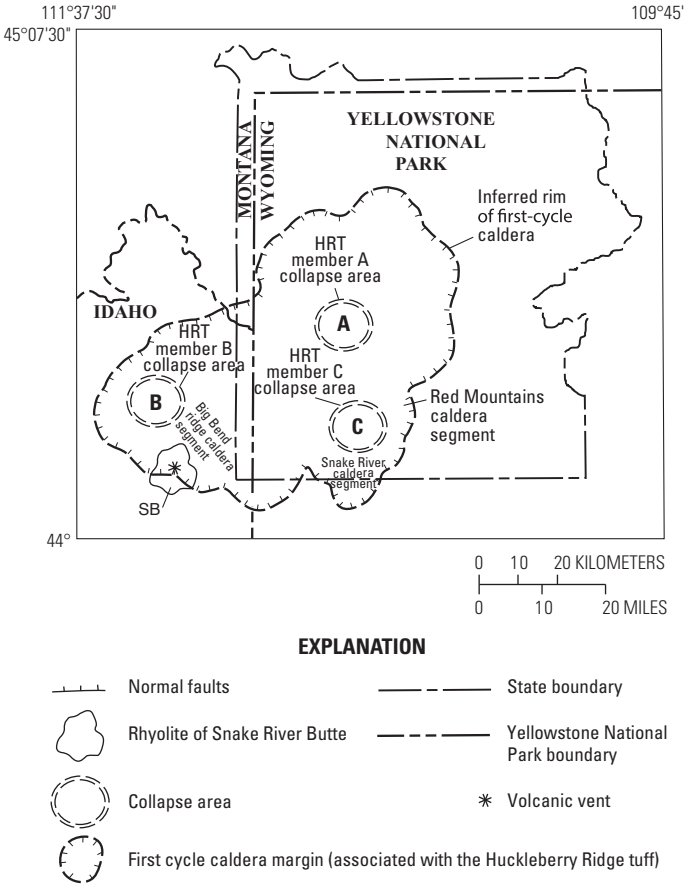

Figure 13. Map showing locations of vent areas for the members of the Huckleberry Ridge Tuff (HRT) relative to the first cycle caldera margins. The vent and distribution of the pre-HRT Snake River Butte (SB) is also shown. From Christiansen and others (2001).

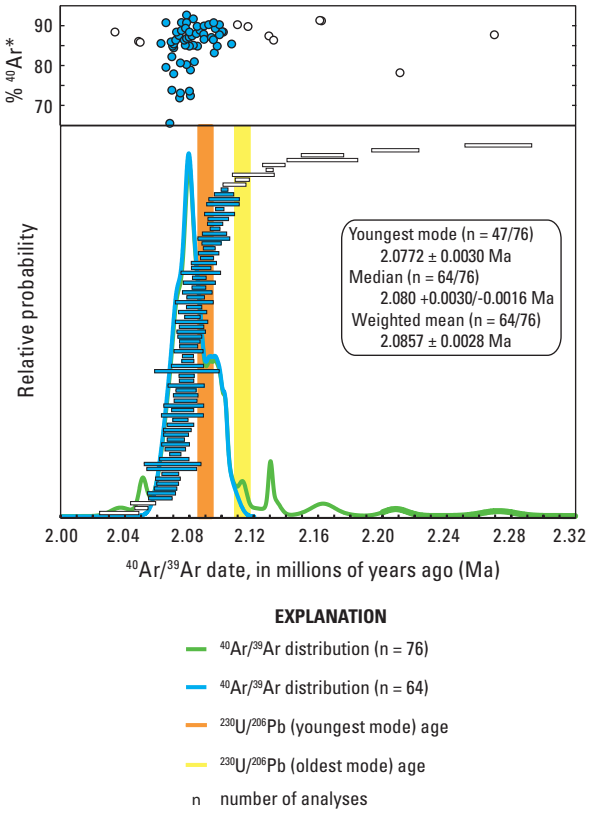

Figure 14. *A*, High precision $^{40}Ar/^{39}Ar$ dates for single sanidines and isotope dilution thermal ionization mass spectrometry (ID-TIMS) $^{206}Pb/^{238}U$ dates for single zircons from the Huckleberry Ridge Tuff (Rivera and others, 2014). Ranked single crystal dates (blue and white bars) along with their corresponding contents of radiogenic argon showing a multi-modal distribution of dates (green curve) that is also observed in other Yellowstone rhyolites (Gansecki and others, 1996; Stelten and others, 2015. The older outliers (white bars) are likely to represent recycled sanidine antecrysts (Rivera and others, 2014) or analyses biased by excess argon (Singer and others, 2014). A young population of sanidine dates (blue bars) yield a distribution (blue curve) suggesting an eruption age of 2.08 Ma. *B*, The apparent eruption age from the $^{40}Ar/^{39}Ar$ dating is approximately 30–40,000 years younger than the youngest mode of $^{206}Pb/^{238}U$ dates derived for associated zircons (Rivera and others, 2014). The dates for the HRT have been used to refine the early Pleistocene geomagnetic timescale.

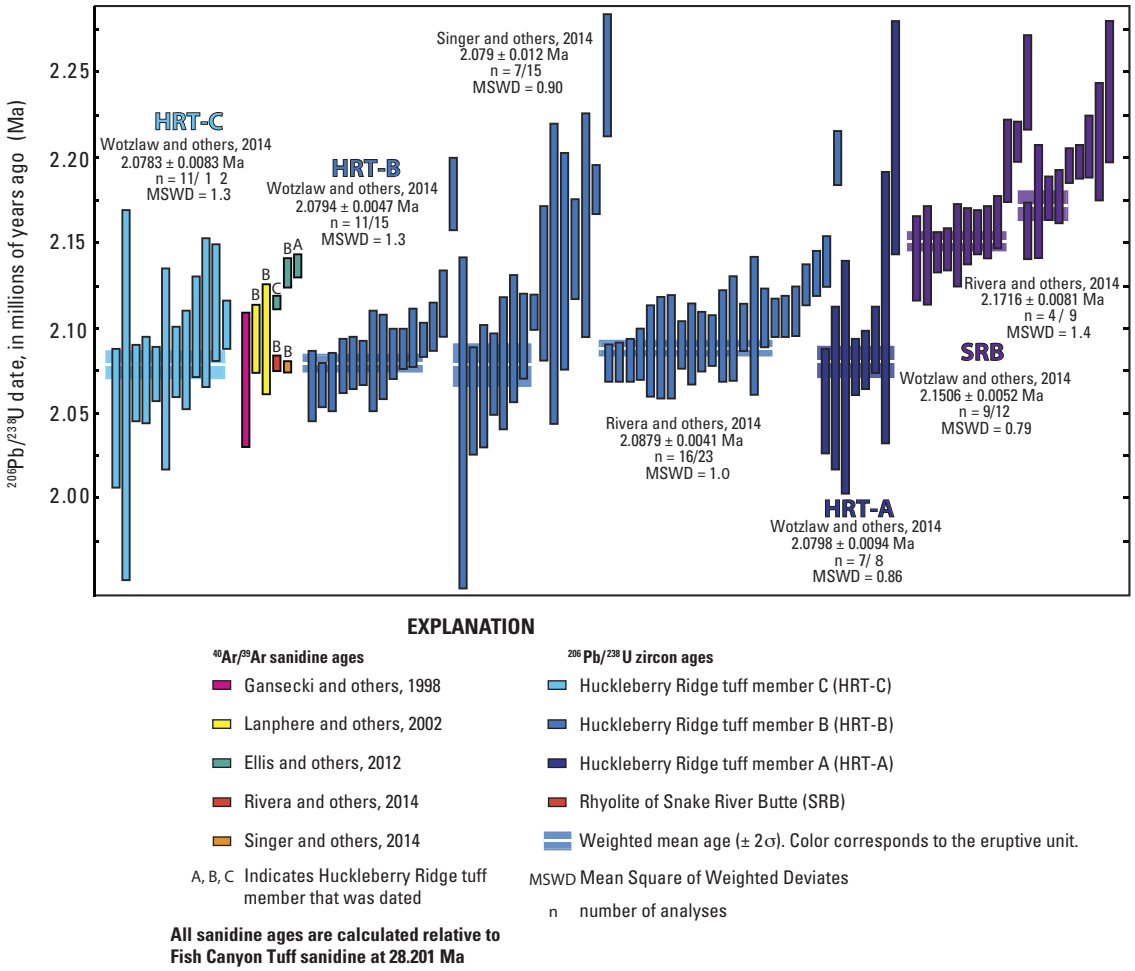

Figure 15. Chart of isotope dilution thermal ionization mass spectrometry (ID-TIMS) $^{206}Pb/^{238}U$ dates for zircons from Huckleberry Ridge Tuff (HRT), including members A, B, and C, and the pre-HRT rhyolite of Snake River Butte (SRB). For comparison, sanidine $^{40}Ar/^{39}Ar$ dates for the different members are plotted. Modified from Wotzlaw and others (2015).

determined for LCT zircons (Matthews and others, 2015; Wotzlaw and others, 2015).

Like the older rhyolites of the Yellowstone Hot Spot (Nash and others, 2006) the radiogenic (lead-strontium-neodymium) isotope compositions of HRT whole rocks (Hildreth and others, 1991) and the hafnium-isotope compositions of HRT zircons (Wotzlaw and others, 2015) indicate ~15–50 percent addition of melted Archean basement to mantle-derived magma (McCurry and Rodgers, 2009; Wotzlaw and others, 2015). Zircons from the HRT members fall into two hafnium-isotope populations (fig. 16), with epsilon hafnium (ε_{Hf}) values of approximately -22 (members A, C) and -6 (members A, B). Member A zircons with similar crystallization ages but different hafnium isotope compositions indicate the mixing of at least two isotopically diverse reservoirs of rhyolite (Wotzlaw and others, 2015). Intercrystal hafnium isotope variation within each of these two zircon populations (fig. 16) suggests the two rhyolite reservoirs were assembled from smaller and isotopically heterogeneous magma batches. The relatively normal and limited intercrystal and intracrystal variation $d^{18}O$ values (fig. 16) of HRT zircons suggest the mixing of Archean crust and mantle-derived melts occurred at a level too deep to assimilate much shallow and hydrothermally altered rock (Wotzlaw and others, 2015). Trace element zoning in HRT zircons appears to record 30–40 percent fractional crystallization over a temperature range of ~700–850 °C (Rivera and others, 2014b; Wotzlaw and others, 2015).

Return to Hwy 26 along Meadow Creek Road.

32.2 Turn left (north) onto Hwy 26.

33.7 Turn right (east) onto Hwy 26 Business.

34.7 Turn left (west) onto Idaho State Highway 48 in Ririe, and veer right.

35.1 Turn left onto East County Road.

43.2 Turn right (east) onto Hwy 20, and head east toward the towns of Rigby and Rexburg.

89.4 Stop 1.2 Mesa Falls Tuff along Hwy 20 between Ashton and Island Park. Pull off onto turnout on right side of Hwy 20. At this stop, the MFT is exposed in the roadcut along west side of Hwy 20. *Be very careful when viewing this outcrop. It is located on the side of a busy highway. Stay a safe*

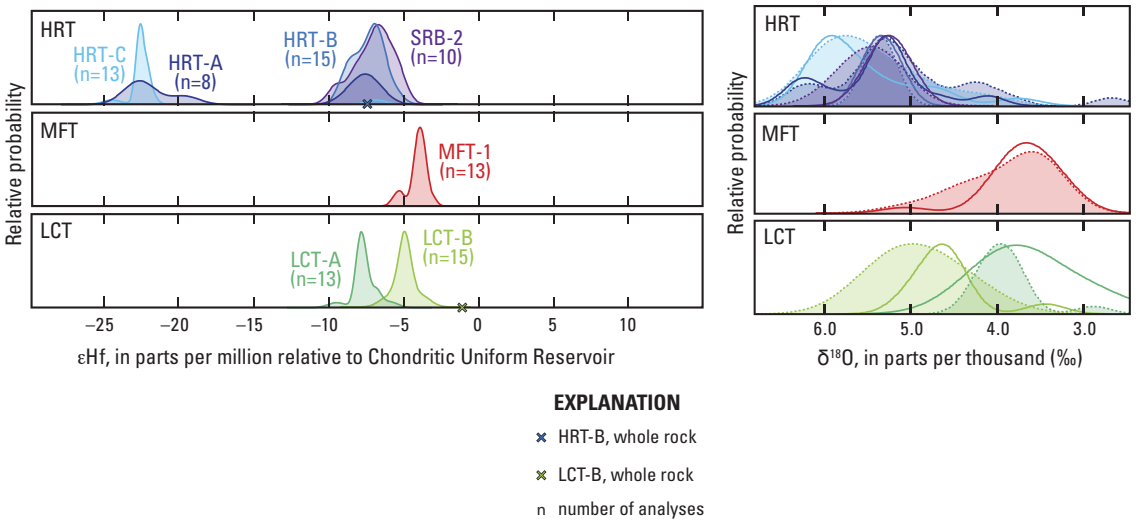

Figure 16. Graph showing distribution of Hf and O isotope compositions for single zircons from Huckleberry Ridge Tuff (HRT), Mesa Falls Tuff (MFT), and Lava Creek Tuff (LCT), and the pre-HRT Snake River Butte (SRB). The Hf isotopic compositions are reported in epsilon units, calculated as $[(^{176}Hf/^{177}Hf_{Sample})/^{176}Hf/^{177}Hf_{CHUR(0)}) -1]*10{,}000$, where $^{176}Hf/^{177}Hf_{CHUR(0)} = 0.282772$ (Vervoort and Blichert-Toft, 1991). CHUR = Chondritic Uniform Reservoir. For comparison, whole rock Hf isotope values for HRT and LCT are shown by crosses. Distributions of oxygen isotope compositions include values for cores of single zircons (dashed lines) and rims (solid lines). Modified from Wotzlaw and others (2015).

distance from the shoulder of the road and be careful if you decide to cross the highway.

The MFT is distributed over more than 2,700 km^2 primarily around the Island Park area. At Thurmon Ridge (fig. 17) to the northwest, and around Upper Mesa Falls to the southeast, the MFT is as much as ~150 m thick, but is commonly 30–70 m thick (Christiansen, 2001). Here, the MFT is on the inside of the caldera rim and directly overlies a thin bed of unconsolidated loess, which in turn overlies gray welded HRT (fig. 18). The basal 5–6 m of the MFT is composed of a white, planar-bedded, and well-sorted fallout deposit, which mantles the underlying paleotopography and reflects the early Plinian stage of the MFT eruption (Christiansen and Blank, 1972; Neace and others, 1986). The basal fallout contains as much as 70 percent crystals (Neace and others, 1986). In contrast, the pumice from the overlying portion of the MFT contains ~30 percent crystals (Neace and others, 1986). This relative enrichment in crystals within the basal fallout indicates loss of glass relative to crystals in the eruption column (Neace and others, 1986). The MFT contains the typical Yellowstone rhyolite mineral assemblage of sanidine, quartz, plagioclase, iron-rich clinopyroxene, magnetite, zircon, chevkinite, ilmenite, and fayalite, but also contains the hydrous minerals allanite and hornblende (Christiansen, 2001; Rivera and others, 2016). Sanidine and quartz phenocrysts in the Mesa Falls rhyolite are as large as several centimeters (cm) in size (Christiansen, 2001). Locally, pumice clasts in the Mesa Falls ignimbrite are as much as 30 cm in size, which is large relative to those in the other ignimbrites of the Yellowstone Plateau (Christiansen, 2001). The glass composition and mineralogy of the MFT fallout is distinct from either the HRT or LCT (Christiansen, 2001), this correlates the fallout to distal tephra, formerly called the Pearlette-S ash (Izett, 1981), which occurs in middle Pleistocene deposits of the southern Rocky Mountains and the Great Plains (fig. 12, Izett and Wilcox, 1982). The upper portion of the basal unit is coarser with more pumice and shows low-angle cross-bedding and channeling, which may reflect the passage of dilute pyroclastic currents, and in some places the passage of pyroclastic flows (Neace and others, 1986; Christiansen, 1982, 2001). Overlying the basal unit is a main ignimbrite body composed of pink-colored pyroclastic flow units (fig. 18), which are unwelded, show vapor-phase alteration, and contain pumice lapilli and blocks (Christiansen, 1982, 2001; Neace and others, 1986).

$^{40}Ar/^{39}Ar$ dating of MFT sanidines indicates an eruption age of 1.300±0.001 Ma (Rivera and others, 2016). $^{206}Pb/^{238}U$ dates for MFT zircons suggests this batch of caldera-forming rhyolite was generated, stored, and differentiated over an interval of, at most, several tens of thousands of years (Rivera and others, 2014b; 2016; Wotzlaw and others, 2015). The Hf isotope composition of MFT zircons is distinct from those associated with the older HRT and younger LCT. The low $\delta^{18}O$ composition of MFT minerals (+5.5 to +6.0‰ quartz, Hildreth and others, 1984) indicates remelting-assimilation of shallow hydrothermally altered crust, while the hafnium isotope composition of MFT zircons suggests a lower crustal source, which at times provided variable amounts of an Archean crustal component to ascending silicic melts (Wotzlaw and others, 2015). These observations are consistent with geochemical modeling indicating multistage generation of low $\delta^{18}O$ rhyolites from normal $\delta^{18}O$ crust (Watts and others, 2010).

Figure 17. Shaded relief map showing physiography of the Island Park region, defined by the semi-circular scarp of the Henrys Fork and Big Bend Ridge caldera segments.

Figure 18. Photographs showing (*A*) Present-day roadcut exposure of Huckleberry Ridge Tuff (HRT) and Mesa Falls Tuff (MFT) along U.S. Route 20 between Ashton and Island Park, Idaho; and (*B*) the same roadcut section as pictured in Hamilton (1965). Section is approximately 18 meters high. From bottom-to-top, the section is composed of 1, welded HRT: 2, unconsolidated loess that is now mostly covered by slope wash; 3 and 4, base of MFT composed of non-welded white and well-sorted crystal-rich ash fallout whose top contains abundant pumice lapilli; and 5, partly welded MFT ignimbrite.

Continue on Hwy 20.

92.7 Additional exposures of MFT in roadcuts along the east side of Hwy 20.

93.2 Pass Anderson Mill Canyon road.

106.6 Turn right (east) onto Mesa Falls Scenic Byway.

106.8 Stop 1.3 Island Park basin, and Big Bend and Henrys Fork caldera rims. Park in turnout on the north side of road. This stop provides an overview of the Island Park basin, with the margins of the Big Bend Ridge and Henrys Fork calderas visible to the west. The Island Park basin is located in the westernmost area of the Yellowstone Plateau volcanic field, and represents the transition from the rhyolite-dominated Yellowstone Plateau to the basalt-dominated SRP. The topography of the Island Park basin reflects the volcanic activity from the three different caldera cycles associated with the Yellowstone Plateau over the last 2.1 m.y. (figs. 17, 19). This stop is in the approximate vent location of HRT member B (fig. 13, Christiansen, 2001). The southwestern and western portions of the Island Park basin are bounded by Big Bend Ridge, which represents the margin of the caldera associated with eruption of the HRT. To the southeast, along the Big Bend Ridge, is the pre-HRT Snake River Butte. The northwestern portion of the basin is bounded by Thurmon Ridge, which represents the overlapping margins of the first cycle caldera associated with eruption of the HRT, and the Henrys Fork caldera associated with eruption of the MFT (Christiansen, 2001). The eastern portion of the basin is bounded by the flow margins of the thick rhyolitic lava flows associated with the third and youngest caldera cycle, which form the Madison Plateau. These rhyolite lavas represent pre-Lava Creek effusive activity as well as the post-collapse effusive volcanism that has filled Yellowstone caldera and compose the Plateau Rhyolite. In the southwest portion of the basin, the scarp is a composite of several structural faults. Originally envisioned as a single

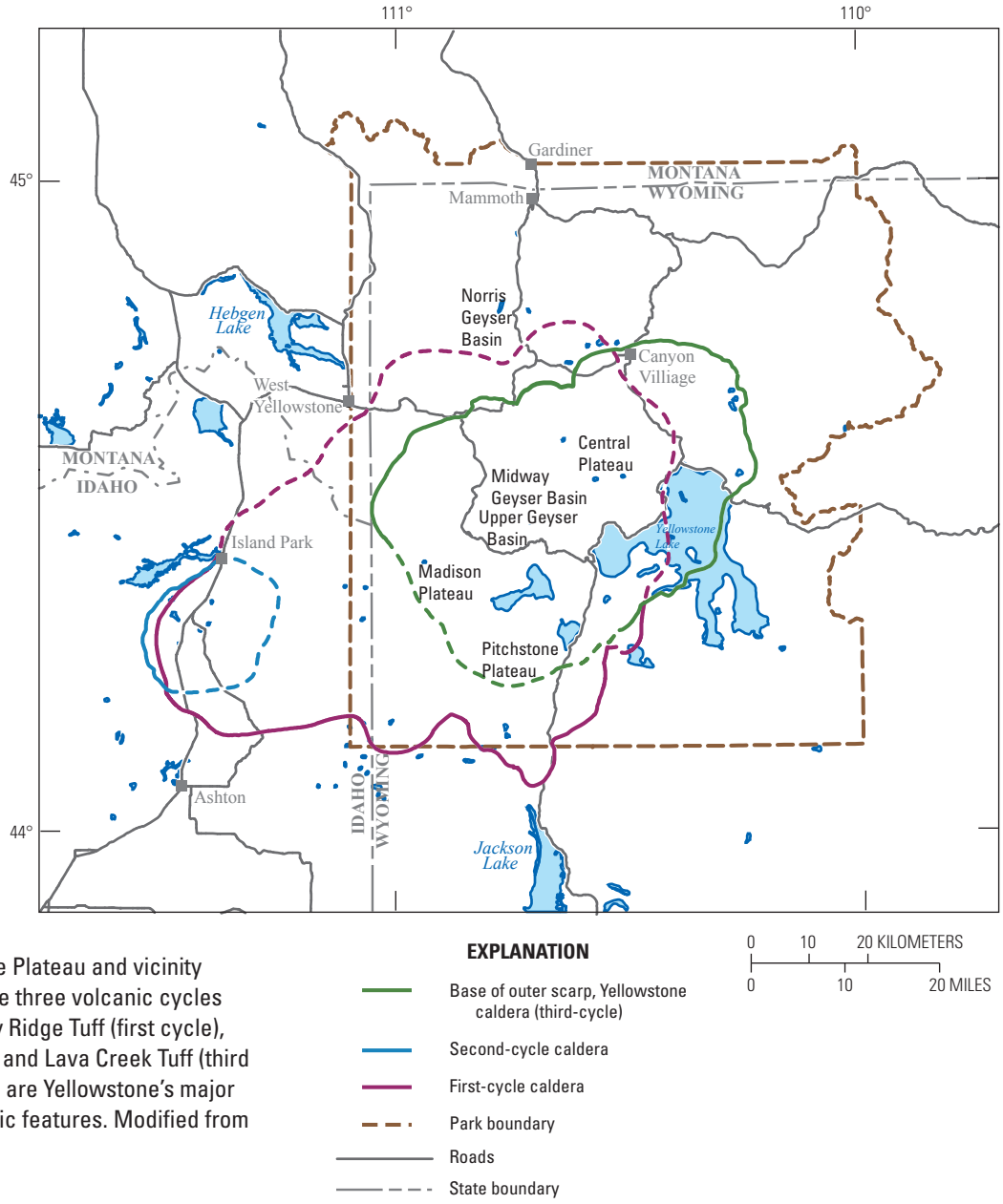

Figure 19. Map of Yellowstone Plateau and vicinity showing caldera outlines for the three volcanic cycles responsible for the Huckleberry Ridge Tuff (first cycle), Mesa Falls Tuff (second cycle), and Lava Creek Tuff (third cycle) ignimbrites. Also labeled are Yellowstone's major geyser basins and physiographic features. Modified from Christiansen and others (2007).

caldera by Hamilton (1965), later detailed field mapping and stratigraphy by R.L. Christiansen revealed that the circular basin resulted from the processes associated with the other caldera cycles.

The volcanic products associated with the second caldera cycle are primarily exposed in the Island Park area, and they have been key to understanding the progressive magmatic evolution responsible for the bigger first and third caldera cycles, as well as the transition from voluminous rhyolite magmatism to the basaltic magmatism characterizing the SRP. The second cycle rocks record the generation and caldera-forming eruption of the MFT rhyolite followed by cessation of the rhyolitic magma chamber and postcollapse effusion of the rhyolitic domes composing the Island Park Rhyolite (Christiansen, 1982, 2001). During this rhyolitic volcanism, basalt vented outside of the main focus of rhyolitic activity, suggesting a persistent locus of shallow silicic magma generation (Christiansen, 2001). The eruption of pre-Lava Creek basalts within Island Park signaled the final cooling and solidification of the second cycle subvolcanic reservoir to the point that basaltic magmas could begin erupting. As a result, this portion of the Yellowstone Plateau has subsided and been partly buried by lavas from the eastern SRP, thus capturing the transition from rhyolitic to basaltic dominated volcanism.

Return to Hwy 20 and turn left (south) toward Harriman State Park.

108.0 Turn right (west) onto Green Canyon Road (Forest Road 167).

108.5 Pass entrance to Harriman State Park.

110.4 Turn left (south) onto unmarked gravel road.

110.6 Stop 1.4 Pleistocene lava flow of the caldera-filling Gerrit Basalt. Park at former quarry with outcrops of basalt. Walk approximately 100 m to the west to reach rubbly exposures of basalt. At this location, the rubbly flow top and tumuli of the 29±9 ka (George and others, 2015) Pinehaven basalt are exposed (fig. 20). Much of the Island Park basin and floor of Henrys Fork caldera have been covered by basaltic lava flows; in the western portion of the basin these basalts include tholeiites associated with the SRP. The Pinehaven basalt is one of the flows of the Gerrit Basalt that have yielded K-Ar and $^{40}Ar/^{39}Ar$ dates between ~450 ka (Christiansen, 2001) and ~30 ka (George and others, 2015). The Gerrit basalts cover much of the Island Park area and overlie the MFT and domes of the Island Park Rhyolite. Flows from the Gerrit Basalt have yielded elevated $^{3}He/^{4}He$ signatures of ~16 times the ratio in air (R_a), suggesting a deep mantle source for Yellowstone basalts (Abedini and others, 2006; Graham and others, 2009). Eruption of basaltic magma in the caldera floor has been attributed to final cooling and solidification of the shallow silicic magma reservoir that otherwise impedes the ascent and eruption of basalt during the earlier stages of the caldera cycle (Smith, 1979; Christiansen, 1984, 2001).

Return to Green Canyon Road, turn right (east) and return to Hwy 20.

113.1 Intersection of Green Canyon Road and Hwy 20. Turn left (north) onto Hwy 20. Continue along Hwy 20 toward the town of West Yellowstone, Montana.

141.4 Exposures of HRT in roadcuts along Hwy 20 over Targhee Pass.

151.6 Turn right (south) onto U.S. Highway 191 (North Canyon Street) through downtown West Yellowstone.

151.9 Turn left (east) onto Yellowstone Avenue, and proceed toward west entrance to Yellowstone National Park.

152.4 Entrance to Yellowstone National Park.

164.4 Stop 1.5 Yellowstone caldera rim and pre-caldera lavas near Harlequin Lake. Turn into large pullout on the right

Figure 20. Photograph of rubbly tumulus on a lava flow of Gerrit Basalt exposed on the western portion of Island Park.

(south) side of road. The west entrance road to Yellowstone National Park and the Madison River follow the margins of Yellowstone caldera, the (now) lava-filled 45 × 85 km caldera that formed as a result of the LCT eruption (Christiansen, 2001). To the north (fig. 21), LCT member A is exposed in the dramatic cliff, which is the topographic edge of Yellowstone caldera. The cliffs to the south across the Madison River are 300 m high and are the eroded flow edge of the post-LCT West Yellowstone flow, one of the voluminous lavas (~41 km^3) of the Plateau Rhyolite that filled Yellowstone caldera (Christiansen and others, 2007). The LCT overlies the pre-caldera Harlequin Lake and Mount Haynes flows of the Mount Jackson Rhyolite (Christiansen and Blank, 1972), which are exposed across the road in the low hills at the base of the caldera rim (fig. 21). Based on their distribution around the caldera and apparent proximity to their vents, the Mount Jackson flows appear to have erupted along the zone that subsequently became the ring-fracture zone of Yellowstone caldera (Christiansen, 2001). The Harlequin Lake flow yields a sanidine $^{40}Ar/^{39}Ar$ date of 830.0±7.4 ka and the Mount Haynes flow yields a date by the same technique of 701.6±1.6 ka (Troch and others, 2017). Hence, the Mount Haynes flow erupted ~70 k.y. before the LCT. Christiansen and Blank (1972) note that the upper glassy portions of the Mount Jackson Rhyolite flows are well preserved in contact with the overlying LCT, suggesting little erosion and in turn a geologically brief time before the Lava Creek eruption. Aside from their apparent eruption ages, these precaldera flows significantly differ in their pyroxene assemblages, with the Mount Haynes rhyolite containing a clinopyroxene to orthopyroxene ratio of 9:1, and the Harlequin Lake rhyolite containing only orthopyroxene (Troch and others, 2017). The oxygen isotope compositions of Harlequin Lake flow quartz and sanidines are somewhat lower than for the Mount Haynes flow, but elevated relative to second cycle rhyolites (Troch and others, 2017). The average oxygen isotope compositions of Mount Haynes quartz indicate equilibrium melt in the range of normal (+5.8–6.3‰) rhyolitic melts, with values resembling those for the LCT, and elevated relative to second cycle and older Mount Jackson Rhyolite flows (Hildreth and others, 1984; Bindeman and Valley, 2001; Troch and others, 2017). Sanidines from the Harlequin Lake flow have lead isotope compositions resembling those from the MFT and other second cycle rhyolites, whereas the Mount Haynes flow sanidines more closely resemble the LCT (Troch and others, 2017), which together with the oxygen isotopes suggest that these flows mark a transition in the petrology characterizing the second and third cycles.

From here, continue east on West Entrance Road.

165.9 Madison Junction. Turn left onto Grand Loop Road and continue east.

167.4 Stop 1.6 Lava Creek Tuff Member A at Tuff Cliff. Turn left into parking lot for Tuff Cliff picnic ground. At this stop, member A of the LCT (LCT-A) is well exposed in the dramatic cliff that marks the margin of Yellowstone caldera (fig. 22). Member A represents the first portion of the LCT to be erupted (Christiansen, 2001), and is elsewhere overlain by member B (LCT-B). Abundant lapilli of phenocryst-bearing pumice are evident in the cliff outcrops and talus boulders, but are friable because the ignimbrite here has endured vapor-phase crystallization.

The LCT-A and LCT-B members each have eruptive volumes of ~500 km^3, but differ in their composition, mineralogy, vent regions, and regional distribution (Christiansen and Blank, 1972; Christiansen, 2001). Based on isopachs and phenocryst-lithic distributions, LCT-A vented from the western portion of the caldera, whereas LCT-B vented from

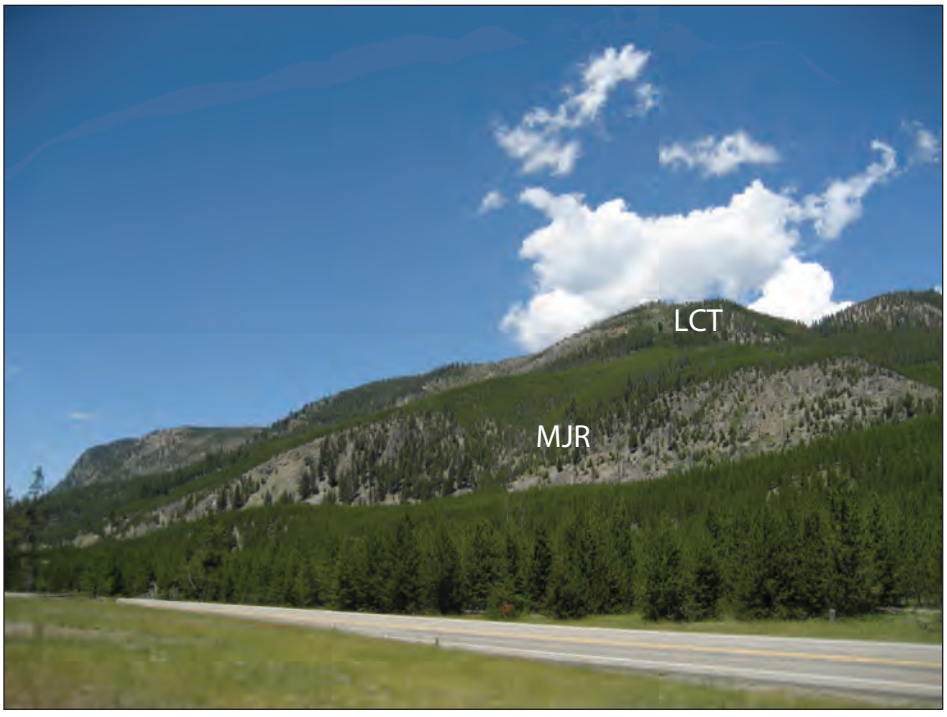

Figure 21. Photograph showing view north across U.S. Highway 20. Low hill and its exposed outcrop along the northwestern rim of Yellowstone caldera are composed of pre-Lava Creek Tuff flows of the Mount Jackson Rhyolite (MJR). The Mount Haynes and Harlequin Lake flows are exposed here. The peaks behind MJR are composed of Lava Creek Tuff (LCT) exposed along the caldera margin. Relief from road to top of MJR is about 200 meters, and about 450 meters to top of LCT cliff.

Figure 22. Photograph looking North from Tuff Cliff picnic area showing exposure of lower Lava Creek member A at Tuff Cliff. Relief from road to top of cliff in this view is about 180 meters.

the eastern portion (Christiansen, 2001). The two members have conformable contacts and form a compound cooling unit suggesting rapid emplacement (Christiansen, 2001). A principal difference between the two LCT members is the presence of hornblende (Christiansen and Blank, 1972), which is otherwise rare in Yellowstone rhyolites, as well as the light rare earth element-rich accessory mineral allanite, in LCT-A (Hildreth, 1981). In contrast, LCT-B lacks hornblende and allanite, and contains iron-rich clinopyroxene as its main mafic silicate phase (Hildreth, 1981). Eruptive temperature estimates for the LCT from iron-titanium oxides range from ~800–900 °C (Hildreth and others, 1984), although the rims of LCT zircons yield crystallization temperatures as low as ~740 °C (Matthews and others, 2015). Glass inclusions in Lava Creek quartz crystals contain H_2O concentrations of ~3.5 weight percent and CO_2 concentrations of 200–800 parts per million (ppm), corresponding to crystallization and melt entrapment pressures of 100–200 megapascals (MPa) if the melts were volatile-saturated (Gansecki, 1998). Distal tephra correlated with LCT-A ignimbrite occurs east of Yellowstone in areas of northern Wyoming, whereas tephra correlated with LCT-B ignimbrite occurs over a wide area of the western United States including locations in coastal California (Izett and Wilcox, 1982).

The $^{40}Ar/^{39}Ar$ dating of bulk LCT sanidine by Lanphere and others (2002) yielded a date of 639±2 ka, which becomes 655 ka when recalculated using up-to-date revisions for the ages of commonly used argon fluence monitors (Matthews and others, 2015). Recent $^{40}Ar/^{39}Ar$ dating of single LCT sanidines (Matthews and others, 2015; Jicha and others, 2016; Mark and others, 2017) suggests the Lanphere and others (2002) bulk sanidine date may have been skewed older by the unresolved presence of xenocrysts. Each of these recent studies identified a majority population of young sanidine (fig. 23) indicating an eruption age of 631.3±4.3 ka (Matthews and others, 2015), 630.9±2.7 ka (Jicha and others, 2016) or 627.0±1.7 ka (Mark and others, 2017), with their differences reflecting somewhat different calibration factors (Mark and others, 2017). The youngest $^{206}Pb/^{238}U$ dates for LCT zircons from high precision isotope-dilution thermal ionization mass spectrometry (ID-TIMS) (Wotzlaw and others, 2015) and high spatial resolution secondary ion mass spectrometry (SIMS; Matthews and others, 2015) analyses are consistent with the $^{40}Ar/^{39}Ar$ dating (fig. 24). The spread of intracrystal and intercrystal U-Pb crystallization ages suggests that the LCT magma was developed over an interval of 35 k.y. or less, perhaps a short as a few thousand years (fig. 24; Matthews and others, 2015; Wotzlaw and others, 2015). An eruption age of around 630 ka is supported by the stratigraphic position of distal LCT-B fallout within pluvial sediments of the western United States (Sarna-Wojcicki and others, 1984), as well as near-shore marine sediments (Dean and others, 2015) deposited at the Marine Isotope Stage 15-16 boundary. This boundary is dated to about 630 ka by astrochronology (Lisiecki and Raymo, 2005) and ^{230}Th dating of speleothems (Cheng and others, 2013).

Distal tephra that is correlated to member A covers a much smaller area than that correlated to member B (Izett and Wilcox, 1982), despite the comparable volumes of their ignimbrites (Christiansen, 2001). Distal LCT-B tephra blanketed much of the western United States (fig. 12), with ~2,400 km between the furthest correlated locations in southern Saskatchewan, Canada, and south central Texas (Izett and Wilcox, 1982; Sarna-Wojcicki and others, 1987). Early tephrochronologic studies referred to distal LCT-B tephra as the Pearlette O

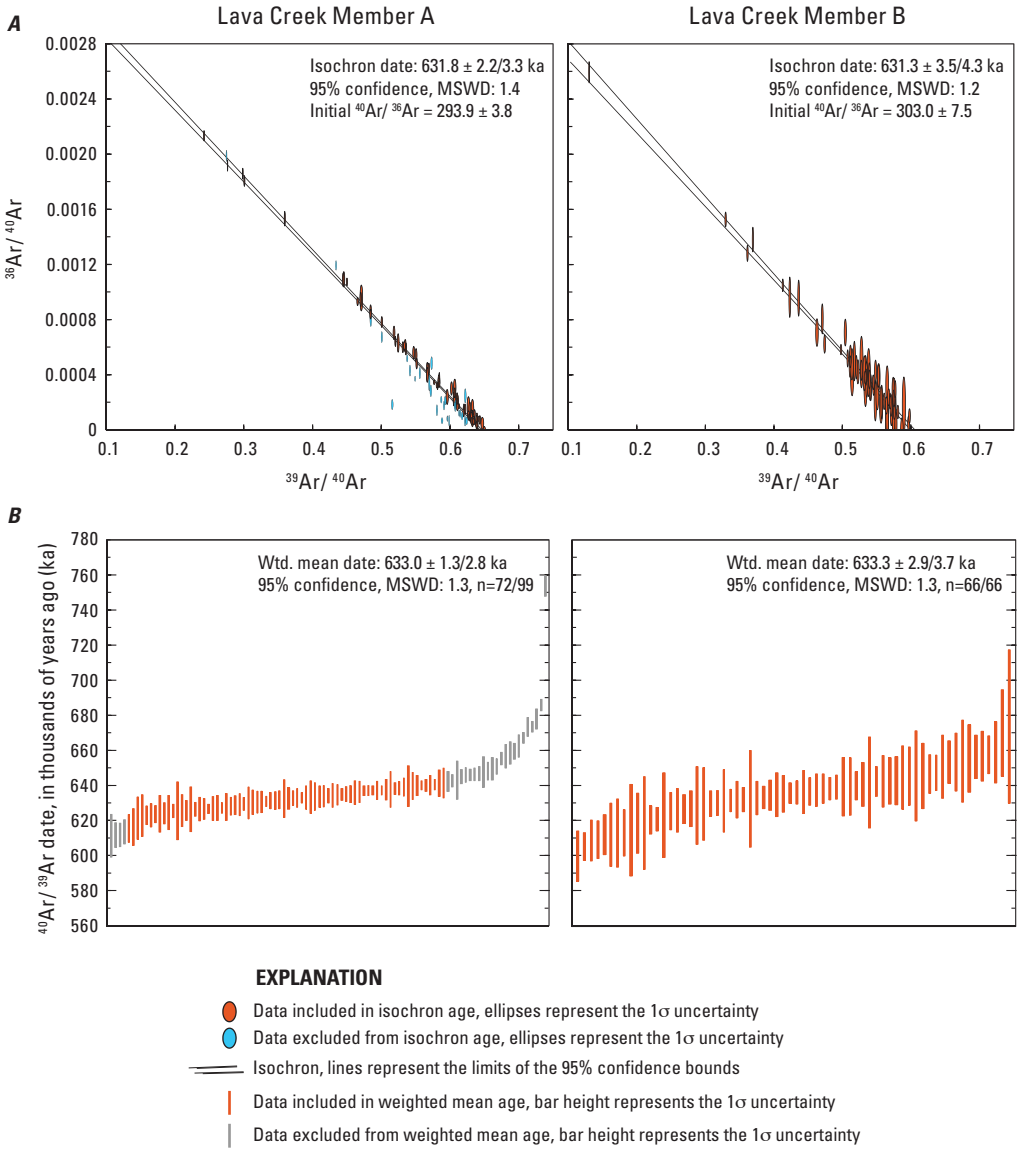

Figure 23. Graphs of *A*, Sanidine inverse isochron plot, and *B*, age-ranked single crystal $^{40}Ar/^{39}Ar$ dates for members A and B of Lava Creek Tuff from Matthews and others (2015). The somewhat high initial $^{40}Ar/^{36}Ar$ suggests the presence of excess argon and in turn an approximately 630 ka eruption age (Matthews and others, 2015). Single sanidine $^{40}Ar/^{39}Ar$ dating by Jicha and others (2016) and Mark and others (2017) confirms an approximately 630 ka eruption age.

(Izett and others, 1970; Naeser and others, 1973) and Wascana (Westgate and others, 1977) tephras of the United States and Canada. Distal LCT-B tephra occurs in numerous sedimentary sequences in the western United States (Izett, 1981; Izett and Wilcox, 1982) and has served as an important chronostratigraphic marker.

Turn left and continue eastward on Grand Loop Road.

170.7 Pass Gibbon Falls along the Gibbon River marking edge of Yellowstone caldera.

174.1 Pass Beryl Spring on the west side of road.

175.5 Pass entrance to Artist's Paint Pots hydrothermal area.

179.2 Turn right (east) onto Norris Canyon Road, and head east toward Canyon Village.

180.8 Turn right onto one-way Virginia Cascade Drive, which follows the Gibbon River.

181.8 Stop 1.7 Lava Creek Tuff along Gibbon River at Virginia Cascade. Park in turn off on the left side of Virginia Cascade Drive. *Watch for traffic along the narrow road*. Both LCT-A and -B are well exposed in the canyon at Virginia Cascade along the Gibbon River (fig. 25). Here, the two members form steep jointed outcrops above and below the road. The contact between the two members corresponds to a decrease in welding intensity and crystal content, as well as the presence of a 20–30 cm thick bed of well-sorted crystal

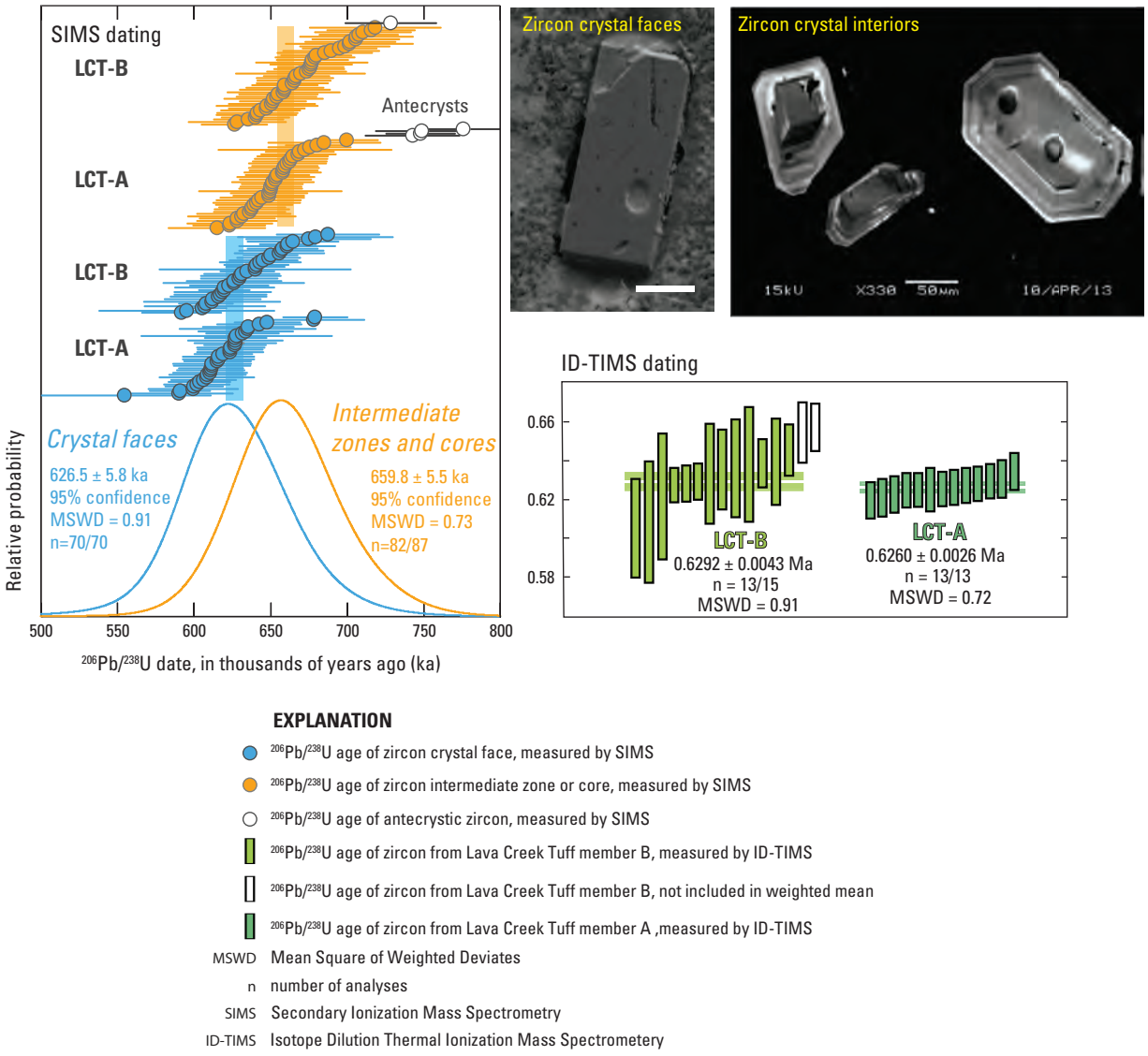

Figure 24. Secondary ion mass spectrometry (SIMS) $^{206}Pb/^{238}U$ dates for the crystal faces and interiors of single zircons from members A and B of Lava Creek Tuff (Matthews and others, 2015). The difference between dates for the crystal faces and interiors suggests crystallization over approximately 35 k.y., although reverse zoning of trace elements in many of the crystals suggests rejuvenation <10 k.y. before eruption (Matthews and others, 2015). High-precision isotope dilution thermal ionization mass spectrometry (ID-TIMS) Pb/U dates for single whole Lava Creek zircon crystals (Wotzlaw and others, 2015) is consistent with the SIMS dating of Matthews and others (2015) and provides precise constraints on the final crystallization of the Lava Creek magma.

ash fallout, which marks the base of LCT-B (Christiansen and Blank, 1972; Christiansen, 2001). The presence of this ash bed, together with the changes in welding and crystal content, has been interpreted by Christiansen (2001) to reflect a pause or change in the nature of the LCT eruption. At this location, the bedded ash is approximately at the road level but is poorly exposed because of slope wash (Christiansen, 2001). Good exposures of the bedded ash occur near Flagg Ranch, Wyoming (Matthews and others, 2015). The outcrops of LCT-B above the road are partly to moderately welded and devitrified with platy and vertical jointing (fig. 25). Phenocryst content increases upward through the member (Christensen, 2001).

LCT-A below the road forms large resistant joint columns of welded devitrified tuff, in some zones rich in lithophysae, and contains about 30 percent phenocrysts. This part of LCT-A is stratigraphically higher than the LCT-A observed at Stop 1.7 (Christiansen, 2001).

Zircons and sanidines from the LCT members at this and the last stop have compositions that correspond their position in the stratigraphy. Zircons from the earliest erupted portion of LCT-A have rims with the highest uranium concentrations, lowest crystallization temperatures, and least amount of core-to-rim zoning (fig. 26), whereas zircons from LCT-B including its basal bedded ash have a greater degree of zoning, rims with

Figure 25. Photograph showing outcrops of Lava Creek Tuff member B at Virginia Cascade in Yellowstone National Park. Contact with upper portion of member A is near the road level. Photograph from Matthews and others (2015).

lower uranium concentrations, and higher apparent crystallization temperatures (Matthews and others, 2015). Many of the LCT zircons contain cores with high uranium concentrations, as much as 5,000 ppm, which indicates crystallization from highly fractionated melts. These highly evolved cores are overgrown by mantles and rims that have less evolved compositions, suggesting maturation of the LCT magma body occurred along on an up-temperature path (Matthews and others, 2015). Sanidine crystals from the lower part of LCT-A and upper portion of LCT-B are relatively unzoned in cathodoluminescence (CL) images, whereas those in the upper part of LCT-A and basal bedded ash of LCT-B have bright-CL rims with high barium concentrations, which suggest crystallization after addition of less evolved silicic magma (Matthews and others, 2015).

The oxygen and hafnium isotope compositions of the cores and rims of LCT zircons are distinct between the two members (fig. 16), suggesting that two physically separated yet coeval bodies of rhyolite were tapped for eruption (Wotzlaw and others, 2015). The hafnium and oxygen isotope signatures suggest mixing of Archean crust, mantle-derived magma, and low $\delta^{18}O$ hydrothermally altered rocks from the shallow subvolcanic environment (Wotzlaw and others, 2015).

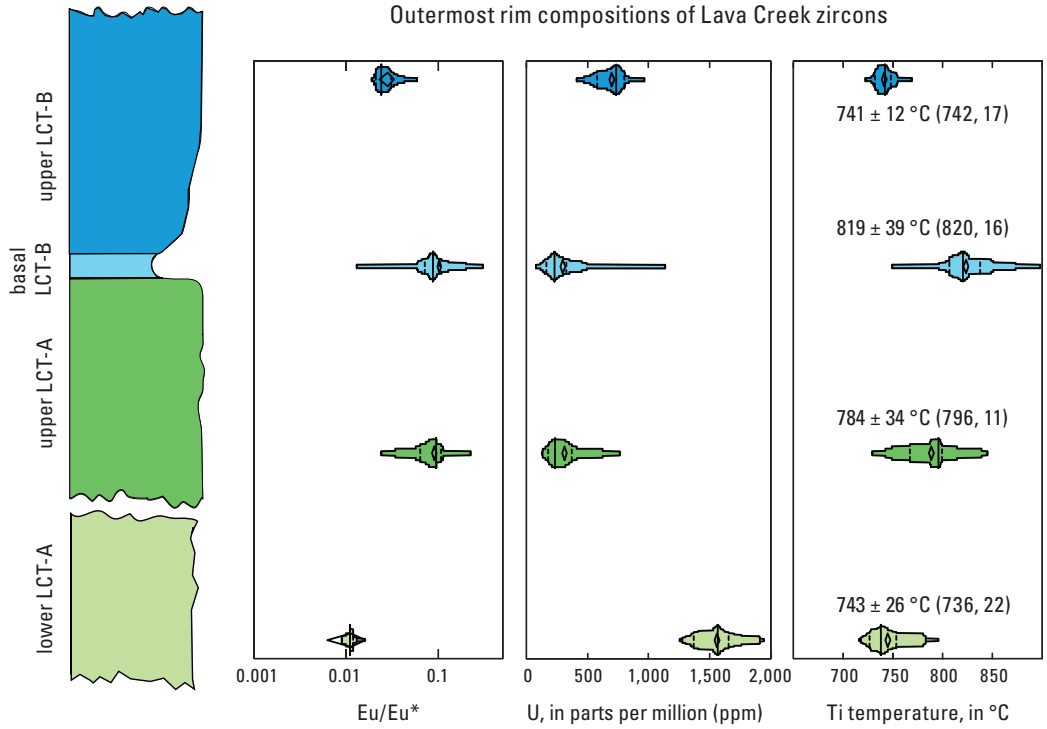

Figure 26. Chart showing concentrations of uranium, titanium-in-zircon temperatures, and magnitudes of europium anomalies recorded by the crystal faces (outermost rims), of zircons from different parts of the Lava Creek Tuff (LCT) stratigraphy. The europium anomaly is calculated as [EuCN/(SmCN0.5 * GdCN0.5)], where CN indicates the measured elemental concentrations have been normalized to chondritic values. Zircons from the lowermost portion of LCT member A (LCT-A) have the most evolved compositions (highest uranium, lowest Eu/Eu*), consistent with the compositions of LCT-A glass. Mean titanium-in-zircon temperatures and their standard deviation are noted, followed by median values and number of data. From Matthews and others (2015).

Continue driving along Virginia Cascade Drive and return to Norris Canyon Road.

182.8 Turn left onto Norris Canyon Road and return to West Yellowstone.

Day 2

Overview

The second day will focus on the Island Park area and its products of pre- and post-caldera volcanism of the first and second caldera cycles. See figure 27 for a geologic map and the locations of the field stops. Stops will include the oldest rhyolite (Snake River Butte) associated with the first caldera cycle, pre- and post-MFT rhyolites (some of which are exceptionally rich in phenocrysts), basalts that have flooded the Island Park region, and finally post-HRT rhyolites, which are famous for their extreme oxygen-isotope compositions and provide important insights into the generation mechanisms of low $\delta^{18}O$ rhyolites.

Day 2 Road Log

0.0 Begin the day's trip in West Yellowstone, Montana, at the intersection of Hwy 20 (Targhee Pass Highway) and U.S. Hwy 191 (Gallatin Road). Reset trip odometer, proceed west on Hwy 20 toward Island Park, Idaho.

47.9 Turn left (east) onto Anderson Mill Road (Forest Road 164) and proceed east into Island Park basin.

49.3 Pass rounded outcrops of welded MFT.

50.4 Fork in road. Turn left (east) to remain on Anderson Mill Road.

51.3 Intersection with Sheep Spur 1 Road. Veer right to stay on Anderson Mill Road.

52.1 Continue through intersection.

52.8 Stop 2.1 Rhyolite of Snake River Butte and Big Bend Ridge caldera margin. Park near intersection. To the south, the wooded Snake River Butte and margin of the Big Bend Ridge caldera are exposed. Snake River Butte (SRB) is a crystal-rich pre-HRT rhyolite lava dome that erupted from the southern portion of the Island Park area (figs. 27, 28), possibly along an incipient ring-fracture zone. It is the oldest recognized product of silicic volcanism on the Yellowstone Plateau (Christiansen, 2001). The caldera-forming eruption of the HRT and associated caldera collapse truncated the SRB flow, resulting in a cross-section exposure along the Big Bend Ridge (Hamilton, 1965; Christiansen, 1982, 2001). Sanidine from the SRB dated by Obradovich (1992) yielded a K-Ar date of 1.99±0.02 Ma, but the SRB rhyolite can be observed to underlie the HRT (Christiansen, 1982, 2001). Zircons from the SRB rhyolite yield $^{206}Pb/^{238}U$ dates with a population at ~2.16 Ma (fig. 15) or about 70–80 k.y. before eruption of the HRT (Rivera and others, 2014; Wotzlaw and others, 2015). The SRB zircons have trace element compositions, a crystallization age spectrum (Rivera and others, 2014), and hafnium isotope compositions (Wotzlaw and others, 2015) like the oldest zircons documented in the HRT (Rivera and others, 2014; Singer and others, 2014; Wotzlaw and others, 2015), suggesting an unerupted residuum of SRB rhyolite was recycled by the later caldera-forming HRT magma (Rivera and others, 2014; Wotzlaw and others, 2015). Like the HRT, the SRB rhyolite and its constituent minerals record crystallization from a melt with normal $\delta^{18}O$ values (fig. 16) and little input from hydrothermally altered crust (Hildreth and others, 1984; Bindeman and others, 2008; Wotzlaw and others, 2015). In addition, the SRB and HRT rhyolites yield the least radiogenic lead isotope compositions of the Yellowstone rhyolites (Doe and others, 1982; Hildreth and others, 1991), which provides insight into the isotopic baseline for Yellowstone rhyolites prior to shallow-level assimilation.

Return to Hwy 20 by way of Anderson Mill Road.

64.8 Turn right (north) onto Hwy 20 heading towards West Yellowstone.

73.4 Turn left (west) onto North Antelope Flat Road (Forest Road 168).

77.2 Pass intersection with Forest Road 170

77.9 Stop 2.2 Tuff of Lyle Spring along caldera margin. At this stop, pumiceous ignimbrite of the tuff of Lyle Spring, a unit of the Big Bend Ridge Rhyolite, is exposed along roadcuts at the wall of the first cycle caldera (fig. 29). Rhyolites of the Big Bend Ridge Rhyolite represent flows and minor pyroclastic deposits associated with the first and second caldera cycles. The rhyolites associated with the first cycle, including the Headquarters and Blue Creek flows, have low $\delta^{18}O$ values and yield Ar/Ar dates of ~1.96 Ma, whereas the flows associated with the second cycle have higher $\delta^{18}O$ values and isotopic compositions resembling MFT (Hildreth and others, 1984; Christiansen, 2001). The Big Bend Ridge Rhyolites, including the tuff of Lyle Spring, Bishop Mountain, and Green Canyon flows, have yielded K-Ar dates of ~1.2–1.3 Ma for their sanidines (Obradovich, 1992), suggesting they are temporally related to the second caldera cycle (Christiansen, 2001). However, field relations appear to indicate these rhyolites predate the MFT (Christiansen, 1982, 2001), in turn indicating some of their reported K-Ar dates are too young. The tuff of Lyle Spring has yielded a sanidine K-Ar date of 1.32±0.02 ka (Obradovich, 1992). The tuff of Lyle Spring and the Bishop Mountain flow are noteworthy because they are amongst the rare Yellowstone rhyolites that contain a hydrous major mineral, in this case biotite. Hornblende occurs in the lower portion of the LCT, and as an accessory mineral in the MFT and post-MFT domes of the Island Park Rhyolite (Christiansen, 2001). The oxygen isotope composition of quartz from the tuff of Lyle Spring and the Bishop Mountain flow resembles the MFT and other second cycle rhyolites, with $\delta^{18}O$ values (~5–6‰) that record a rebound from the exceptionally low values (2–3‰) of the earlier Blue Creek and Headquarters flows of the first cycle (Hildreth and others, 1984; Bindeman and Valley, 2001).

Figure 27. Geologic map of the Island Park area with Day 2 field trip stops shown by green numbered circles. Map scale is 1:125,000. Modified from Christiansen (2001).

Figure 28. Photograph of Snake River Butte looking south from within the Big Bend Ridge caldera segment. Top of butte is about 175 meters higher than the road in the foreground, and about 1.2 kilometers to the south.

Figure 29. Photograph from North Antelope Flat Road looking North showing exposures of vapor-phase altered ignimbrite of the tuff of Lyle Spring along. The tuff of Lyle Spring is one of the few Yellowstone rhyolites with a biotite as a major phase mineral.

Return to Hwy 20 using North Antelope Flat Road

82.4 Turn left (north) onto Hwy 20.

85.8 Turn right (east) onto Mesa Falls Scenic Byway.

87.9 Gerrit Basalt is exposed in road cuts.

89.9 Turn left (east) onto North Hatchery Butte Road. The low hills to the left (north) of the road make up Osborne Butte.

90.3 Stop 2.3 Osborne Butte. Park along the road and walk ~75 m north to rounded exposures of Osborne Butte rhyolite that are rich in phenocrysts (figs. 30, 31). Osborne Butte is one of several crystal-rich rhyolite domes of the Island Park Rhyolite, which stand above the floor of the Island Park basin and post-date the Mesa Falls eruption (fig. 27). The steep-sided morphology and concentric flow pattern of this ~100-m-high dome suggest endogenous growth (Christiansen, 2001). Osborne Butte, Silver Lake, Lookout, and Warm River butte domes define a 30-km-long and 7-km-wide northwest-trending lineament of eruption vents (fig. 27). Recent $^{40}Ar/^{39}Ar$ dating of sanidine suggests that these domes were erupted during the 1.2943±0.0026 Ma (Warm River Butte flow) to 1.2190±0.0146 Ma (Lookout Butte flow) interval (Troch and others, 2017). This lineament parallels not only fault zones associated with the resurgent areas of the Yellowstone caldera, but also parallels major tectonic fault zones and the Teton Range to the southeast, suggesting a structural control (Christiansen, 2001). Sanidine $^{40}Ar/^{39}Ar$ dates for Osborne Butte indicate an eruption age of 1.2784±0.0054 Ma (Troch and others, 2017), likely only tens of thousands of years after the MFT eruption. The lavas of the Island Park Rhyolite are distinct on the Yellowstone Plateau because they contain as much as 40 percent phenocrysts (Troch and others, 2017), often several centimeters in size (fig. 31), which is much more crystalline in terms of size and abundance than the <20 percent phenocryst content of the same mineral assemblage that characterizes the MFT. Glomerocrysts composed primarily of pyroxenes, plagioclase, and oxides, but lacking sanidine and quartz, occur in the Osborne Butte rhyolite and are interpreted to represent cumulate material left over from the crystal-melt

Figure 30. Photograph showing exposures of crystal-rich Island Park Rhyolite at Osborne Butte.

Figure 31. Close-up photograph of crystal-rich rhyolite of the Osborne Butte flow, with approximately 40 percent crystals including phenocrysts of sanidine, quartz, and plagioclase.

fractionation that led to the Island Park Rhyolite (Troch and others, 2017). The lead isotope compositions of sanidines from the crystal-rich Island Park rhyolites indicate an affinity to the MFT rhyolite and the second cycle (Troch and others, 2017).

Return to Mesa Falls Scenic Byway.

90.7 Turn left (south) onto Mesa Falls Scenic Byway.

99.5 Stop 2.4 Upper Mesa Falls overlook. Turn right into Upper Mesa Falls and drive down to park in the overlook parking lot. Note that this parking lot requires a fee ($5.00 as of August, 2017). Walk down to the overlook past lava flows of Gerrit Basalt to observe a cliff-forming section of MFT directly across the falls (fig. 32). Upper Mesa Falls is the location for the principal reference section for the MFT, with about 140 m of exposed thickness (Christiansen and Blank, 1972). The lower portion of the section is composed of welded devitrified tuff with abundant large phenocrysts, and the upper portion is a vapor-phase zone (Christiansen and Blank, 1972; Neace and others, 1986). Crystal content decreases upsection from ~40 percent to 25 percent crystals (Neace and others, 1986). This exposure represents MFT that ponded within the Big Bend Ridge caldera and later was exposed by the Henrys Fork River. The overlook is located at the edge of an erosional terrace, which was produced by an earlier period of incision by the ancestral Henrys Fork River. This terrace was later inundated by lava flows of Gerrit Basalt, which rest unconformably on the welded devitrified portion of the MFT and form the current lava bench at the level of the overlook (Christiansen, 2001). Field mapping and paleomagnetism has correlated the bench-forming basalt at the overlook to the ~30 ka Pinehaven flow (George and others, 2015) observed at Stop 1.4 (fig. 20), indicating that this lava flow spilled into the ancestral Henrys Fork canyon and traveled ~25 km downstream (George and others, 2015). Scattered outcrops and benches of older basalts and hyaloclastite occur upstream and downstream of Upper Mesa Falls, and represent older episodes when basaltic lavas spilled into and flowed down the ancestral Henrys Fork canyon (George and others, 2015).

Return to Mesa Falls Scenic Byway (Idaho State Highway 47) and turn right (south). Continue on Mesa Falls Scenic Byway to Ashton.

102.1 Turnout for Lower Mesa Falls.

108 Cross Warm River, a tributary to the Henrys Fork River.

111.8 Veer right, continue on Hwy 47 toward Ashton.

116.8 Turn left (south) onto Hwy 20 heading toward Twin Falls.

126.6 Turn right onto East 700 North road.

127.7 Turn right (north) and cross bridge across Henrys Fork River.

127.8 Turn left (west) onto East 700 North road.

128.5 Turn right (north) onto Sand Creek Road. Proceed north.

143.6 Veer left, continue on Sand Creek Road.

144.5 Turn left (west) onto Snowshoe Beetle Road.

145.3 Stop 2.5 Headquarters flow near Sand Creek Reservoir. Park next to jagged outcrops of devitrified, spherulitic, and flow banded rhyolite of the post-HRT Headquarters flow. Phenocrysts include plagioclase, sanidine, and quartz (Christiansen, 1982). The Headquarters (fig. 33) and Blue Creek rhyolite flows share nearly identical low $\delta^{18}O$ mineral and glass values (Hildreth, 1984; Bindeman and Valley, 2001), radiogenic lead-strontium isotope compositions (Hildreth and others, 1991), and sanidine Ar/Ar dates (Rivera and others, 2017) consistent with the latter flow underlying the former (Christiansen, 2001). These are key petrologic units at Yellowstone because they are the oldest rhyolites heralding the considerable depletion of $^{18}O/^{16}O$ ratios that is characteristic of most of the rhyolites on the Yellowstone Plateau. Sanidines from the Headquarters and Blue Creek flows yield Ar/Ar dates of 1.9476±0.0037 Ma and 1.9811±0.0035, respectively (Rivera and others, 2017). These flows, and the newly identified low-$\delta^{18}O$ Sheridan Reservoir flow that is located to the north and yields a uranium-lead zircon crystallization date of 2.07±0.19 Ma (Watts and others, 2011), appear to have vented from within the HRT caldera (Watts and others, 2011). The similar isotopic compositions and eruption ages of the Headquarters and Blue Creek flows suggest both units record the same general time interval and state of the magmatic system ~95–130 k.y. after the first cycle caldera collapse associated with the HRT. Quartz phenocrysts from the Headquarters

Figure 32. Photograph of Mesa Falls Tuff (MFT) at the principal reference section exposed along the Henrys Fork River at Upper Mesa Falls (Christiansen and Blank, 1973). The exposed cliff at the falls is about 40 meters (m) high, but the thickness of the MFT in the section is about 140 m (Christiansen and Blank, 1973). A resistant welded and devitrified zone makes up the lower portion of the MFT at this location and grades upward into a less-resistant vapor-phase zone (Christiansen and Blank, 1973; Neace and others, 1986). Apparent horizontal layering reflects lithologic variations and variable erosion of different pyroclastic flow beds (R. Christiansen, oral comm., 2017). The sequence represents a single cooling unit. Near the canyon rim, the Mesa Falls Tuff is overlain by Lava Creek Tuff and in turn Gerrit Basalt (Christiansen and Blank, 1973; Christiansen, 2001).

flow yields $\delta^{18}O$ values of about +4‰ (Hildreth and others, 1984; Bindeman and Valley, 2001), suggesting a melt value of +3.5‰ and a drop of ~3–4‰ below the normal $\delta^{18}O$ values characterizing the HRT (Hildreth and others, 1984; Bindeman and Valley, 2001). The remarkably low $\delta^{18}O$ of these flows indicates parental magma with a large component of hydrothermally altered shallow crust (Hildreth and others, 1984; Bindeman and Valley, 2001; Bindeman and others, 2008). Based on the presence of zircon xenocrysts in the Blue Creek flow (described at the next stop), at least some of this hydrothermally altered crust may have been intracaldera rhyolite related to the HRT (Bindeman and others, 2008).

Head back east on Snowshoe Beetle Road.

146.1 Enter Sand Creek Reservoir campground.

146.8 Turn left onto road toward Blue Creek Reservoir.

146.9 Veer right on road toward Blue Creek Reservoir.

147.7 Quarry for basaltic cinders located on the west side of road. This represents a vent area for basalts of the SRP.

148.8 Stop 2.6 Blue Creek flow at Blue Creek Reservoir. Park in the turnaround near Blue Creek Reservoir. To the west, the margin of the Blue Creek flow is exposed as dark cliff-forming outcrops with vertical jointing (fig. 34). Like the Headquarters flow, the Blue Creek flow is characterized by very low $\delta^{18}O$ values. Blue Creek zircons yield an average $\delta^{18}O$ value of about +2‰ (Bindeman and Valley, 2001), although with up to ~6‰ variation within single zircons including high- and low-$\delta^{18}O$ cores (Bindeman and others, 2008). Ion microprobe $^{206}Pb/^{238}U$ dating of Blue Creek zircons reveals the presence of inherited crystals (from older, first cycle rhyolites) dating back to ~2.3 Ma (Bindeman and others, 2008). This inheritance and variability in oxygen isotope composition within and between Blue Creek zircons indicates remelting of multiple source rocks with different $\delta^{18}O$ (Bindeman and others, 2008). A rimward decrease of oxygen-isotope compositions characterizes the Blue Creek zircons, which is consistent with cannibalization of hydrothermally altered first-cycle rhyolites and the immersion and re-equilibration of inherited crystals in low $\delta^{18}O$ melt (Bindeman and Valley, 2001). Based on the scale of this zoning and experimentally established kinetics of oxygen diffusion, Bindeman and Valley (2001) calculated that the Blue Creek zircons were immersed in low $\delta^{18}O$ melt for no more than 10 k.y. before eruption.

Figure 33. Photograph of margin of post-Huckleberry Ridge Tuff and low $\delta^{18}O$ Headquarters flow near Sand Creek Reservoir.

Figure 34. View to west at turnaround near Blue Creek Reservoir. The cliff exposure is the eroded margin of the low $\delta^{18}O$ Blue Creek flow. Distance to flow is 0.4 kilometer. Relief is 220 meters.

Similar applications of diffusion geochronometry to other Yellowstone rhyolites (Bindeman and Valley, 2001; Till and others, 2015; Loewen and others 2017) have also yielded short timescales between remelting and eruption.

Return to West Yellowstone.

Day 3

Overview

The third day of the field trip will focus on examining extracaldera basaltic and rhyolitic volcanism at Yellowstone. Including:

- Extracaldera rhyolitic magmas with various petrographic characteristics that are contemporaneous with the post-Lava Creek Tuff (LCT) magmatism at Yellowstone,
- Several Yellowstone basalts including an excellent exposure of columnar jointed basalt,
- A mixed basalt-rhyolite complex, and
- Hydrothermal discharge features associated with extracaldera volcanism.

The trip begins at the west entrance to Yellowstone National Park, continues east along the northern margin of Yellowstone caldera to Norris, and then heads north to Mammoth along a region of abundant normal faulting that hosts the majority of Yellowstone's extracaldera volcanism. See figures 35 and 36 for maps showing the location of the field trip stops as well as geologic features of interest.

Day 3 Road Log

0.0 Start at west entrance to Yellowstone National Park. Reset trip odometer.

1.4 Turn left onto unnamed road.

1.6 Stop 3.1 Madison River Basalt. Park at the end of the road and walk a short distance down a dirt path to the edge of the Madison River. Dense basalt crops out at the base of Madison River on both sides. This is a flow of the Madison River Basalt (fig. 37), a plagioclase and olivine-phyric basalt (Christiansen, 2001), which yields an $^{40}Ar/^{39}Ar$ date of 530±60 ka (Bennett, 2006). Several more outcrops of Madison River Basalt that erupted from several different vents can be found to the north and northwest of this location (fig. 36). Just over the northern riverbank is the Riverside flow, an extracaldera rhyolite that yields a sanidine $^{40}Ar/^{39}Ar$ date of 526±3 ka (Nastanski, 2005) and is part of the Roaring Mountain Member of the Plateau Rhyolite (Christiansen, 2001). Madison River Basalt and the Riverside flow represent some of the first-erupted extracaldera magmas following the caldera-forming eruption of the LCT, and are broadly contemporaneous with the early Upper Basin Member rhyolites, which represent some of the first eruptions into the newly formed Yellowstone caldera (Christiansen, 2001). The contemporaneous eruption of basalt, extracaldera rhyolites, and intracaldera rhyolite has occurred throughout the post-Lava Creek volcanic history of Yellowstone.

Although the timing of post-LCT basaltic and rhyolitic (both extracaldera and intracaldera) volcanism is broadly contemporaneous, there appears to be no geochemical evidence that these suites of magmas are directly related. Instead, Yellowstone basalts, extracaldera rhyolites, and intracaldera rhyolites have distinct isotopic compositions (Hildreth and others, 1991; Pritchard and Larsen, 2012; Stelten and others, 2015), which require a distinct source for each suite (fig. 6). For example, isotopic data demonstrate that intracaldera Yellowstone rhyolites (and the caldera-forming eruptions) have isotopic compositions intermediate between Yellowstone basalts and their potential crustal sources (fig. 6). This characteristic suggests that Yellowstone rhyolites are derived from a hybridized source region in the lower- to mid-crust (Hildreth and others, 1991;Christiansen, 2001; Watts and others, 2010; Pritchard and Larsen, 2012; Wotzlaw and others, 2015). The extracaldera rhyolites have lower $^{143}Nd/^{144}Nd$ and higher $^{87}Sr/^{86}Sr$ than the intracaldera rhyolites, which indicates a relatively larger crustal influence during their formation (fig. 6; Hildreth and others, 1991; Pritchard and Larson, 2012; Pritchard and others, 2013).

The coeval nature of post-LCT basaltic volcanism around the margins of Yellowstone caldera while rhyolitic volcanism, both intracaldera and extracaldera, was active suggests a rejuvenation of the system with basaltic magmatism, which resulted in

- Eruption of peripheral basalts,
- Melting of local crust outside of Yellowstone caldera to form the extracaldera rhyolites, and
- Melting of a hybridized crustal source that underlies Yellowstone caldera to form the intracaldera rhyolites (fig. 7; Stelten and others, 2013).

1.8 Drive to main road (Hwy 20) and turn left.

12.5 Excellent view of the northern margin of the ~114 ka West Yellowstone flow to the south.

13.9 Madison Junction. Turn left onto Hwy 89 towards Norris/Mammoth.

18.7 Stop 3.2 Gibbon Falls. Turn right into parking area for Gibbon Falls. South of here the Gibbon River crosses from a slumped caldera block into the main caldera basin. The falls represents headwater retreat along the Gibbon River from the inner caldera scarp and is held up by densely welded LCT. The Nez Perce Creek flow, a ~148 ka intracaldera rhyolite flow forms the skyline to the south. To the north, the outer caldera rim is capped by LCT-A (fig. 38).

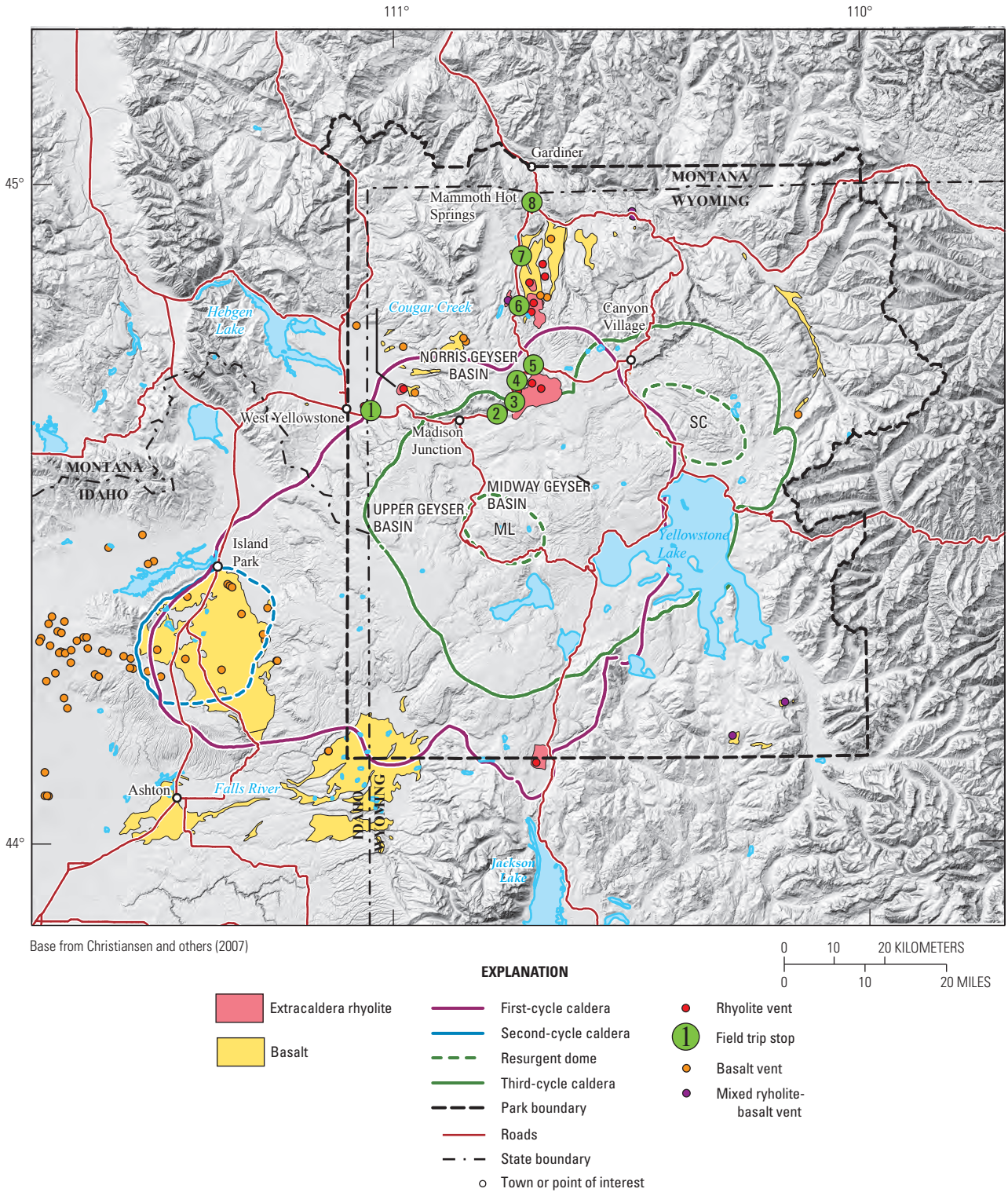

Figure 35. Map of Yellowstone National Park and vicinity showing extracaldera rhyolites and basalts that erupted after the caldera-forming eruption of the Lava Creek Tuff. ML, Mallard Lake resurgent dome; SC, Sour Creek resurgent dome. Modified from Christiansen and others (2007).

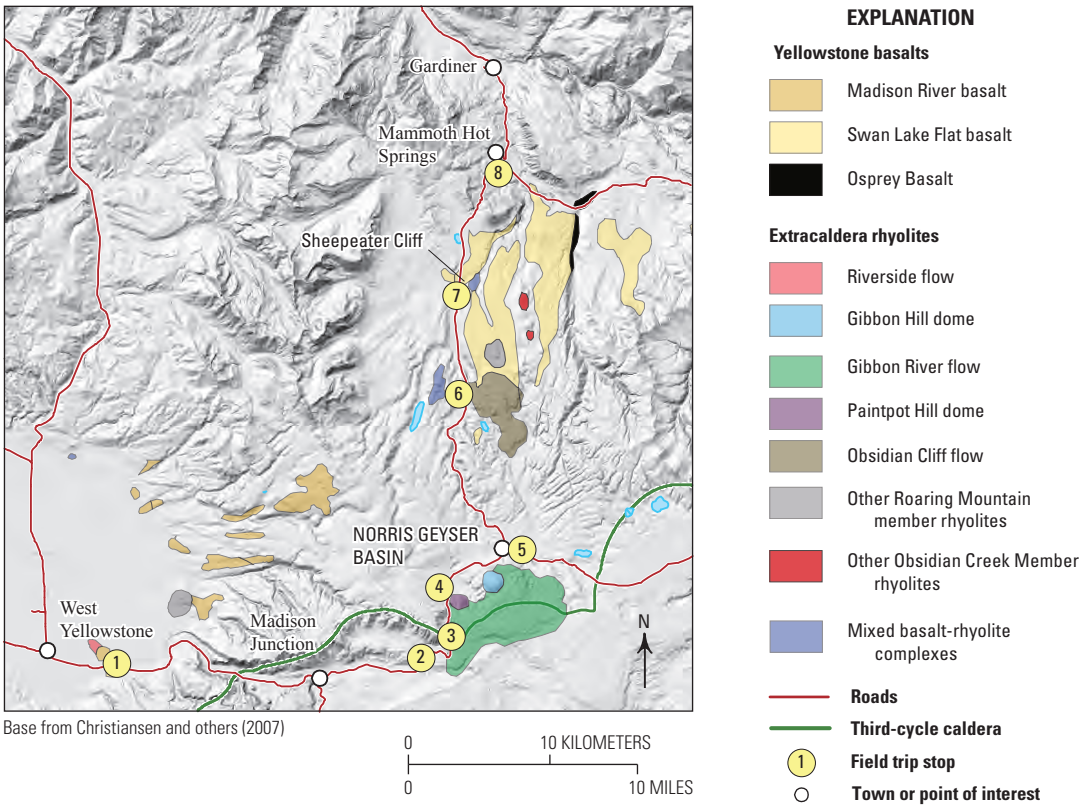

Figure 36. Map showing close-up view of Day 3 field trip stop locations. Extracaldera basalts and rhyolites are included for reference. Modified from Christiansen and others (2007).

Figure 37. Photograph of outcrop of Madison River Basalt along the Madison River, west of Yellowstone caldera. Basalt outcrop is approximately 1 meter high relative to the river level.

Continue north on Hwy 89 towards Norris. Note the hydrothermal discharge features on the side of the road as we drive through Gibbon River Canyon.

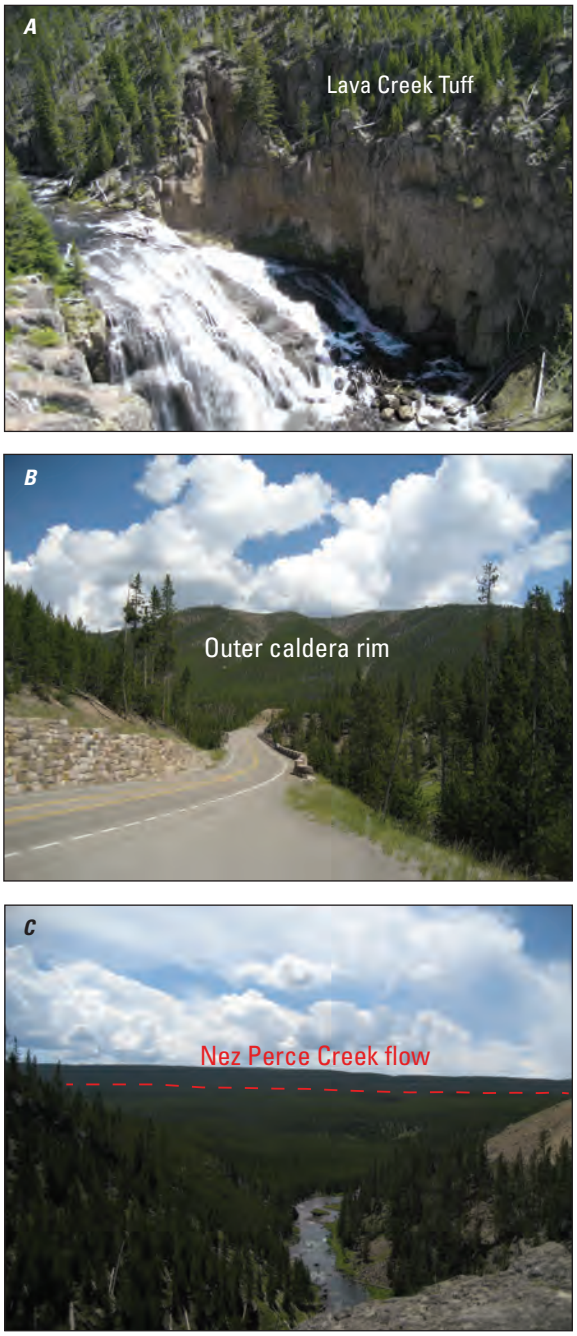

Figure 38. Photographs of Gibbon Falls. *A,* View of Gibbon Falls cutting into densely welded Lava Creek Tuff. It is approximately 23 meters from the base of the waterfall to the top of the outcrop. Gibbon Falls is located on a slumped caldera block at the northern margin of Yellowstone caldera. *B,* View looking north from the Gibbon Falls parking area. The outer caldera rim can be seen. *C,* View looking south from the Gibbon Falls parking area. The approximately 148,000-year-old Nez Perce Creek flow forms the skyline to the south.

23.0 Stop 3.3 Gibbon River flow. Park in the roadside turnout on left. We are stopped at the northern end of Gibbon River Canyon. To the southwest is a tilted fault block of LCT-A, located just outboard of the outer caldera scarp. To the east is the Gibbon River flow, an extracaldera rhyolite of the Roaring Mountain Member (fig. 39). The Gibbon River flow, with an eruption age of 107.6±7.1 ka based on $^{40}Ar/^{39}Ar$ dating of sanidine (Dallegge, 2008), vented near the northern caldera margin and flowed both into and out of Yellowstone caldera (Christiansen, 2001). The Gibbon River flow is distinct from other Roaring Mountain Member rhyolites because it contains ~10 percent phenocrysts of sanidine, quartz, and minor plagioclase, opaque minerals, olivine, and amphibole (Wooton, 2010), whereas other Roaring Mountain Member rhyolites are nearly aphyric.

Based on feldspar compositions and trace elements, Wooton (2010) concluded that the Gibbon River flow is composed of three compositionally distinct magmas that erupted simultaneously. To understand mixing between intra and extracaldera rhyolites at the margin of Yellowstone caldera, Stelten and others (2013) compared (1) ^{238}U-^{230}Th crystallization ages, trace-element concentrations, and Hf-isotope ratios in zircons, and (2) lead isotope compositions, major-element, and barium concentrations in individual sanidine crystals from the Gibbon River flow to the nearby Solfatara Plateau flow and Hayden Valley flow, which erupted at 102.8±7.6 ka and 102±4 (Christiansen and others, 2007), respectively (fig. 39).

The Gibbon River flow rhyolite hosts one zircon population and one sanidine population that are compositionally distinct from the same minerals hosted in the Hayden Valley flow or other intracaldera rhyolites (fig. 40). However, the Solfatara Plateau flow contains multiple populations of sanidine and zircon crystals, some of which are identical to those found in the coeval Gibbon River and Hayden Valley flows. These data suggest that the Solfatara Plateau flow rhyolite was formed by mixing the rhyolitic magma that fed the extracaldera Gibbon River flow with magma at the margin of the main subcaldera reservoir that had fed the Central Plateau Member flows. A detailed field and geochemical study by Befus and Gardner (2016) demonstrated that the Solfatara Plateau flow is heterogeneous in trace element composition, and the portion sampled by Stelten and others (2013) is likely to be a volumetrically minor compositional component of the Solfatara Plateau flow. Nevertheless, the zircon and sanidine data described above demonstrate that extracaldera magma mixed with the margin of the main subcaldera reservoir during the genesis of the Solfatara Plateau, Gibbon River, and Hayden Valley rhyolites.

Continue north along Hwy 89.

23.5 Turn right into parking area for Paintpot Hill dome.

23.7 Stop 3.4 Paintpot Hill dome and associated hydrothermal features. We are now located at the southern end of the Norris-Mammoth corridor, the location of abundant north-south oriented normal faulting as well as extracaldera basaltic and rhyolitic volcanism. Paintpot Hill dome is a small rhyolite dome located in the foreground to the southeast, which erupted

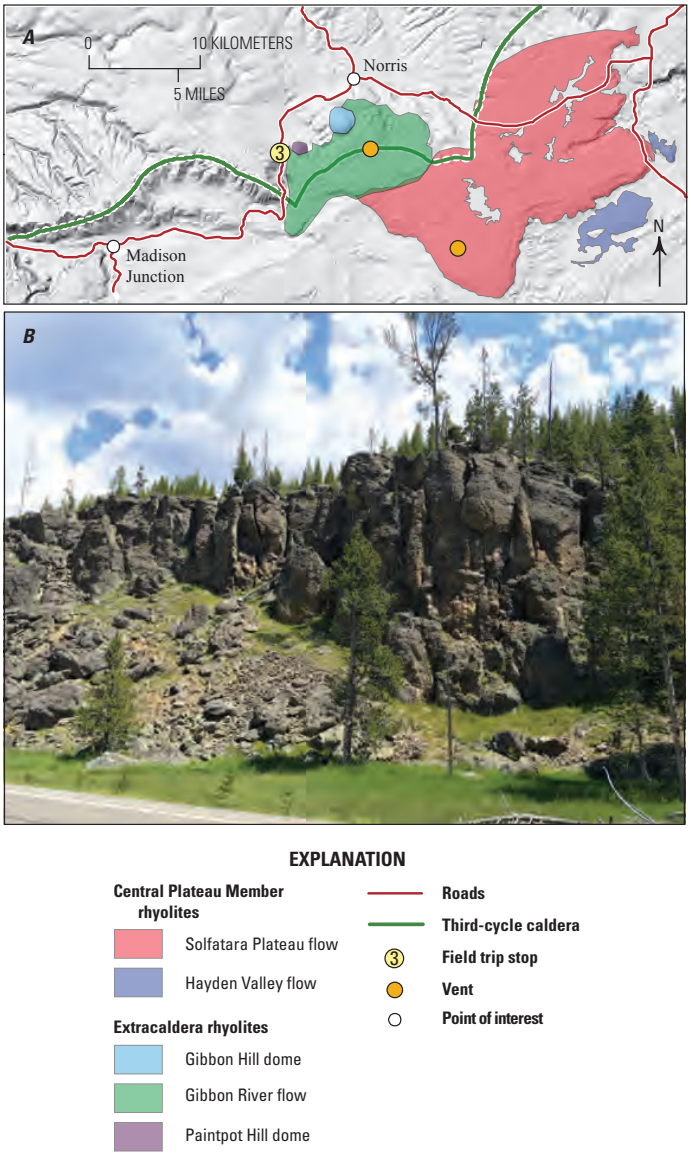

Figure 39. Gibbon River flow. *A*, Close-up map showing the northern margin of Yellowstone caldera, the extracaldera Gibbon River flow, Paintpot Hill dome, and Gibbon Hill dome, as well as the intracaldera Solfatara Plateau and Hayden Valley flows. The Gibbon River flow erupted approximately 108 ka near the northern margin of Yellowstone caldera. The Solfatara Plateau and Hayden Valley flows are intracaldera rhyolites (part of the Central Plateau Member rhyolites) that erupted approximately 103 ka near the northern margin of Yellowstone caldera (coeval with the Gibbon River flow). The vent location for the Hayden Valley flow is not known. Map modified from Christiansen and others (2007). *B*, Photograph of outcrop of the Gibbon River flow at Stop 3.3 of the field trip (annotated on map A). The outcrop shown here is approximately 12 meters tall.

at 208.1±4.9 ka based on $^{40}Ar/^{39}Ar$ sanidine dating (Nastanski, 2005; fig. 41). Paintpot Hill Dome is an extracaldera rhyolite, which is part of the Obsidian Creek Member. Obsidian Creek Member rhyolites are exclusively found in the Norris-Mammoth Corridor and are distinguished from Roaring Mountain Member rhyolites based on petrography. The Obsidian Creek Member rhyolites are porphyritic with quartz, sanidine, and plagioclase, whereas the Roaring Mountain Member rhyolites are sparsely porphyritic to aphyric. In fact, the Obsidian Creek Member rhyolites petrographically resemble some of the intracaldera rhyolites.

To the east Gibbon Hill dome can be seen. Gibbon Hill dome is an extracaldera rhyolite of the Obsidian Creek Member, which erupted at 134.3±2.6 ka based on $^{40}Ar/^{39}Ar$ dating (Nastanski, 2005). From this vantage point, the Gibbon River flow can be seen forming the skyline behind Gibbon Hill and Paintpot Hill domes (fig. 41). The majority of the extracaldera rhyolites of both the Obsidian Creek and Roaring Mountain Members are located to the north-northeast along the Norris-Mammoth Corridor.

This location also provides excellent examples of the hydrothermal features for which Yellowstone National Park is famous (fig. 42). We will walk along the short 1.8 km (round trip) Artist's Paint Pots Trail located at the southeast end of the parking lot. Along this trail there are more than 50 springs, geysers, vents, and mud pots for viewing. The large clear hot springs represent areas of unrestricted discharge of thermal waters from the hydrothermal system. The colors in the pools are typically related to the presence of bacteria colonies, with lighter colors corresponding to higher water temperatures (Fournier and others, 1994). Fumaroles have formed in places where only vapor has found a pathway to the surface, while the geysers reflect the variability of the hot spring system, with the frequency and magnitude of their activity controlled by plumbing geometry, discharge rate, and (or) heat loss (Fournier and others, 1994). The mud pots are not directly fed by the underlying hydrothermal system and instead formed where water collected on the ground surface owing to condensation and oxidation of acid gases and steam (Christiansen and others, 2007). Conversion of H_2S in the steam by bacteria produces sulfuric acid, which acts to alter and break down the surrounding rocks into an impermeable mash of clay minerals that hold water and form mud pots (Fournier and others, 1994). The bubbling of the mud pots reflects continued percolation of gas. We refer the reader to Fournier and others (1994), Hurwitz and Lowenstern (2014), and Morgan and others (2009) for detailed descriptions of the hydrothermal system at Yellowstone. In addition to viewing the spectacular hydrothermal discharge features in this area, this short hike offers a great panoramic view of the surrounding region.

Return to the vehicles and drive back to the main road (Hwy 89; Grand Loop Road).

23.9 Turn right onto Hwy 89/Grand Loop Road.

27.6 Norris Junction. Turn left toward Norris Geyser Basin.

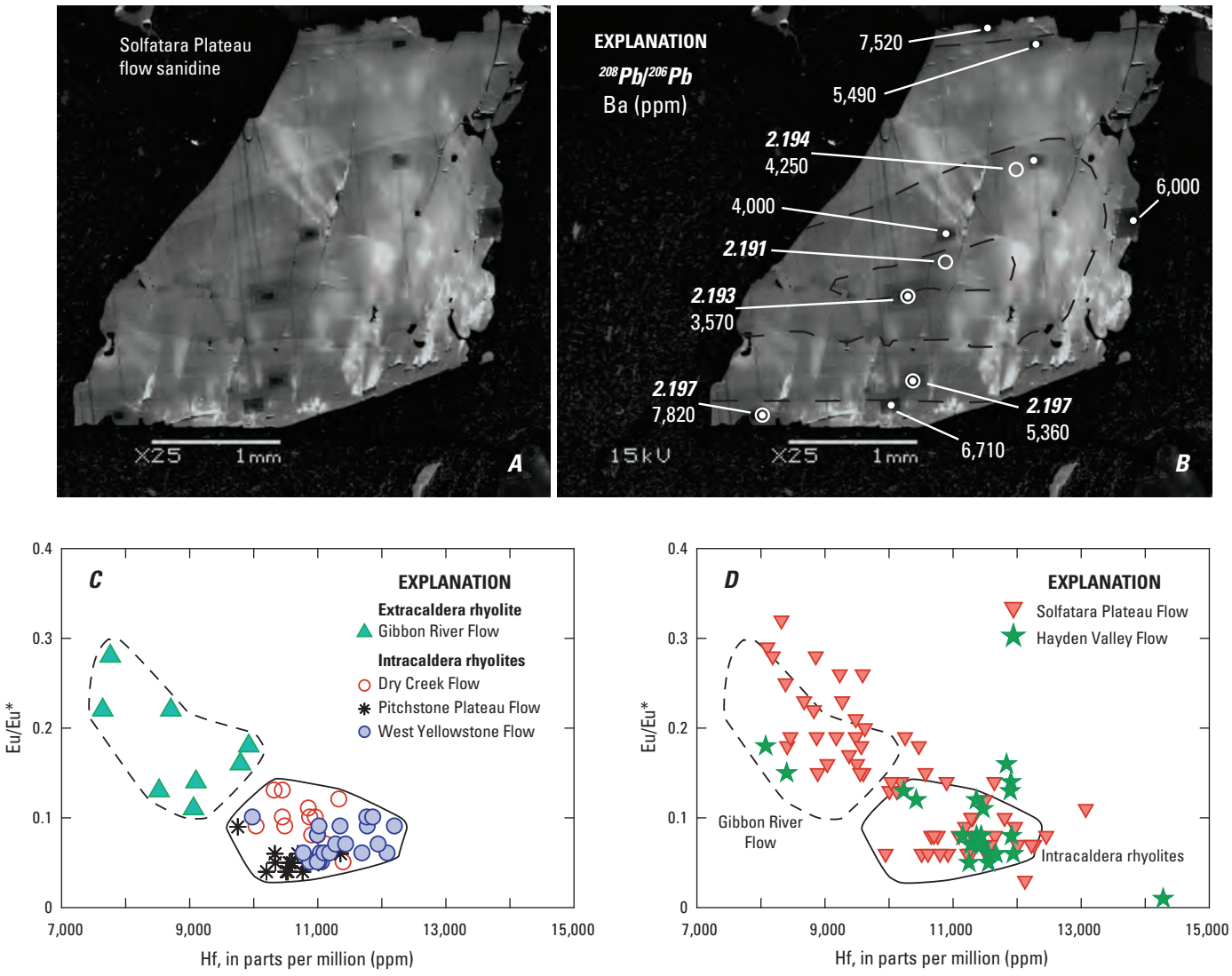

Figure 40. Cathodoluminescence (CL) image of a sanidine grain from the Solfatara Plateau flow that displays multiple zones with distinct lead isotopic composition and barium concentrations. *A,* Unedited image, and *B,* annotated image. The open white circles in *B* represent the locations of lead isotopic analyses performed via laser ablation multi-collector inductively coupled plasma mass spectrometry. The filled white circles in *B* represent the locations of the electron microprobe analyses for major-element and barium concentrations, barium concentrations annotated in parts per million (ppm). The black dashed lines in *B* mark the boundaries between the zones of different CL brightness within the sanidine crystal. Note the systematic zoning from a low barium and low $^{208}Pb/^{206}Pb$ core to high barium and high $^{208}Pb/^{206}Pb$ rim. *C,* Hafnium versus Eu/Eu* (the europium anomaly) for zircons from the extracaldera Gibbon River flow compared to intracaldera rhyolites (Dry Creek flow, Pitchstone Plateau flow, and West Yellowstone flow). Eu/Eu* is calculated as $[Eu_{CN}/(Sm_{CN}^{0.5} * Gd_{CN}^{0.5})]$, where CN indicates the measured elemental concentrations have been normalized to chondritic values, and is used here a proxy for magmatic differentiation (lower Eu/Eu* corresponds to a more evolved melt). *D,* Hafnium versus Eu/Eu* (the europium anomaly) for zircons from the Hayden Valley flow and Solfatara Plateau flow, two intracaldera rhyolites coeval with the Gibbon River flow. Reference fields for Gibbon River flow zircons, main reservoir Central Plateau Member zircons, and Scaup Lake flow zircons are included for comparison. Note how the Solfatara Plateau flow contains zircons similar to those found in the extracaldera Gibbon River flow and the intracaldera rhyolites. Modified from Stelten and others (2013).

Figure 41. Photograph from the parking lot for Paintpot Hill dome (or Artist's Paint Pots Trail). Gibbon Hill dome, and the Gibbon River flow are young, extracaldera rhyolites, which erupted just north of Yellowstone caldera at the southern end of the extensional Norris-Mammoth corridor. For reference, the peak of Paintpot Hill dome is approximately 210 meters above the elevation of the parking lot. $^{40}Ar/^{39}Ar$ dates are from Dallegge (2008) and Nastanski (2005).

Figure 42. Photograph from the Artist's Paint Pots Trail, Yellowstone National Park showing hydrothermal discharge features near Paintpot Hill dome. Photograph by Jon Sullivan.

28.0 Stop 3.5 Norris Geyser Basin. We briefly describe some of the features of Norris Geyser Basin here, but the reader is referred to Fournier and others (1994) and White and others (1988) for more thorough descriptions. Most of the information presented here is based on descriptions from these publications.

Norris Geyser Basin is a large area of hydrothermal activity and can be viewed on two loop trails starting from the visitor center. Norris Geyser Basin is known for having the hottest shallow reservoir of any thermal area in Yellowstone National Park (Fournier and others, 1994). Additionally, Norris Geyser Basin hosts Steamboat Geyser, which is the highest-erupting active geyser in the world (Fournier and others, 1994).

Walk to the Norris Museum visitors center located near the parking lot. Looking north from the Norris Museum visitor center you will see the Porcelain Basin (fig. 43), which is host to numerous geysers. The waters that discharge into Porcelain Basin, and the 100 Spring Plain just beyond Porcelain Basin, are supersaturated with respect to silica but deposit little sinter because of the acidity (pH 3–4) of the water (Fournier and others, 1994). These acidic waters have caused intense surficial alteration of the LCT, which is the lithology that encloses most of Norris Geyser Basin. The white deposits around the Porcelain Basin are not hot-spring precipitates, but instead acid-leached LCT (Fournier and others, 1994). The geysers can be viewed from the platform on the north side of Norris Museum.

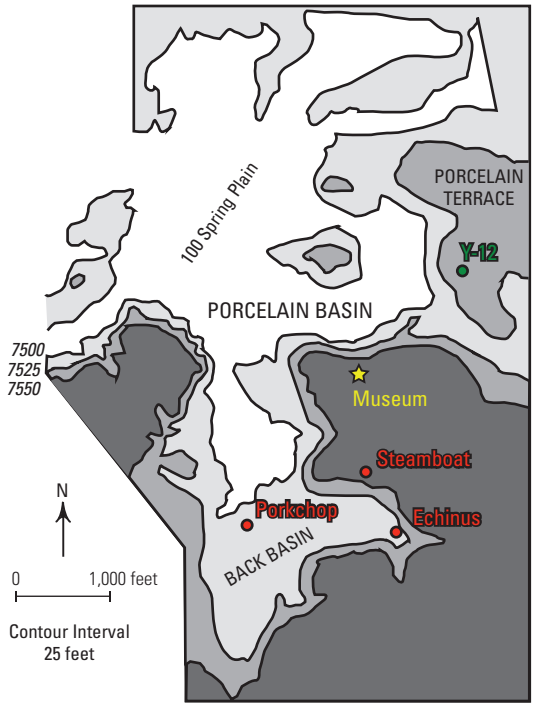

Figure 43. Map of Norris Geyser Basin showing topographic and selected hydrothermal discharge features. The location of U.S. Geological Survey drill hole Y-12 is included for reference. Modified from Fournier and others (1994).

At Porcelain Terrace, located on the east of Porcelain Basin, (fig. 43), the waters being discharged are from the deepest and hottest (275–325 °C) reservoir at Norris Geyser Basin and silica is being deposited faster than any other place in Yellowstone National Park (Fournier and others, 1994). USGS drill hole Y-12 is located at the south edge of Porcelain Terrace, and penetrates through the LCT with temperatures of ~240 °C at a depth of 323 m (Fournier and others, 1994). Drill hole Y-12 was significant because it provided information on the chemical composition of the deep water in the hydrothermal system (Truesdell and others, 1977; Fournier and others, 1994). As you walk though Porcelain Basin, take note of the color of the discharge channels. The vibrant green color seen in some of the areas of hot water reflects the activity of cyanobacteria, which thrive in low pH waters, whereas the areas with yellow, red, and brown colors reflect bacteria that prefer neutral pH environments (Fournier and others, 1994).

To the south-southwest of the Norris Museum is Back Basin (fig. 43). Back Basin is host to numerous geysers including the highest-erupting active geyser in the world, Steamboat Geyser, and Echinus Geyser, which erupts approximately once per hour. Steamboat Geyser produces irregular and infrequent eruptions, which can reach more than 100 m (Fournier and others, 1994). Echinus Geyser has more predictable eruptions, some of which can eject centimeter-sized fragments of pyrite and marcasite (FeS_2), and its slightly acidic waters produce a spiny texture around its pool (Fournier and others, 1994). Other features of interest at this stop include Porkchop Geyser Crater and the explosion debris produced when the Porkchop exploded in September 1989 (Fournier and others, 1994), and Cistern Spring, which is host to a spectacular sinter terrace.

Return to the vehicles and return to the main road.

28.4 Norris Junction. Turn left onto Hwy 89 (Grand Loop Road).

36.8 Stop 3.6 Obsidian Cliff flow. Park at the turnout on the left. At this stop we will examine the flow features and crystallization textures of a glassy extracaldera rhyolite. Across the road to the southeast is Obsidian Cliff, which is the west margin of the Obsidian Cliff flow, part of the Roaring Mountain Member rhyolites. The Obsidian Cliff flow has yielded a $^{40}Ar/^{39}Ar$ date of 105.6±1.0 ka for its obsidian groundmass (Nastanski, 2005. Obsidian Cliff is notably aphyric to sparsely phyric, suggesting it erupted close to its liquidus temperature (Christiansen and others, 2007). The vent for the Obsidian Cliff flow is approximately 1 km to the east of the road (Christiansen, 2001).

Note the large columnar joints at the base of the flow near the road and prominent flow layering near the top of the flow (fig. 44). The flow layering becomes steep and contorted near the top of the flow. Walk across the road to the base of Obsidian Cliff. A close inspection of the talus blocks at the base of the cliff reveals spherulitic and lithophysal obsidian

as well as small-scale flow structures. Lithophysae are hollow spherulitic cavities lined by concentric shells of small crystals, which generally include tridymite, alkali feldspar, and minor accessory minerals that are separated by open interspaces. Small-scale flow structures are apparent and marked by bands of small gray spherulites. Some pinkish spherulites and lithophysae are 1–5 cm in size. The lithophysae of the Obsidian Cliff flow caught the attention of pioneering American petrologist J.P. Iddings, who produced a remarkably detailed description of the occurrence (Iddings, 1888). Lithophysae represent vapor exsolution and crystallization of minerals from the vapor phase at relatively high temperatures before or after solidification of the flow (Breitkreuz, 2013). Iddings (1888) noted that some of the lithophysae have been crushed by surrounding glass that was forced into their cavities, in turn suggesting the glass was viscous at the time of formation. However, using oxygen isotope thermometry, Befus (2016) determined that spherulites in another Yellowstone flow (Pitchstone Plateau) formed in the ~300–580 °C temperature interval, which is below the glass transition of 600–700 °C, indicating crystallization from solid volcanic glass.

The Obsidian Cliff flow was a source of Native American arrowheads around the greater Yellowstone area, and is an archeological resource. **Important Note:** *Do not collect from this location, or others in the National Park, without prior permission from National Park Service.*

Return to the vehicles and continue north on Hwy 89 toward Mammoth.

41.25 Cross the Gardner River bridge.

41.4 Turn right towards Sheepeater Cliff.

41.65 Stop 3.7 Sheepeater Cliff and the mixed basalt-rhyolite of Gardner River. Park in Sheepeater Cliff parking area. At the northwest end of the parking lot is Sheepeater Cliff, which is a spectacular cross-section exposure of a columnar-jointed lava flow of the Swan Lake Flat Basalt (fig. 45). There is a short trail that heads to the northwest where more exposures of columnar jointed basalt can be seen. Swan Lake Flat Basalt is a stratigraphic unit composed of a number of different post-LCT lava flows (Christiansen and Blank, 1972). The basalt exposed at Sheepeater Cliff is derived from Panther Creek volcano located west of the Sheepeater Cliff on the other side of Hwy 89 (fig. 45) and dated at 174±46 ka ($^{40}Ar/^{39}Ar$ date, Bennett, 2006). Other lava flows of the Swan Lake Flat Basalt are located near this area, and include those from the Horseshoe Hill volcanoes to the southeast and Tower Road volcano to the northeast (fig. 45). The basalt that erupted from the Tower Road volcano yields an $^{40}Ar/^{39}Ar$ date of 590±65 ka (Bennett, 2006). The flows of the Swan Lake Flat Basalt are some of the most isotopically primitive basalts at Yellowstone with ε_{Hf} ranging from 3.25 to 5.46 (Stelten and others, 2017) and epsilon neodymium ($\varepsilon_{Nd)}$ ranging from -3.02 to -2.36 (Hildreth and others, 1991), suggesting they experienced little contamination prior to eruption. Because of its primitive isotopic composition, the Swan Lake Flat Basalt has been used as the mantle end-member in mixing models seeking to explain the range of isotopic compositions observed for

Figure 44. Photograph of the south face of Obsidian Cliff. The cliff face is approximately 30 meters tall. Photograph by John Good, U.S. National Park Service, 1965.

the Yellowstone rhyolites (Hildreth and others, 1991; Stelten and others, 2017).

Downstream from the picnic area, and stratigraphically between the basalt and underlying LCT is the mixed basalt-rhyolite complex of Gardner River (fig. 46). The rhyolite end-member of the mixed complex yields a date of 300.5±2.8 ka from $^{40}Ar/^{39}Ar$ dating of sanidine (Nastanski, 2005). Walk downstream along an unmaintained trail about 250 m and after passing the base of another basaltic cliff the trail will cross a low bluff of weathered rhyolite (spherulitic and lithophysal) at the western margin of the complex. Just past this bluff, the mixed basalt-rhyolite lavas are exposed in outcrops along the trail and in cliffs along the stream bank (fig. 46). We will examine outcrops that are mostly rhyolite with basaltic inclusions (fig. 46). However, the outcrops across the river are mostly basalt with rhyolitic inclusions.

The Gardner River complex has been the target of multiple studies over more than a century because it represents a curious example of direct mixing of basalt and rhyolite at Yellowstone. Note that this mafic-felsic mixing, at least at this scale, is not observed in the intracaldera rhyolites. Only one intracaldera rhyolite has been reported to contain rare mafic inclusions (Christiansen and others, 2007). In one of the earliest studies, Iddings (1899) concluded that the rhyolitic component succeeded the basaltic component and partially fused it, resulting in streaking mixtures of basalt and rhyolite at their contacts. A major flaw with this model is that the rhyolite must be intruded at temperatures above the solidus of the basalt. Later, Fenner (1938, 1944) concluded that the rhyolite flow intruded and dissolved deeply eroded older basalt. Using a combination of detailed mapping and petrography, Wilcox (1944) concluded that the rhyolitic and basaltic components of the complex were both liquid at the time of their joint eruption. He showed that the basalt was chilled against the rhyolite, but never the reverse. Additionally, Wilcox showed that quartz and sanidine xenocrysts in the basalt, interpreted to be derived from the rhyolitic component, occur away from the contact with the rhyolite, indicating the basalt was liquid or at least partly liquid when the two magmas mixed. Hawkes (1945) proposed a model similar to Wilcox (1944), but proposed that mixing occurred on the surface. Boyd (1961) and Struhsacker (1978) concluded that the basaltic and rhyolitic melts variably mixed in a composite feeder, because microphenocrysts in the basaltic portions of the unit are aligned with flow banding and minerals in the rhyolitic groundmass.

Based on observations from the Gardner River complex as well as three nearby locations that also preserve basalt-rhyolite mixing, Pritchard and others (2013) concluded that syneruptive mixing between the basalt and rhyolite occurs because of decompression after the rhyolitic magma body is underplated by a basaltic intrusion (fig. 47). The basalt intrusion causes ascent and decompression of the rhyolitic magma, which in turn decompresses the deeper basalt and leads to decreased density and an ascent rate that would be greater than that for the rhyolite. This inversion would result in coeval eruption and mixing of the basalt and rhyolite (fig. 46). See Pritchard and others (2013) for a more detailed description of this model.

Return to the vehicles and return to the main road (Hwy 89).

41.9 Turn right onto Hwy 89.

47.8 Turn left onto Upper Terrace Loop Drive.

47.9 Turn right towards Mammoth Hot Springs overlook.

48.1 Stop 3.8 Mammoth Hot Springs. Park in one of the parking areas for Mammoth Hot Springs. At this stop we will explore the extensive travertine terraces at Mammoth Hot Springs.

In the foreground to the east is the active part of the Main Terrace of Mammoth Hot Springs. The currently active hot spring area at Mammoth is an elongate depositional mound with an area of nearly 1 km^2, which hosts approximately 100 active hot springs (Bargar, 1978). Unlike the many other hydrothermal areas in Yellowstone that primarily deposit silica, Mammoth Hot Springs is a carbonate depositing system and forms large travertine terraces (fig. 48). In fact, Mammoth Hot Springs is the world's largest carbonate depositing spring system (Fournier and others, 1994). Hot spring waters at Mammoth are generally cooler (~73 °C) than hot spring waters discharging at the geyser basins within Yellowstone caldera (Fournier and others, 1994).

The exposed bedrock in the area consists of Mesozoic sandstones and shales (Pierce and others, 1991; Christiansen, 2001). The Mississippian Mission Canyon Limestone underlies the Mesozoic rocks and is a regional aquifer and likely source for carbon in the thermal waters discharging at Mammoth Hot Springs (Pierce and others, 1991). The location of the hot springs is likely a result of the Gardner syncline and local faults (Pierce and others, 1991). The thermal waters at Mammoth are high in dissolved carbonate and sulfate, and release excess CO_2 as they emerge into the lower pressure at the surface, resulting in travertine, which forms ridge-like mounds above the discharge fractures (Fournier and others, 1994). Water that pools and evaporates around these mounds loses CO_2 to the atmosphere and deposits layers of carbonate (Fournier and others 1994). In 1967–8, approximately 77 m of travertine was cored at Mammoth Hot Springs from U.S. Geological Survey drill hole Y-10 (White and others, 1975). Pierce and others (1991) and Sturchio and others (1994) report uranium-series dates for travertine and found that Mammoth Hot Springs deposits have been active since approximately 8.8 ka, whereas travertine deposits atop Terrace Mountain to the south formed about 375 ka. Drill hole Y-10 is noteworthy because of the high $^3He/^4He$ (R_a=8.4) measured in waters from the hole. These high $^3He/^4He$ ratios indicate the helium is at least partly mantle derived and relatively undiluted by crustal helium (Kharaka and others, 1991). In turn, the helium suggests inputs of magmatic heat and volatiles underneath Mammoth Hot Springs (Kharaka and others, 1991).

Across the Gardner River, the visible cliff side of Mount Everts is capped by a mesa-like section of HRT. This Mount Everts location is noteworthy because the base of HRT member A is well exposed, including an ~2.5-m-thick sequence of

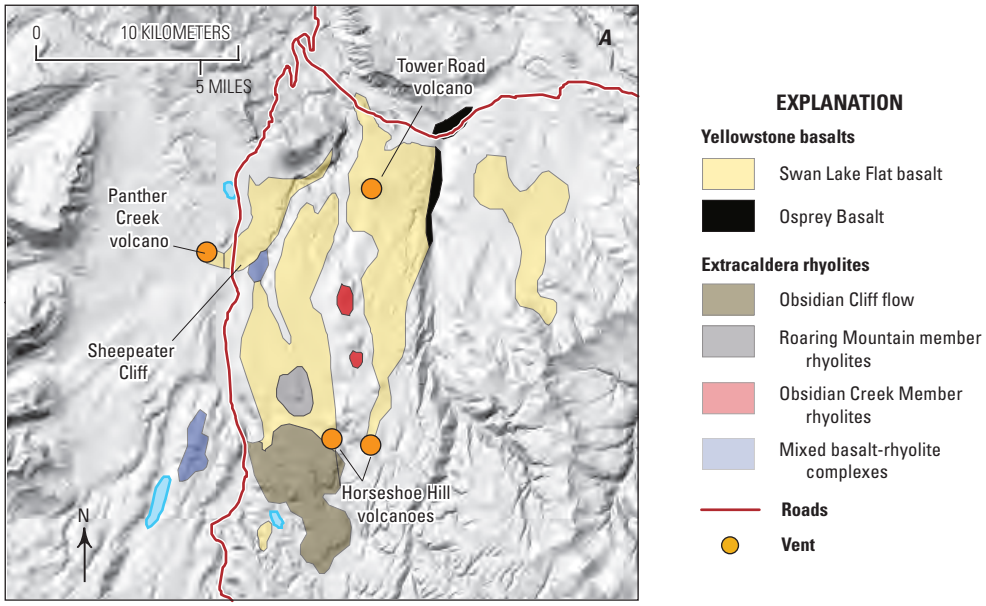

Figure 45. Sheepeater Cliff. *A*, Map of the region around Sheepeater Cliff showing extracaldera basalts, rhyolites, and mixed basalt-rhyolite complexes. The vent locations for the Panther Creek volcano, Tower Road volcano, and Horseshoe Hill volcanoes, which are different eruptions that make up the Swan Lake Flat basalts, are included. Modified from Christiansen and others (2007). Vent location for the Panther Creek volcano is from Bennett (2006). *B*, Photograph of columnar jointed Swan Lake Flat Basalt at Sheepeater Cliffs. Geologist (1.8 meters [m] tall; indicated by yellow circle) is standing at the base of the columnar jointed section of the outcrop. The cliff face of the columnar jointed section is approximately 6 m tall.

Gardner River or Gardiner River?

A careful reader of this field trip guide might notice that references by Fenner (1938, 1944), Hawkes (1945), and Wilcox (1944) use the name Gardiner River, while throughout the field trip guide we use Gardner River. So is it Gardiner River or Gardner River? Well, that depends on when the reference was written.

The U.S. Board on Geographic Names (BGN) is a Federal body created in 1890 to maintain uniform geographic name usage throughout the Federal Government. BGN officially named it Gardiner River in 1930; then in 1960 BGN officially named it Gardner River. So the authors who published before 1960 are correct to use Gardiner River, and authors since 1960 use Gardner River.

Now you know.

Reference Cited

U.S. Board on Geographic Names, 2017, BGN Home: U.S. Board on Geographic Names web page, accessed October 05, 2017 at https://geonames.usgs.gov.

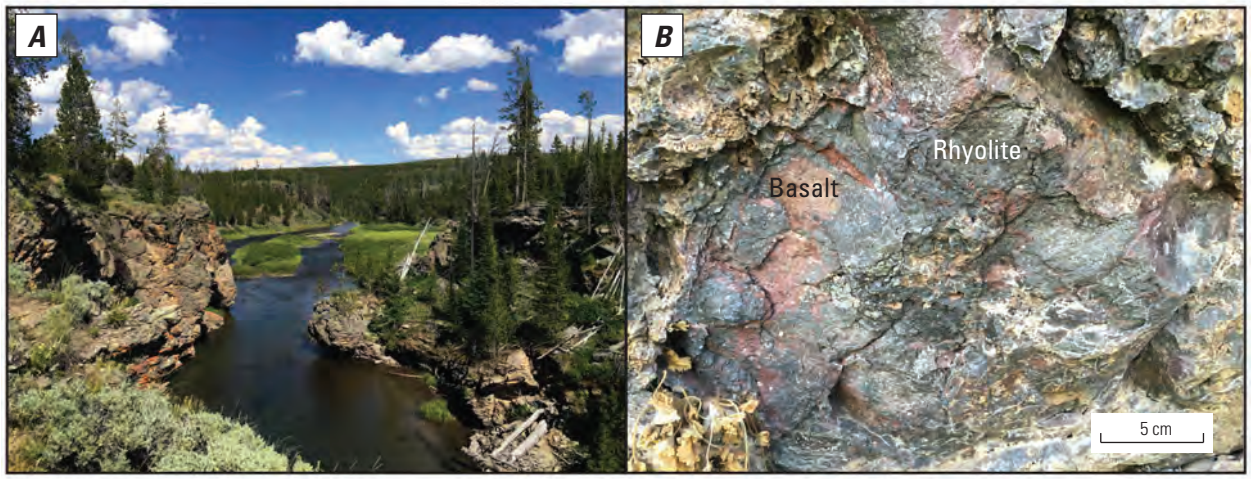

Figure 46. *A*, Photographs of outcrops of the rhyolite-basalt mixed lavas of Gardner River, located downstream of the Sheepeater Cliff parking area. Outcrops in this area are primarily rhyolitic with basaltic inclusions. *B*, Close-up of basalt mixing with rhyolite in the Gardner River complex. Red basalt can be seen hosted in dark obsidian.

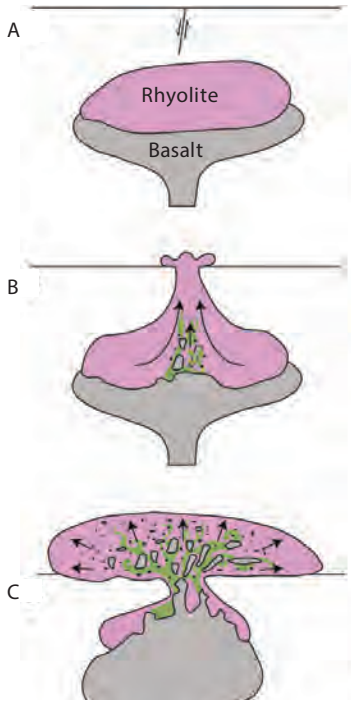

Figure 47. Conceptual model for the formation of mixed basalt-rhyolite complexes at Yellowstone. *A*, A rhyolite magma body is underplated by a basaltic magma body, and both underlie a normal fault. *B*, The rhyolite ascends through the normal fault causing decompression in both the rhyolite and underlying basalt. Rapid decompression of the basaltic magma causes a decrease in the density of the mafic magma. Since the rhyolitic magma has a higher viscosity than the basalt, it is likely that the basaltic magma would rise at a faster rate and initiate mixing. This would allow for coeval eruption and mixing of the basalt and rhyolite. *C*, As the rhyolite flow inflates, basaltic enclaves are pulled into the base of the complex. Modified from Pritchard and others (2013).

continuously bedded and nonwelded fallout marking the start of the HRT eruption (Christiansen, 2001; Myers and others, 2016). The trace element compositions of quartz-hosted glass inclusions, reentrants, and obsidian pyroclasts from this fall deposit suggest the early portions of the HRT eruption tapped multiple cupolas above a larger magma body (Myers and others, 2016).

Head back to the vehicles and return to the main road (Hwy 89).

48.4 Turn right onto Hwy 89 (Grand Loop Road) toward Norris.

80.3 Madison Junction. Turn right on West Entrance Road (Hwy 20) towards the west entrance of the park and the town of West Yellowstone.

93.8 Arrive at the west entrance to Yellowstone National Park. Continue straight to the town of West Yellowstone for lodging.

Figure 48. Time-series photographs of travertine buildup at Narrow Gauge spring, Mammoth Hot Springs. *A*, Photograph taken September 16, 2008. *B*, Photograph taken July 20, 2009. From Housel and others (2010).

Day 4

Overview

On Day 4 we will examine the post-LCT intracaldera volcanism at Yellowstone. Topics to be discussed include the petrogenesis of the post-caldera rhyolites, the mechanisms and timescales of rhyolite generation, the nature of the magma reservoir at Yellowstone caldera, and the different eruptive styles of the post-caldera volcanism. See figures 5 and 49 for maps showing the location of the field-trip stops as well as geologic features of interest.

Day 4 Road Log

0.0 Start at west entrance to Yellowstone National Park. Head east.

13.5 Madison Junction. Turn right and head south on Grand Loop Road toward Old Faithful.

14.0 Turn right onto the one-way Firehole Canyon Drive. This road follows the Firehole River through a canyon with the West Yellowstone flow on the west side of the river and the Nez Perce Creek flow on the east side.

14.4 Stop 4.1 The West Yellowstone flow and models for rhyolite generation at Yellowstone. Pull into turnout on left. To the west across the Firehole River, a dramatic cliff of rhyolite marks the little modified margin of the West Yellowstone flow. The West Yellowstone flow is a Central Plateau Member rhyolite that erupted at 114.0±1.2 ka based on $^{40}Ar/^{39}Ar$ dating (fig. 50; Christiansen and others, 2007). Internal flow layering with variable dip is apparent in these cliff outcrops. The West Yellowstone flow is one of the most voluminous post-caldera eruptions at Yellowstone with a volume of ~40 km^3 (Christiansen and others, 2007). On the east side of the road is the flow margin of the ~6 km^3 Nez Perce Creek flow, which is another Central Plateau Member rhyolite and yields an $^{40}Ar/^{39}Ar$ date of 148.3±5.1 ka (Christiansen and others, 2007).

The Central Plateau Member rhyolites represent the youngest eruptive episode at Yellowstone caldera (from ~170 to ~70 ka; Christiansen, 2001; Christiansen and others, 2007; Stelten and others, 2015). The Central Plateau Member rhyolites were likely erupted episodically in four or five pulses separated by 15 to 30 k.y. (Christiansen and others, 2007), and the West Yellowstone flow and Nez Perce Creek flow represent rhyolites that erupted during different pulses.

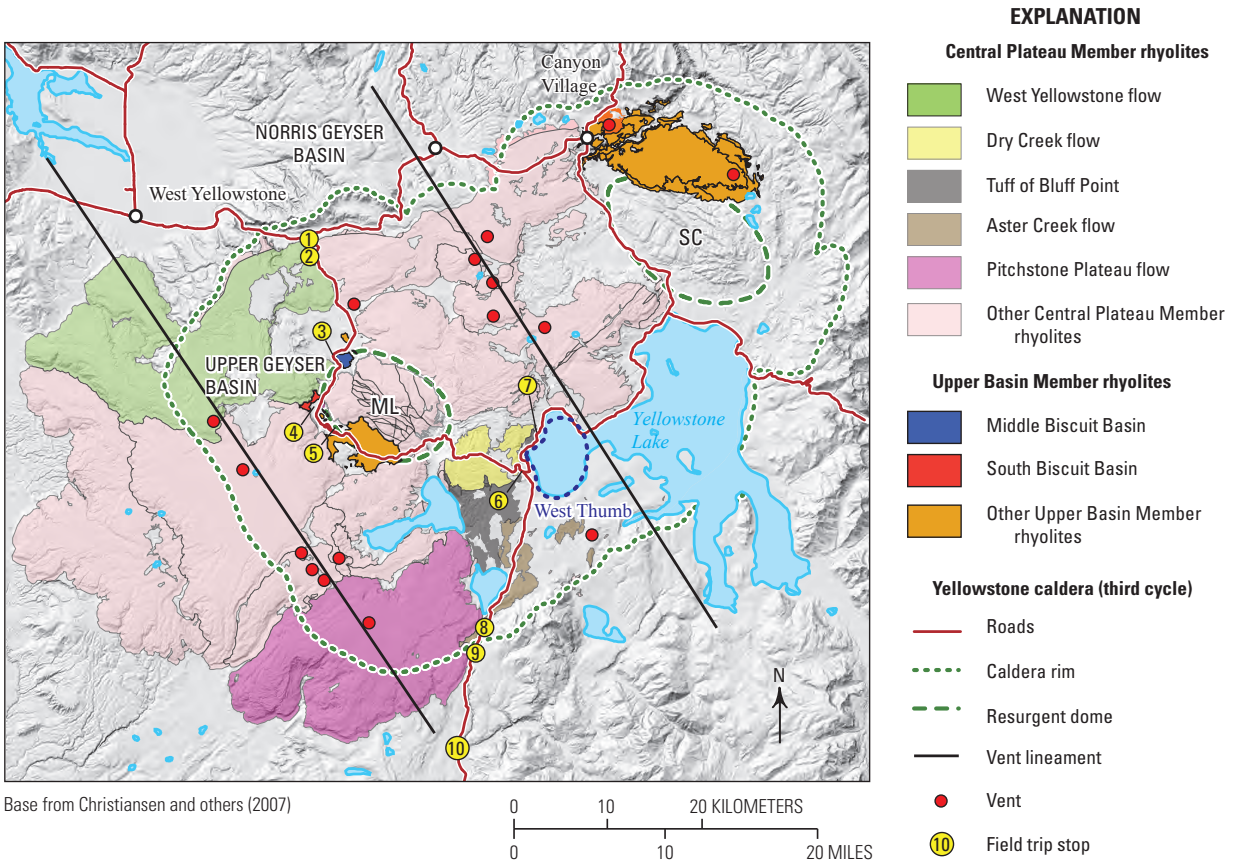

Figure 49. Close-up map of Yellowstone caldera showing major geologic features of interest and the field trip stop locations. Units that are visited on Day 4 of the field trip are highlighted. Vents for the lava flows from the younger Central Plateau Member rhyolites (approximately 170–70 ka) form two linear northwest trending vent zones across the caldera. ML, Mallard Lake resurgent dome; SC, Sour Creek resurgent dome. Modified from Christiansen and others (2007).

The origin and compositional evolution of the Central Plateau Member rhyolites has been the topic of multiple studies over the past decade or so. A key consideration in these studies has been the presence or absence and the source of recycled zircons because they yield important clues about the petrogenesis of Yellowstone rhyolites. Several studies have performed ^{238}U-^{230}Th dating of zircon crystals from the Central Plateau Member rhyolites and initially found contrasting results. Vazquez and Reid (2002) measured ^{238}U-^{230}Th dates for sectioned Central Plateau Member zircon interiors and found the zircons typically have crystallization ages that are tens of thousands of years older than their eruption age, and concluded these zircons record crystallization events that preceded eruption by a similar amount of time (fig. 51). In a later study, Watts and others (2012) similarly dated sectioned Central Plateau Member zircons, albeit for a smaller number of crystals than Vazquez and Reid (2002), but instead found ^{238}U-^{230}Th dates suggesting majority crystallization close to the eruption age (fig. 51). Citing the apparent paucity of antecrystic zircons found by Watts and others (2012), Loewen and Bindeman (2015) concluded that the Central Plateau Member rhyolites were heated above their zircon saturation temperatures prior to eruption (to dissolve pre-existing zircon) and then were cooled to allow crystallization of new zircon shortly before eruption.

Stelten and others (2015) resolved this uncertainty about zircon crystallization and the presence of antecrystic zircons in Central Plateau Member rhyolites by performing detailed 238U-230Th dating and trace-element analysis of crystal surfaces and sectioned interiors for a larger number of zircons than previous studies (fig. 51). The extended range of crystallization ages found by Stelten and others (2015) demonstrate that the interiors (or cores) of zircons from Central Plateau Member rhyolites are typically tens of thousands of years older than their eruption age and thus are antecrysts inherited from older episodes of Yellowstone magmatism, whereas the zircon surfaces crystallized from their host melt shortly before eruption (fig. 51). In addition, they found that Central Plateau zircons record decreasing crystallization temperatures over time (fig. 52). Accordingly, the Central Plateau Member rhyolites could not have been heated above zircon saturation such that preexisting zircons in the source region were entirely dissolved. Instead, material from the preceding episodes of magmatism must have been remobilized by younger Central Plateau Member rhyolite eruptions, and additional zircon growth must have occurred shortly before eruption.

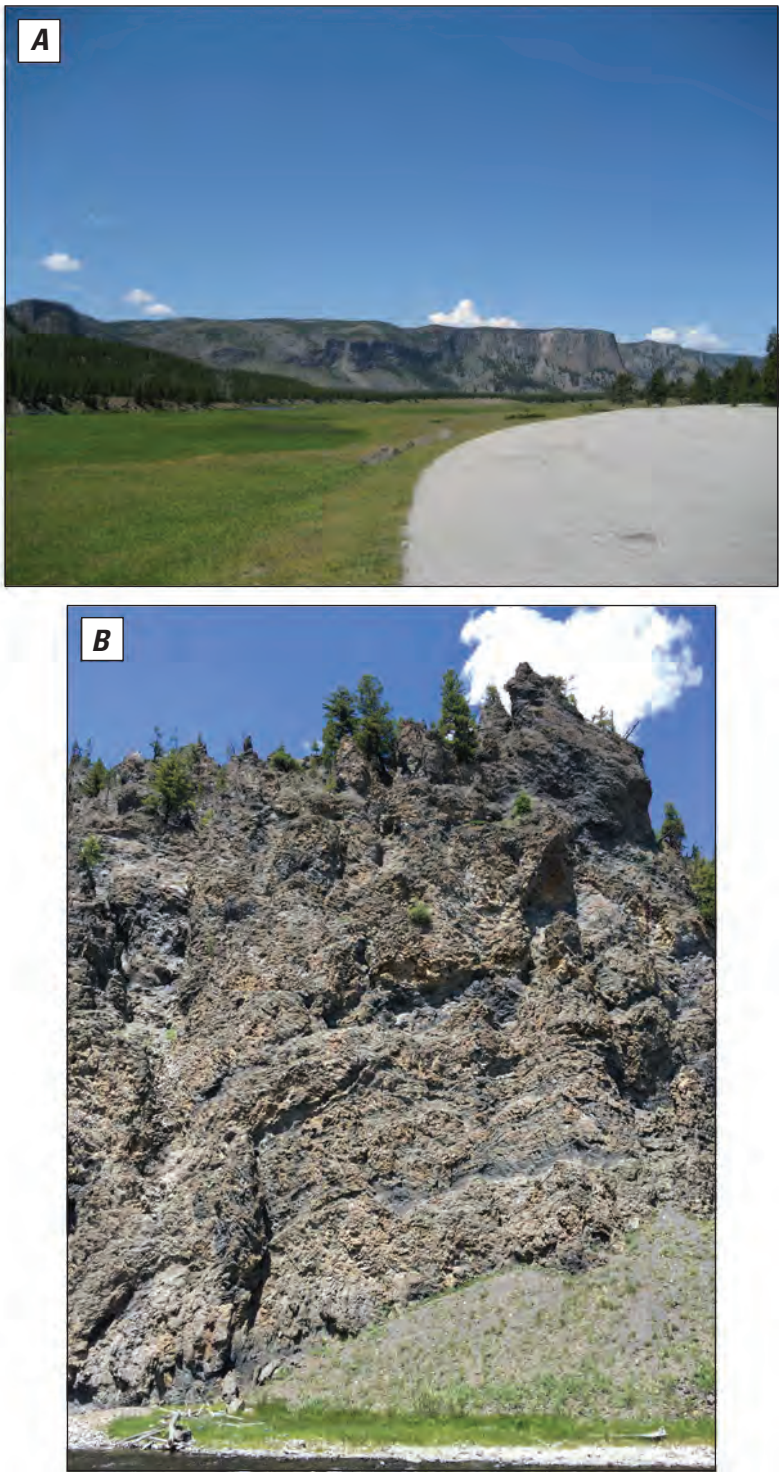

Figure 50. *A*, Cliff exposure of the approximately 114 ka West Yellowstone flow along the Madison River, east-northeast of Stop 4.1. The West Yellowstone flow is part of the most recent eruptive episode at Yellowstone Plateau (approximately 170–70 ka), which produced the Central Plateau Member of the Plateau Rhyolite. In general, the West Yellowstone flow here is approximately 475 meters (m) thick. *B*, West Yellowstone flow exposed along the west side of Firehole Canyon at Stop 4.1. The flow front in this area is approximately 250 m thick.

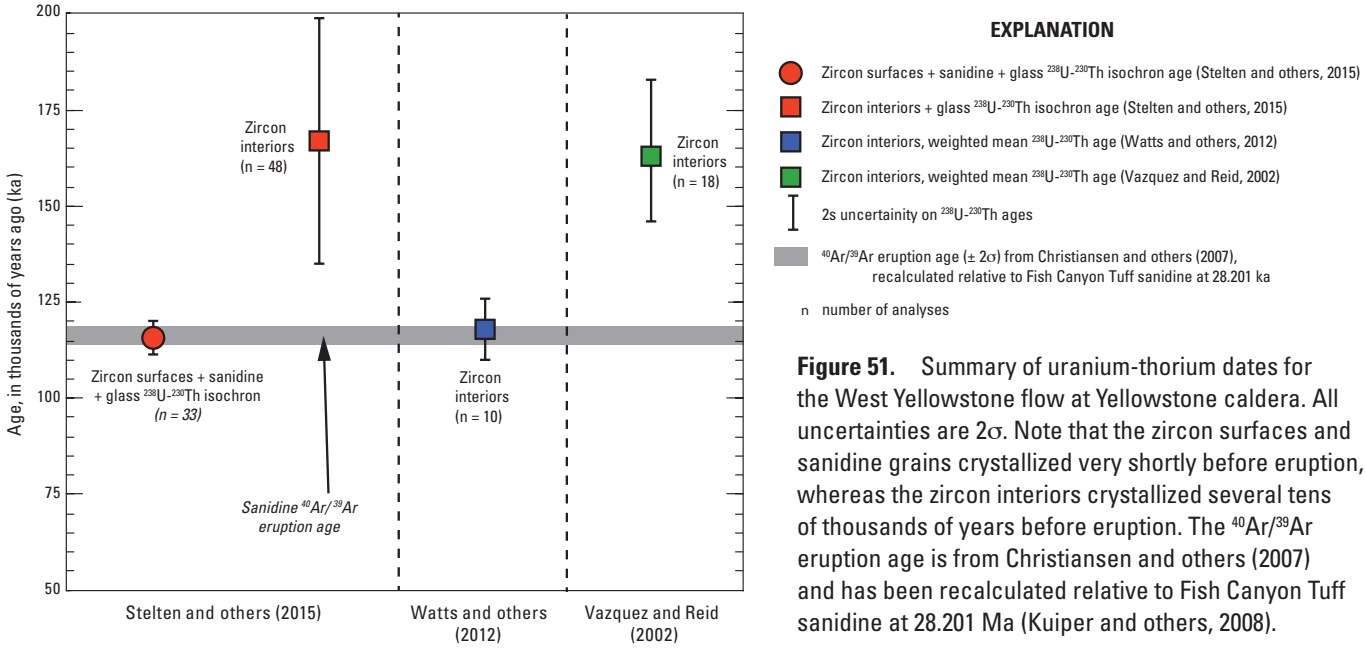

Figure 51. Summary of uranium-thorium dates for the West Yellowstone flow at Yellowstone caldera. All uncertainties are 2σ. Note that the zircon surfaces and sanidine grains crystallized very shortly before eruption, whereas the zircon interiors crystallized several tens of thousands of years before eruption. The $^{40}Ar/^{39}Ar$ eruption age is from Christiansen and others (2007) and has been recalculated relative to Fish Canyon Tuff sanidine at 28.201 Ma (Kuiper and others, 2008).

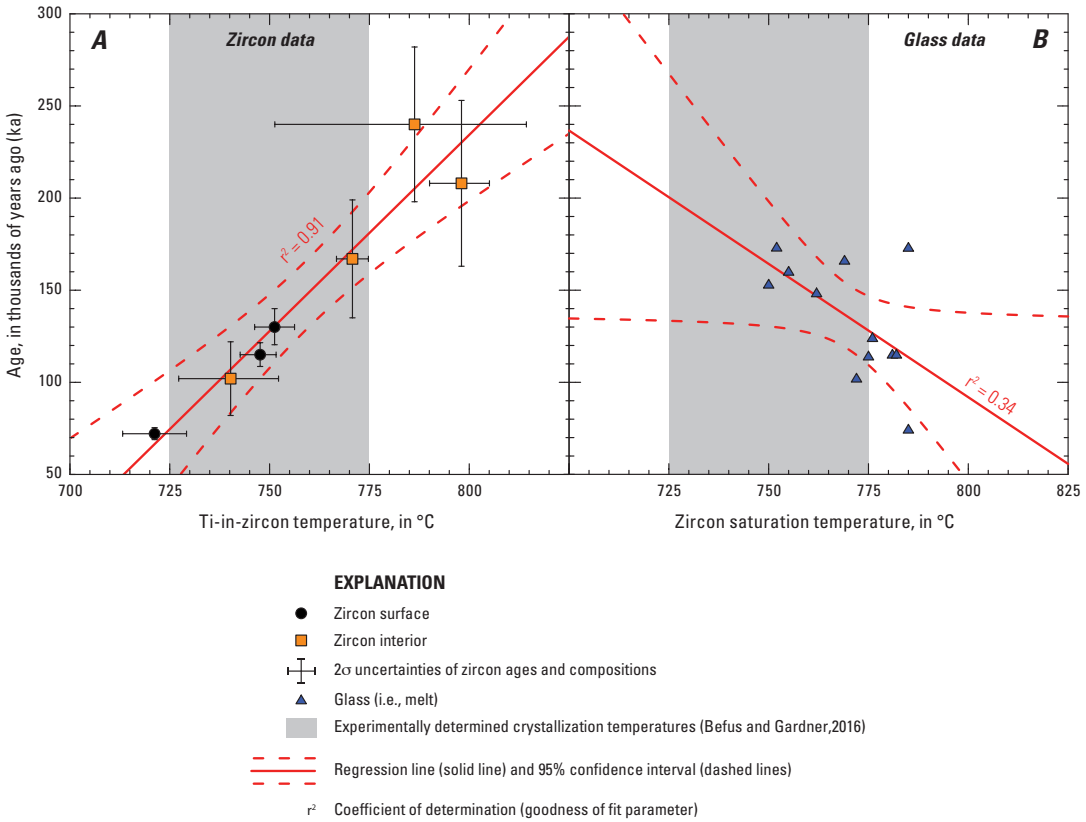

Figure 52. Graphs showing summary of zircon thermometry for the Central Plateau Member rhyolites. *A*, Average zircon ^{238}U-^{230}Th crystallization age versus average titanium-in-zircon crystallization temperature for Central Plateau Member zircons (data from Stelten and others, 2015). Note that the Central Plateau Member zircons display a linear decrease in crystallization temperature with age. The solid red line represents a linear fit to the data and the dashed lines represent the 95 percent confidence intervals on the regression line. *B*, Eruption age (K-Ar or $^{40}Ar/^{39}Ar$) versus zircon saturation temperatures for Central Plateau Member rhyolite glasses. Note that zircon saturation temperatures may show a slight increase though time, although the correlation is weak. The grey field in each graph corresponds to experimentally constrained crystallization temperatures determined for the Central Plateau Member rhyolites by Befus and Gardner (2016).

In addition, Stelten and others (2015) performed ^{238}U-^{230}Th dating of phenocrystic sanidine from the same rhyolites and showed that the sandines crystallized at the same time as the zircon surfaces (within a few thousand years of eruption; fig. 53). Stelten and others (2015) concluded that these data indicate the Central Plateau Member rhyolites were generated by extracting melt and antecrystic zircons from a long-lived (150–250 k.y.) crystal mush, whereas the larger sanidine crystals remain trapped in the locked crystal network (accounting for the lack of inherited sanidine). The extracted melts plus antecrystic zircons are then amalgamated into a liquid-dominated magma body, which resides in the crust for ≤1 k.y. before being erupted. Loewen and Bindeman (2015) provided an alternative model for the petrogenesis of the Central Plateau Member rhyolites based on zircon saturation temperatures (fig. 52), in which the rhyolites are generated by equilibrium melting of a shallow feldspar-rich source region, which may be in mushy or a subsolidus state. In a more recent study, Loewen and others (2017) concluded that the interiors of quartz from the 124 ka (Christiansen and others, 2007) Summit Lake flow are antecrystic and reflect incomplete resorption of crystals recycled from deeper in the magmatic system after an episode of recharge and thermal rejuvenation of intrusions and (or) crystal mush, similar to the Stelten and others (2015) model for CPM zircons. Using titanium-in-quartz geospeedometry, Loewen and others (2017) calculated only years or decades between recycling and eruption.

Continue south on Firehole Canyon Drive.

14.8 Stop 4.2 Marginal flow breccia of the Nez Perce Creek flow and the synglacial West Yellowstone flow. Pull into the turnout on left side of the road in Firehole Canyon. *Be careful for traffic on this narrow road.* The location of the Firehole River Canyon is likely to have been topographically controlled by the contact between the West Yellowstone and Nez Perce flows (Fournier and others, 1994). On the east side of the road behind the turnout, the brecciated flow margin of the Nez Perce Creek flow is exposed in the roadcut. The autoclastic breccia of the flow margin is characterized by many blocks of perlitic rhyolite (fig. 54). This perlitic breccia suggests the margin of the Nez Perce Creek flow contacted a small body of water, causing high-temperature hydration of the rhyolite (Christiansen, 2001; Bindeman and Lowenstern, 2016). Locally, the flow breccia is mingled with larger domains of flow banded rhyolite from the interior of the lava, which reflects dynamic interaction between the viscous and fluid interior of the flow and the outer carapace of quenched and broken blocks (Fournier and others, 1994).

The West Yellowstone flow is noteworthy for its map-scale features, which suggest synglacial emplacement (fig. 54). Large reentrants are apparent on the eastern portion of the West Yellowstone flow, which suggests flow of the rhyolite lava around areas that contained a stagnating or retreating glacier (Christiansen, 2001). Richmond (1986) notes that erratics of basalt are found on the margins of the West Yellowstone rhyolite, but not on its top, consistent with emplacement against a glacier. Given the ~114 ka $^{40}Ar/^{39}Ar$ date, the glacier responsible for the reentrants may reflect glacial advance during the global shift to a cooler climate during substage D of Marine Isotope Stage 5. (Pierce, 2003).

Continue south on Firehole Canyon Drive.

16.2 Turn right onto Hwy 191.

20.1 After crossing Nez Perce Creek, the ~153 ka Elephant Back flow can be seen to the east (left).

21.3 Enter Upper Geyser Basin.

24.3 Stop 4.3 Middle Biscuit Basin flow. Park in the turnout on the left, just past the parking area for Grand Prismatic Spring. To the west is Grand Prismatic Spring, the largest hot spring in the United States.

The forested hill immediately to the east is the Middle Biscuit Basin flow, one of the rhyolites of the Upper Basin Member of the Plateau Rhyolite (Christiansen and Blank, 1972; Christiansen, 2001). Nice exposures of rhyolite occur in the roadcut at the road level. To the south and southeast beyond the Middle Biscuit Basin flow is the uplifted Mallard Lake resurgent dome. Originally mapped as one unit with discontinuous outcrops across the basin, the Biscuit Basin flow is one of the first intracaldera eruptions that followed the caldera collapse associated with the Lava Creek eruption (Christiansen, 2001). Based on differences in geochemistry and geochronology, recent studies have recognized that the original informal Biscuit Basin map unit is actually composed of multiple units, which are now called the South, North and East Biscuit Basin flows (Bindeman and others, 2008; Watts and others, 2011). The original flow is now termed the Middle Biscuit Basin flow, and has yielded a sanidine $^{40}Ar/^{39}Ar$ date of 516±14 ka (Gansecki and others, 1996). Field relations suggest that eruption of the Biscuit Basin rhyolites preceded resurgence. The Upper Basin Member rhyolites are relatively distinct in that they tend to have a greater proportion of plagioclase and more calcic feldspar relative to the older and younger rhyolites of the third cycle (Christiansen, 2001). The Middle Biscuit Basin flow is notable for its low $\delta^{18}O$ melt value of ~1.1‰ (Hildreth and others, 1984; Bindeman and Valley, 2001; Bindeman and others, 2008), and for zircon crystals with diverse oxygen isotope compositions (fig. 55). These zircons typically have high $\delta^{18}O$ values in their cores (similar to LCT and pre-LCT rhyolites) and have low $\delta^{18}O$ values in their rims, which are in equilibrium with their host melt (Bindeman and others, 2008; Watts and others, 2012). The low $\delta^{18}O$ values and zircons with crystallization ages of up to ~2.1 Ma have led to the interpretation that the Middle Biscuit Basin flow was generated by remelting of deeply buried hydrothermally altered intracaldera rocks composed of HRT and pre-LCT Yellowstone rhyolites, or their unerupted equivalents, owing to heating by mafic or silicic magmas that ponded beneath the caldera (Bindeman and others, 2008). This model accounts for

- Low $\delta^{18}O$ melt composition of the Middle Biscuit Basin rhyolite, which is inferred to be derived from melting hydrothermally altered rocks,

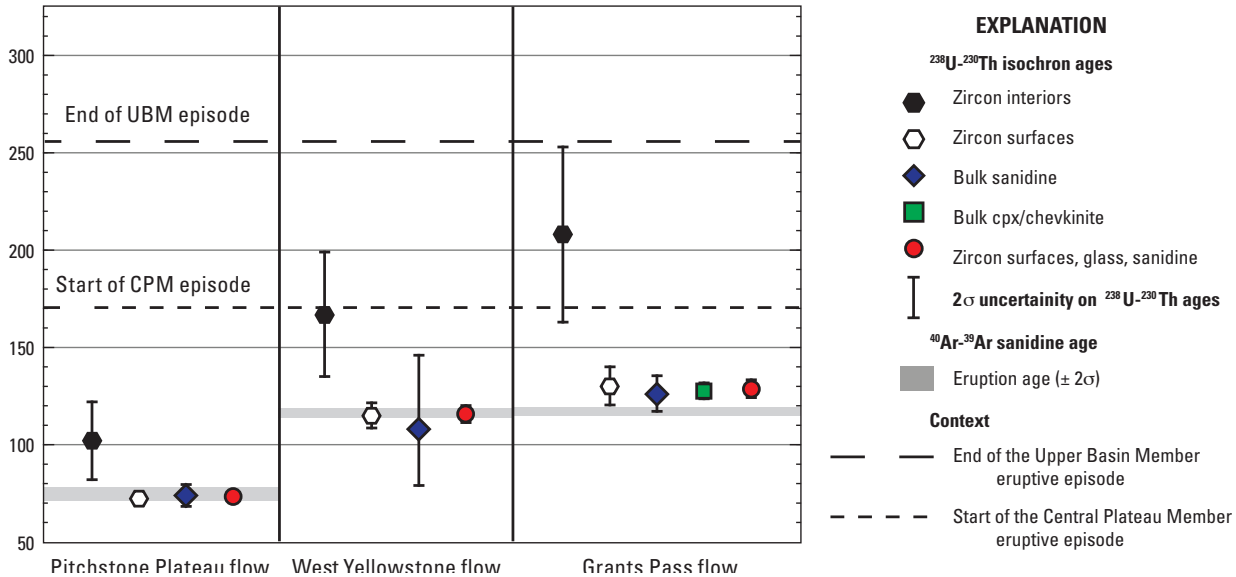

Figure 53. Summary of ages for the Central Plateau Member rhyolites from Stelten and others (2015). The green square in the Grants Pass flow panel corresponds to a ^{238}U-^{230}Th crystallization age measured for a clinopyroxene separate. The horizontal dashed lines denote the timing of the late Upper Basin Member (UBM) rhyolites and the start of the Central Plateau Member (CPM) eruptive episode. Note that for each rhyolite the zircon interiors are tens of thousands of years older than both the eruption age of the host rhyolite and the age of the zircon surfaces and major phases. The $^{40}Ar/^{39}Ar$ eruption ages for the late Upper Basin Member rhyolites are from Bindeman and others (2008) and Christiansen and others (2007). The $^{40}Ar/^{39}Ar$ eruption age for the West Yellowstone flow is from Christiansen and others (2007).

- Presence of inherited zircon cores with high $\delta^{18}O$ that crystallized from pre-LCT melts with originally higher $\delta^{18}O$ (before hydrothermal alteration), and
- Low $\delta^{18}O$ values of the zircon rims, which grew from their low $\delta^{18}O$ host melt.

In support of a remelting origin for the early Upper Basin Member rhyolites is the presence of pyroxenes in the Middle Biscuit Basin flow with exsolution lamellae, which are consistent with recycling of crystals from subsolidus intrusions (Vazquez and others, 2009).

Continue south on Hwy 89/Hwy 20.

27.8 Stop 4.4 The South Biscuit Basin and East Biscuit Basin flows. Turn right into the Biscuit Basin parking area and park. Walk along the boardwalk at the west end of the parking area. This path will take you over the Firehole River and though Biscuit Basin, which has numerous hydrothermal discharge features including hot springs and geysers. Some hydrothermal features to note include Rusty Geyser, Sapphire Pool, Jewel Geyser, Shell Geyser, Avoca Spring, and Mustard Springs. Exit the Biscuit Basin loop at its western end and follow the trail towards Mystic Falls. Hike along this trail for approximately 0.5 mile to an excellent exposure of the South Biscuit Basin flow. The South Biscuit Basin flow has yielded a $^{40}Ar/^{39}Ar$ date of 261±17 ka (Watts and others, 2012) and is part of the Upper Basin Member of the Plateau Rhyolite. To the west, 114 ka West Yellowstone flow overlies the South Biscuit Basin flow and forms a prominent plateau. To the east, the Mallard Lake resurgent dome can be seen. The abundant hydrothermal activity to the southeast is at Upper Geyser Basin.

The South Biscuit Basin flow and the petrographically identical Scaup Lake flow (Till and others, 2015) are part of the formal Upper Basin Member (Christiansen and Blank, 1972), although recent geochemical and geochronologic studies have demonstrated these two rhyolites are transitional in their isotopic composition between early Upper Basin Member and the subsequent Central Plateau Member magmatism (Vazquez and Reid, 2002; Girard and Stix, 2009, 2010; Watts and others, 2012), and yield indistinguishable $^{40}Ar/^{39}Ar$ dates that are ~220 k.y. younger than the next youngest Upper Basin Member rhyolite (Christiansen and others, 2007; Watts and others, 2012). These characteristics suggest a common magma chamber and coeval volcanism for the two flows (Till and others, 2015).

Petrography and mineral compositions indicate that the South Biscuit Basin and Scaup Lake rhyolites were generated, like the older Upper Basin Member rhyolites, by remelting of shallow lithologies. Both rhyolites contain clinopyroxene phenocrysts with cores that display exsolution lamellae, which has been taken to implicate recycling of crystal residue from subsolidus intrusions (Vazquez and others, 2009; Till and others, 2015). In addition, their zircons have heterogeneous $\delta^{18}O$ values, which point to remelting of hydrothermally altered upper crustal rocks (fig. 54; Bindeman and others, 2008; Watts and others, 2012). Several observations suggest that the Scaup Lake and South Biscuit Basin rhyolites were reheated prior to

Figure 54. *A*, Photograph of rhyolitic flow breccia from the approximately 148-ka Nez Perce Creek flow. Outcrop is about 7 meters tall. *B*, Map of West Yellowstone flow showing glacial reentrants and the field trip stops. These reentrants are interpreted to be areas where the movement of ~114 ka West Yellowstone flow was impeded by the presence of a glacier (the lava flowed around the glacier).

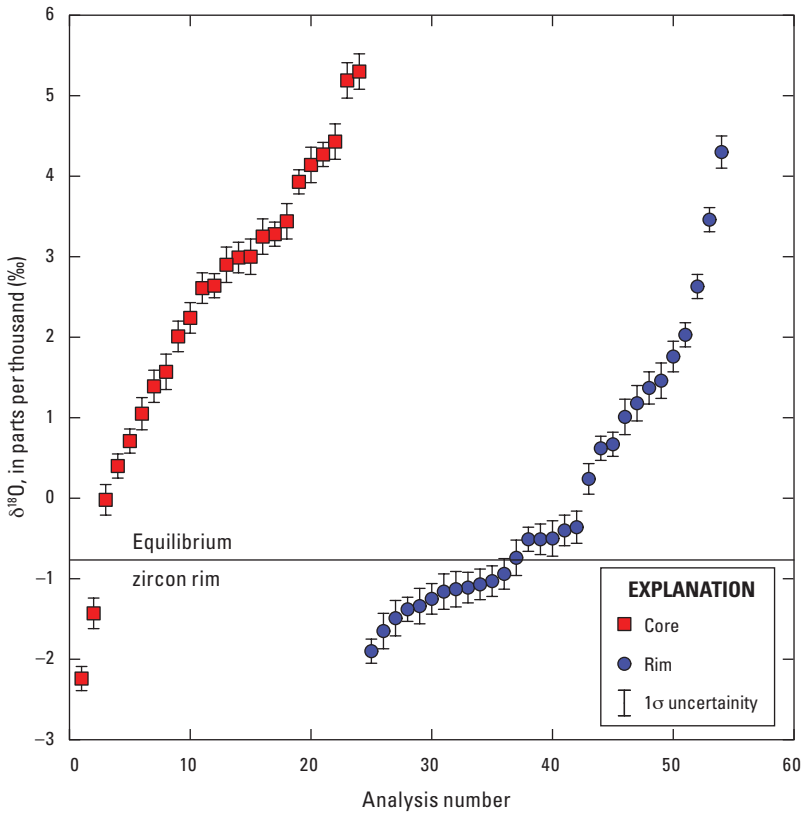

Figure 55. Oxygen isotope data for zircons from the Middle Biscuit Basin flow. The x-axis is arbitrary. Note that zircon cores tend to have higher oxygen isotopic compositions than the zircon rims, and most zircon rims have oxygen isotopic compositions that are in, or close to, equilibrium with their host melt (equilibrium value shown by the horizontal solid line). Data from Bindeman and others (2008).

eruption, likely by the influx of a hotter, less evolved silicic magma, including

- Clinopyroxenes from both rhyolites are reversely zoned with higher magnesium/iron rims than their cores (Vazquez and others, 2009; Till and others, 2015),
- Scaup Lake plagioclase and sanidine phenocrysts have ubiquitous and sharply bounded rims enriched in barium, strontium, and calcium (fig. 56; Till and others, 2015), and
- Scaup Lake quartz crystals have relatively high titanium rims suggesting renewed crystallization from higher temperature silicic magma (Vazquez and others, 2009).

Alternatively, these high titanium rims could reflect magma mixing that resulted in lowered melt titanium activity and in turn increased titanium concentrations in newly grown quartz (Vazquez and others, 2009), the consequence of renewed quartz growth at lower pressures after magma ascent (Thomas and Watson, 2012), accelerated quartz growth rates (Huang and Audetat, 2012), and/or buildup of titanium-rich crystal-melt boundary layers (Pamukcu and others, 2016).

Using geospeedometry, Till and others (2015) quantified the time between rejuvenation and eruption of the Scaup Lake rhyolite at no more than about 40 years because its sanidines do not show diffusional exchange of barium and strontium across the inner boundary of their rims (fig. 56*B*). However, an apparent record of magnesium diffusion across these same boundaries suggests a timescale of only 10 months before eruption (Till and others, 2015). A similar approach has yielded short timescales for other Yellowstone rhyolites. Loewen and others (2017) used the low degree of titanium diffusion across the rim-interior boundaries of antecryst-cored quartz phenocrysts to determine durations as short as 3–5 years between rejuvenation, fractionation, and final eruption and emplacement of the 124-ka Summit Lake flow rhyolite.

In addition to viewing the South Biscuit Basin flow at this location, the East Biscuit Basin flow can be seen as a small, forested hill located approximately 1.2 miles to the southeast. Similar to the other Biscuit Basin flows, the East Biscuit Basin rhyolite is a low $\delta^{18}O$ (~1‰) dome, which erupted near the Mallard Lake resurgent dome. There are currently no published dates for the East Biscuit Basin flow, but it appears to be one of the oldest of the post-LCT rhyolites (Watts and others, 2012). Girard and Stix (2009) first recognized the East Biscuit Basin flow because of its low whole-rock SiO_2 (~70 percent) relative to the other Biscuit Basin rhyolites (>72 percent SiO_2), as well as its lack of quartz and sanidine in the plagioclase-dominated phenocryst assemblage. East Biscuit Basin zircons have a range of $\delta^{18}O$ values that are not in equilibrium with their host melt, suggesting the rhyolite reflects remelting of hydrothermally altered lithologies of pre-LCT age (Watts and others, 2012).

Return to the vehicles and drive back to the main road (Hwy 191/Hwy 20).

28.0 Turn right onto Hwy 191/Hwy 20 towards Old Faithful.

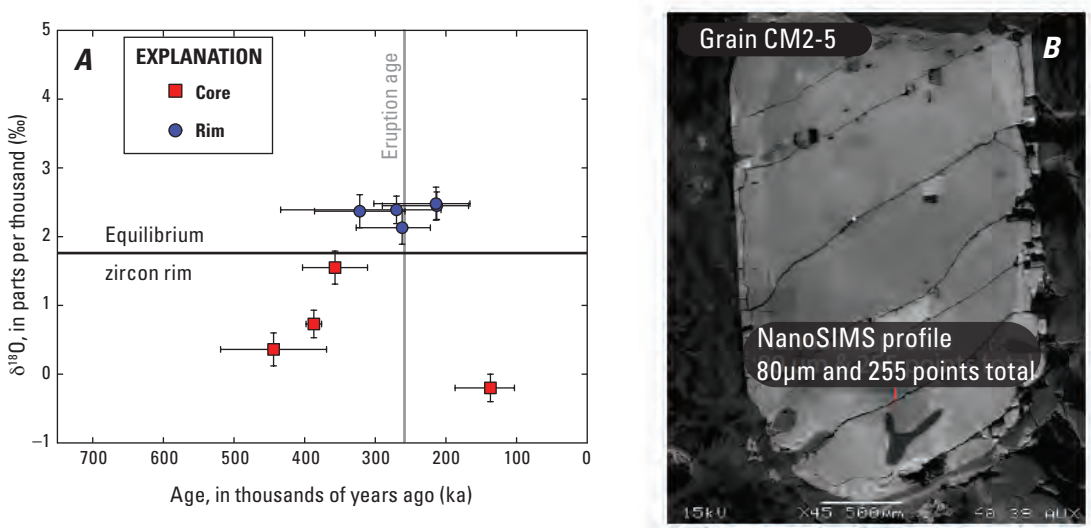

Figure 56. *A*, Graph of oxygen isotopic data versus age for single zircons from the South Biscuit Basin flow. Note that the zircon cores have lower oxygen isotopic compositions than the zircon rims. This suggests the South Biscuit Basin flow was formed by remelting of low $\delta^{18}O$ upper crustal rocks (Bindeman and others, 2008). Graph modified from Watts and others (2012). *B*, Cathodoluminescence image of a sanidine grain from the South Biscuit Basin flow. Note the bright rim on the sanidine. This bright rim is more calcic and has higher concentrations of feldspar compatible trace elements such as strontium and barium than does the crystal core, suggesting growth from a hotter less-fractionated melt. Image modified from Till and others (2015).

28.3 Turnout on right. You can park here and hike along the Daisy Trail (trailhead on the other side of the road) to get to the East Biscuit Basin flow.

29.9 Exit right to Old Faithful.

31.6 Stop 4.5 Old Faithful. No trip to Yellowstone would be complete without observing the most famous geyser in the United States, Old Faithful! Old Faithful typically erupts every 60 minutes to 120 minutes. The prediction of when Old Faithful will erupt is largely dependent on the duration of the previous eruption. Eruptions from Old Faithful range from ~30 to 55 m in height and eruptions normally last 1½ to 5½ minutes (Fournier and others, 1994). Long eruptions are typically followed by long intervals (70–120 minutes) whereas short eruptions are typically followed by shorter intervals (30–65 minutes) (Fournier and others, 1994). We refer the reader to White (1967) and Fournier and others (1994) for detailed descriptions of the hydrothermal systems at Yellowstone.

A variety of food options are available at this stop including the Old Faithful Inn Dining Room, Old Faithful Lodge Cafeteria, and the Obsidian Dining Room. Gift shops are also available.

Return to main road (Hwy 191/Hwy 20) when done.

33.3 Merge south onto Hwy 191/Hwy 20/Grand Loop Road towards Jackson.

41.0 Turnout on right near Isa Lake. The Mallard Lake resurgent dome can be seen to the north.

46.9 Continental divide.

50.6 Stop 4.6 Duck Lake explosion crater. Park where there are turnouts on both sides of the road. To the north-northeast is Duck Lake, a hydrothermal explosion crater just to the west of Yellowstone Lake (fig. 57) and at the edge of the Dry Creek flow, a ~166 ka Central Plateau Member rhyolite. Duck Lake has an average diameter of 617 m and a maximum water depth of 18 m (Christiansen and others, 2007). The crater is rimmed by an explosion breccia composed of silicified clasts of sinter, obsidian, tuff of Bluff Point, lake sediments, and cemented beach sand (Morgan and others, 2009). At Yellowstone, a record of hydrothermal explosions is only preserved for events that occurred after the last glacial cycle (Pierce and others, 2002; Christiansen and others, 2007), and there have been about 20 large post-glacial hydrothermal explosion events (Morgan and others, 2009). Most of the largest hydrothermal explosion craters are found within Yellowstone caldera, but some are located in the Norris-Mammoth corridor (Morgan and others, 2009).

Continue south on Hwy 191/Hwy 20/Grand Loop Road towards Jackson.

51.0 Turn left onto Hwy 20 towards West Thumb.

54.6 Stop 4.7 Tuff of Bluff Point and West Thumb caldera. Park on the shoulder just before a roadcut exposure of the tuff of Bluff Point on the north side of the road. *Be safe and mindful of traffic on this busy road*. If it looks difficult to park here, there is a turnout at 40.9 miles. At this outcrop you can observe the tuff of Bluff Point in contact with the Dry Creek flow (fig. 58), which yield indistinguishable sanidine $^{40}Ar/^{39}Ar$ dates of 173.1±4.9 ka and 166±9 ka respectively (Christiansen and others, 2007). Abundant pumice clasts as well as a gradation in the degree of welding and appearance of fiamme (dark, vitric lenses in welded tuff) can be observed in this outcrop of tuff of Bluff Point. The relative age between

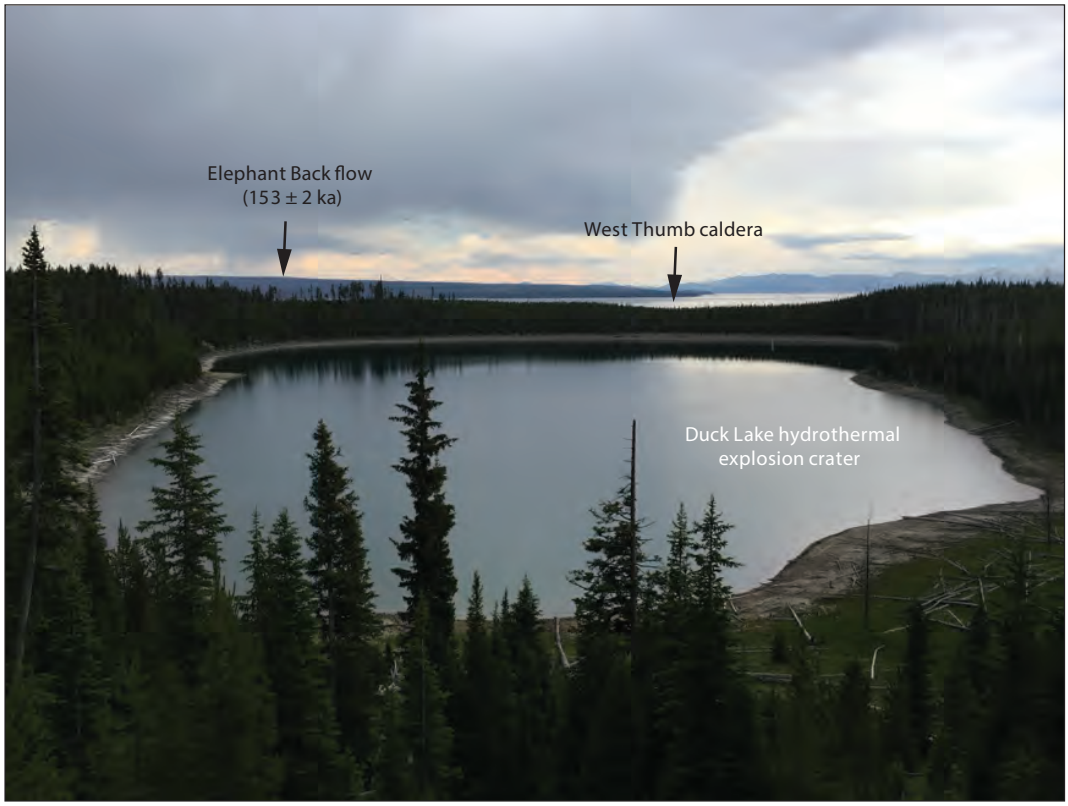

Figure 57. Photograph looking east over Duck Lake, a large Holocene (~6–4 ka) hydrothermal explosion crater. The West Thumb of Yellowstone Lake can be seen in the background. Duck Lake has an average diameter of 617 meters (m) and a maximum water depth of 18 m (Christiansen and others, 2007).

the two units is obscured by slope wash at this roadcut, but mapping has established that the tuff of Bluff Point is stratigraphically younger than the Dry Creek flow (Christiansen, 2001; Christiansen and others, 2007). However, field relations exposed elsewhere between these two units suggest that the tuff of Bluff Point was emplaced onto the Dry Creek flow while it was flowing (Christiansen, 2001). The eruption of the tuff of Bluff Point is thought to have created West Thumb caldera (fig. 49), which is now marked by the West Thumb of Yellowstone Lake (Christiansen, 2001) located southeast of the road. Based on his field observations, Christiansen (2001) suggested that the tuff of Bluff Point could be a late-stage explosive phase from the Dry Creek vent, which appears to have been located where the West Thumb caldera is today.

The tuff of Bluff Point has a volume of ~50 km^3 (Christiansen and others, 2007) and is one of only two Central Plateau Member eruptions that produced extensive pyroclastic deposits (Christiansen, 2001). The other large pyroclastic deposit is the tuff of Cold Mountain Creek, which yields an ^{40}Ar/^{39}Ar date of 143±5 ka (Christiansen and others, 2007) and crops out west of Shoshone Lake in the Yellowstone backcountry. Although small relative to the enormity of Yellowstone caldera, the West Thumb caldera is comparable in size to the caldera forming Crater Lake, Oregon.

Continue heading north-northeast along Hwy 20 and find a place to turn around.

54.9 Turn around using the turnout on the left.

58.3 Turn left onto Hwy 191 towards Jackson.

66.0 Continental divide.

69.7 View of Lewis Lake on the right.

73.5 Stop 4.8 Southern margin of Yellowstone caldera at Lewis Falls (optional stop). Cross Lewis River bridge and park at the turnout on the right. We are located just inside of the southeastern fault scarp of Yellowstone caldera, which trends northeast from this location along the west side of the Red Mountains (Christiansen, 2001). There is no clear topographic expression of the caldera margin west of the Lewis River because the margin has been inundated by the Pitchstone Plateau flow. At this location, the Lewis River cuts into the 155±3 ka (K-Ar date; Obradovich, 1992) Aster Creek flow of the Central Plateau Member and forms Lewis Falls (fig. 59). The Pitchstone Plateau flow forms the skyline to the west.

Continue south along Hwy 191 towards Jackson.

74.7 Stop 4.9 Pitchstone Plateau flow. Park at turnout on left. Here the eastern margin of the Pitchstone Plateau flow can be observed (fig. 60).

The Pitchstone Plateau flow is the largest of the Central Plateau Member rhyolites, with a volume of ~70 km^3 (Christiansen, 2001; Christiansen and others, 2007). The Pitchstone Plateau flow is the youngest rhyolite erupted at Yellowstone and yields a sanidine ^{40}Ar/^{39}Ar eruption age of 74.9±3.4 ka (Stelten and others, 2015). Despite its large volume, the Pitchstone Plateau flow is remarkably homogeneous in its mineral composition and only displays limited trace-element variations in its glass composition (Loewen and Bindeman, 2015).

Stelten and others (2015) performed ^{238}U-^{230}Th dating and trace-element analysis of Pitchstone Plateau zircon crystal surfaces and sectioned crystal interiors (fig. 60). Results from

Figure 58. Panoramic photograph of outcrops of the approximately 173 ka tuff of Bluff Point and ~166 ka Dry Creek flow along Grand Loop Road (U.S. Highway 20). Note geologist at the base of the outcrop for scale. Be careful when walking next to or across the road and watch for traffic.

Figure 59. Photograph of Lewis Falls on the Lewis River. Here, the Lewis River cuts into the approximately 155 ka Aster Creek flow. The waterfall is approximately 9.1 meters (30 feet) tall.

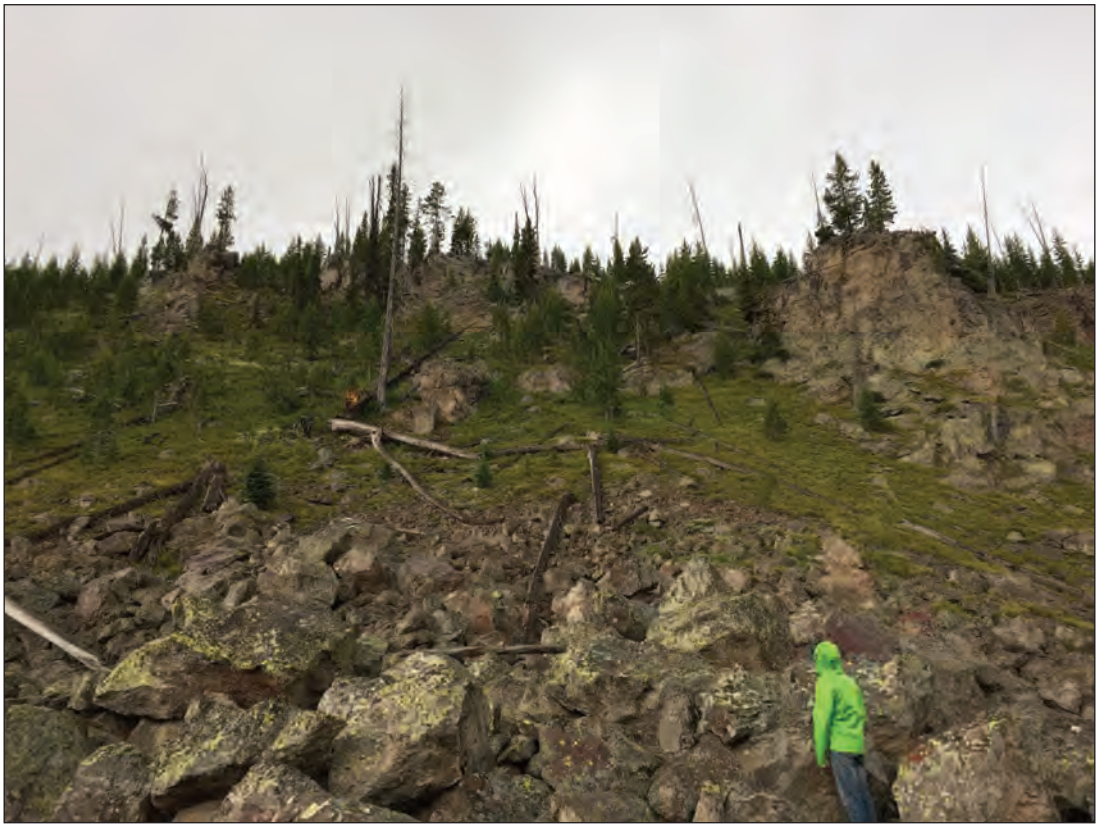

Figure 60. Photograph of a cliff along margin of the ~75 ka Pitchstone Plateau flow. The Pitchstone Plateau flow is the youngest and most voluminous (~70 cubic kilometers) of the post-Lava Creek Tuff intracaldera rhyolites at Yellowstone. The cliff exposure seen from this location is approximately 70 meters tall.

this study demonstrate that the interiors or cores of the Pitchstone Plateau zircons have an average crystallization age of 102±20 ka (Stelten and others, 2015), but the zircon surfaces crystallized shortly before eruption at 72.1±3.2 ka. In addition, Stelten and others (2015) performed ^{238}U-^{230}Th dating of Pitchstone Plateau sanidines and showed that this major phase crystallized at 73.9±5.6 ka and therefore coeval with the zircon surfaces (fig. 53). This same relation was observed for zircons and sanidines from several other Central Plateau Member rhyolites and suggests these rhyolites were derived from a long-lived (~150 k.y.) source region, from which antecrystic zircons are recycled and eruptible bodies of melt-dominated magma only reside for ~1 k.y. before eruption (Stelten and others, 2015).

The range of crystallization ages recorded by the autocrystic and antecrystic domains in zircons from the Pitchstone Plateau flow and other Central Plateau Member rhyolites (Stelten and others, 2015) is greater than observed for zircons from the rhyolites associated with the major caldera-forming eruptions of the three cycles. As described earlier in this guide, multiple studies using different techniques (Rivera and others, 2014; Matthews and others, 2015; 2016; Wotzlaw and others, 2015) reveal zircons in the caldera-forming rhyolites yield crystallization ages that only range to a few tens of thousands of years older than eruption. This difference may indicate the absence of a long-lived source like the one that fed the Central Plateau Member magmas.

Return to the vehicles and continue south on Hwy 191 towards Jackson.

76.6 LCT is exposed in roadcuts and across the river.

82.2 Stop 4.10 Moose Falls flow. Park in the turnout on the left side of the road just before Moose Falls. We will walk down a short trail to view the Moose Falls rhyolite flow at Moose Falls (fig. 61). The Moose Falls flow is somewhat unique because it is the only young extracaldera rhyolite located southeast of Yellowstone caldera although it lies just within the first-cycle caldera margin (Christiansen, 2001). The rhyolite exposed at the falls is a spherulitic vitrophyre, which locally displays flow layering that fans upward, suggesting flow to the east (Bonnichsen and others, 1989). This rhyolite has yielded a sanidine $^{40}Ar/^{39}Ar$ date of 80.6±4.6 ka (Christiansen and others, 2007). Despite its location outside of

Figure 61. Photograph of Moose Falls flow exposed at Moose Falls on Crawfish Creek. The approximately 81 ka Moose Falls flow is a unit of the Central Plateau Member rhyolites even though it erupted outside of Yellowstone caldera. It is worth noting that the Moose Falls flow erupted near the first-cycle caldera margin. Moose Falls is approximately 9.1 meters (30 feet) tall.

Yellowstone caldera, the Moose Falls flow is considered to be a unit of the Central Plateau Member (Christiansen and others, 2007). The Moose Falls flow appears to have erupted along an extension of the northwest-southeast trending lineament of Central Plateau Member vents within the western portion of Yellowstone caldera. An affinity to the Central Plateau Member rhyolites is supported by a hafnium isotopic composition of -5.83 ε_{Hf}, which is within the -6.36 to -5.69 ε_{Hf} range of hafnium isotope compositions that characterize Central Plateau Member rhyolites (Stelten and others, 2017).

Continue south on Hwy 191 towards Jackson.

83.5 Southern entrance to Yellowstone National Park.

90.4 Enter Grand Teton National Park.

106.4 Park at the turnout on the right for an excellent view of the Grand Tetons.

140.8 Enter Jackson, Wyoming. Find hotel for the night.

References Cited

Abedini, A.A., van Soest, M., Hurwitz, S., and Kennedy, B.M., 2006, Helium isotopes in basalt-hosted olivines from the Yellowstone Plateau—Implications on volcanic processes: EOS, Transactions of the American Geophysical Union, v. 87, no., 52, Fall Meeting Supplement, Abstract V51D-1700.

Anders, M.H., Geissman, J.W., Piety, L.A., and Sullivan, J.T., 1989, Parabolic distribution of circumeastern Snake River Plain seismicity and latest Quaternary faulting—Migratory pattern and association with the Yellowstone hotspot: Journal of Geophysical Research—Solid Earth, v. 94, no. B2, p. 1589–1621, https://doi.org/10.1029/JB094iB02p01589.

Anders, M.H., Rodgers, D.W., Hemming, S.R., Saltzman, J., DiVenere, V.J., Hagstrum, J.T., Embree, G.F., and Walter, R.C., 2014, A fixed sublithospheric source for the late Neogene track of the Yellowstone hotspot—Implications of the Heise and Picabo volcanic fields: Journal of Geophysical Research—Solid Earth, v. 119, no. 4, p. 2871–2906, https://doi.org/10.1002/2013JB010483.

Bargar, K.E., 1978, Geology and thermal history of Mammoth Hot Springs, Yellowstone National Park, Wyoming: U.S. Geological Survey Bulletin 1444, 55 p., https://pubs.er.usgs.gov/publication/b1444.

Befus, K.S., and Gardner, J.E., 2016, Magma storage and evolution of the most recent effusive and explosive eruptions from Yellowstone Caldera: Contributions to Mineralogy and Petrology, v. 171, no. 4, p. 1–19, https://doi.org/10.1007/s00410-016-1244-x.

Bennett, K.M., 2006, Petrogenesis of Pleistocene basalts in the Norris-Mammoth Corridor, Yellowstone National Park: Las Vegas, University of Nevada, M.S. thesis, 123 p., 1 pl., http://digitalscholarship.unlv.edu/cgi/viewcontent.cgi?article=2119&context=thesesdissertations.

Bindeman, I.N., Fu, B., Kita, N.T., and Valley, J.W., 2008, Origin and evolution of silicic magmatism at Yellowstone based on ion microprobe analysis of isotopically zoned zircons: Journal of Petrology, v. 49, no. 1, p. 163–193, https://doi.org/10.1093/petrology/egm075.

Bindeman, I.N. and Lowenstern, J.B., 2016. Low-δD hydration rinds in Yellowstone perlites record rapid syneruptive hydration during glacial and interglacial conditions: Contributions to Mineralogy and Petrology, v. 171, p. 89, https://link.springer.com/article/10.1007/s00410-016-1293-1

Bindeman, I.N., and Simakin, A.G., 2014, Rhyolites—Hard to produce, but easy to recycle and sequester—Integrating microgeochemical observations and numerical models: Geosphere, v. 10, no. 5, p. 930–957, https://doi.org/10.1130/GES00969.1.

Bindeman, I.N., and Valley, J.W., 2001, Low-$\delta^{18}O$ rhyolites from Yellowstone—Magmatic evolution based on analyses of zircons and individual phenocrysts: Journal of Petrology, v. 42, no. 8, p. 1491–1517, https://doi.org/10.1093/petrology/42.8.1491.

Bindeman, I.N., Watts, K.E., Schmitt, A.K., Morgan, L.A., and Shanks, P.W., 2007, Voluminous low $\delta^{18}O$ magmas in the late Miocene Heise volcanic field, Idaho—Implications for the fate of Yellowstone hotspot calderas: Geology, v. 35, no. 11, p. 1019–1022, https://doi.org/10.1130/G24141A.1.

Bonnichsen, Bill, Christiansen, R.L., Morgan, L.A., Moye, F.J., Hackett, W.R., Leeman, W.P., Honjo, Norio, Jenks, M.D., and Godchaux, M.M., 1989, Excursion 4A—Silicic volcanic rocks in the Snake River Plain–Yellowstone Plateau province, in Chapin, C.E., and Zidek, Jiri, eds., Field excursions to volcanic terranes in the western United States: New Mexico Bureau of Mines and Mineral Resources Memoir 47, p. 135–182.

Boyd, F.R., 1961,Welded tuffs and flows in the rhyolite plateau of Yellowstone Park, Wyoming: Geological Society of America Bulletin, v. 72, no. 3, p. 387–426, https://doi.org/10.1130/0016-7606(1961)72[387:WTAFIT]2.0.CO;2.

Breitkreuz, Christoph, 2013, Spherulites and lithophysae–200 years of investigation on high-temperature crystallization domains in silica-rich volcanic rocks: Bulletin of Volcanology, v. 75, no. 4, p. 705–721, https://doi.org/10.1007/s00445-013-0705-6.

Camp, V.E., 1995, Mid-Miocene propagation of the Yellowstone mantle plume head beneath the Columbia River basalt source region: Geology, v. 23, no. 5, p. 435–438, https://doi.org/10.1130/0091-7613(1995)023<0435:MMPOTY>2.3.CO;2.

Cheng, Hai, Edwards, R.L., Shen, C.-C., Polyak, V.J., Asmerom, Yemane, Woodhead, Jon, Hellstrom, John, Wang, Yongjin, Kong, Xinggong, Spötl, Christoph, and Wang, Xianfeng, 2013, Improvements in ^{230}Th dating, ^{230}Th and ^{234}U half-life values, and U–Th isotopic measurements by multi-collector inductively coupled plasma mass spectrometry: Earth and Planetary Science Letters, v. 371, p. 82–91, https://doi.org/10.1016/j.epsl.2013.04.006.

Christiansen, R.L., 1982, Late Cenozoic volcanism of the Island Park area, eastern Idaho, in Bonnichsen, Bill, and Breckenridge, R.M., eds., Cenozoic geology of Idaho: Idaho Bureau of Mines and Geology Bulletin 26, p. 345–368, http://geology.isu.edu/Digital_Geology_Idaho/papers/B-26ch6-2.pdf.

Christiansen, R.L., 1984, Yellowstone magmatic evolution—Its bearing on understanding large-volume explosive volcanism, *in* Boyd, F.R., ed., Explosive volcanism—Inception, evolution, and hazards: Washington, D.C., National Academy of Sciences, p. 84–95.

Christiansen, R.L., 2001, The Quaternary and Pliocene Yellowstone Plateau Volcanic Field of Wyoming, Idaho, and Montana: U.S. Geological Survey Professional Paper 729-G, 120 p., https://pubs.er.usgs.gov/publication/pp729G.

Christiansen, R.L., and Blank, H.R., Jr., 1972, Volcanic stratigraphy of the Quaternary rhyolite plateau in Yellowstone National Park: U.S. Geological Survey Professional Paper 729-B, 17 p., https://pubs.er.usgs.gov/publication/pp729B.

Christiansen, R.L., and Embree, G.F., 1987, Island Park, Idaho—Transition from rhyolites of the Yellowstone Plateau to basalts of the Snake River Plain, *in* Beus, S.S., ed., Rocky Mountain Section of the Geological Society of America—Centennial Field Guide Volume 2: Boulder, Colo., Geological Society of America, p. 103–108.

Christiansen, R.L., Foulger, G.R., and Evans, J.R., 2002, Upper-mantle origin of the Yellowstone hotspot: Geological Society of America Bulletin, v. 114, no. 10, p. 1245–1256, https://doi.org/10.1130/0016-7606(2002)114<1245:UMOOTY>2.0.CO;2.

Christiansen, R.L., and Hutchinson, R.A., 1987, Rhyolite-basalt volcanism of the Yellowstone Plateau and hydrothermal activity of Yellowstone National Park, Wyoming, *in* Beus, S.S., ed., Rocky Mountain Section of the Geological Society of America—Centennial Field Guide Volume 2: Boulder, Colo., Geological Society of America, p. 165–172.

Christiansen, R.L., Lowenstern, J.B., Smith, R.B., Heasler, Henry, Morgan, L.A., Nathenson, Manuel, Mastin, L.G., Muffler, L.J.P., and Robinson, J.E., 2007, Preliminary assessment of volcanic and hydrothermal hazards in Yellowstone National Park and vicinity: U.S. Geological Survey Open-File Report 2007–1071, 94 p., https://pubs.er.usgs.gov/publication/ofr20071071.

Coble, M.A., and Mahood, G.A., 2012, Initial impingement of the Yellowstone plume located by widespread silicic volcanism contemporaneous with Columbia River flood basalts: Geology, v. 40, no. 7, p. 655–658, https://doi.org/10.1130/G32692.1.

Dallegge, T.A., 2008, ^{40}Ar/^{39}Ar Geochronology of lavas from the Central Plateau Member of Plateau Rhyolite with implications for magma residence times and eruptive reoccurrence intervals, Yellowstone National Park: The Mountain Geologist, v. 45, no. 3, p. 77–98, http://archives.datapages.com/data/mountain-geologist-rmag/data/045/045003/77_rmag-mg450077.htm.

Doe, B.R., Leeman, W.P., Christiansen, R.L., and Hedge, C.E., 1982, Lead and strontium isotopes and related trace elements as genetic tracers in the Upper Cenozoic rhyolite-basalt association of the Yellowstone Plateau Volcanic Field: Journal of Geophysical Research—Solid Earth, v. 87, no. B6, p. 4785–4806, http://onlinelibrary.wiley.com/doi/10.1029/JB087iB06p04785/full.

Ellis, B.S., Mark, D.F., Pritchard, C.J., and Wolff, J.A., 2012, Temporal dissection of the Huckleberry Ridge Tuff using the 40Ar/39Ar dating technique: Quaternary Geochronology, v. 9, p. 34–41, https://doi.org/10.1016/j.quageo.2012.01.006.

Ellis, B.S., Mark, D.F., Troch, J., Bachmann, O., Guillong, M., Kent, A.J.R., and von Quadt, A., 2017b, Split-grain ^{40}Ar/^{39}Ar dating—Integrating temporal and geochemical data from crystal cargoes: Chemical Geology, v. 457, p. 15–23, https://doi.org/10.1016/j.chemgeo.2017.03.005.

Ellis, B.S., Szymanowski, D., Wotzlaw, J.F., Schmitt, A.K., Bindeman, I.N., Troch, J., Harris, C., Bachmann, O., and Guillong, M., 2017a, Post-caldera volcanism at the Heise volcanic field— Implications for petrogenetic models: Journal of Petrology, v. 58, no. 1, p. 115–136, https://doi.org/10.1093/petrology/egx007.

Embree, G.F., and Hoggan, R.D., 1999, Secondary deformation within the Huckleberry Ridge Tuff and subjacent Pliocene units near the Teton Dam—Road log to the regional geology of the eastern margin of the Snake River Plain, Idaho, *in* Hughes, S.S., and Thackray, G.D., eds., Guidebook to the Geology of Eastern Idaho: Pocatello, Idaho, Idaho Museum of Natural History, p. 181–203, http://geology.isu.edu/Digital_Geology_Idaho/papers/gsac3p11.pdf.

Farrell, Jamie, Smith, R.B., Husen, Stephan, and Diehl, Tobias, 2014, Tomography from 26 years of seismicity revealing that the spatial extent of the Yellowstone crustal magma reservoir extends well beyond the Yellowstone caldera: Geophysical Research Letters, v. 41, no. 9, p. 3068–3073, https://doi.org/10.1002/2014GL059588.

Fenner, C.N., 1938, Contact relations between rhyolite and basalt on Gardiner River, Yellowstone Park: Geological Society of America Bulletin, v. 49, no. 9, p. 1441–1484, https://doi.org/10.1130/GSAB-49-1441.

Fenner, C.N., 1944, Rhyolite-basalt complex on Gardiner river, Yellowstone Park, Wyoming—A discussion: Geological Society of America Bulletin, v. 55, no. 9, p. 1081–1096, https://doi.org/10.1130/GSAB-55-1081.

Fournier, R.O., Christensen, R.L., Hutchinson, R.A., and Pierce, K.L., 1994, A field-trip guide to Yellowstone National Park, Wyoming, Montana, and Idaho—Volcanic, hydrothermal, and glacial activity in the region: U.S. Geological Survey Bulletin 2099, 46 p., https://pubs.er.usgs.gov/publication/b2099.

Gansecki, C.A., 1998, $^{40}Ar/^{39}Ar$ geochronology and pre-eruptive geochemistry of the Yellowstone Plateau volcanic field rhyolites: Stanford, Calif., Stanford University, Ph.D. dissertation, 203 p.

Gansecki, C.A., Mahood, G.A., and McWilliams, M.O., 1996, $^{40}Ar/^{39}Ar$ geochronology of rhyolites erupted following collapse of the Yellowstone caldera, Yellowstone Plateau volcanic field— Implications for crustal contamination: Earth and Planetary Science Letters, v. 142, no. 1–2, p. 91–107, https://doi.org/10.1016/0012-821X(96)00088-X.

Gansecki, C.A., Mahood, G.A., and McWilliams, M., 1998, New ages for the climactic eruptions at Yellowstone—Single-crystal $^{40}Ar/^{39}Ar$ dating identifies contamination: Geology, v. 26, no. 4, p. 343–346, https://doi.org/10.1130/0091-7613(1998)026<0343:NAFTCE>2.3.CO;2.

George, A.R., Moore, D.K., Embree, G.F., Champion, D.E., Kuntz, M.A., and Leishman, B., 2015, Origin of lava benches and Upper and Lower Mesa Falls in the Henrys Fork and Warm River canyons, Island Park, Idaho: Geological Society of America Abstracts with Programs, v. 47, no. 6, p. 4, https://gsa.confex.com/gsa/2015RM/webprogram/Paper256048.html.

Girard, Guillaume, and Stix, John, 2009, Magma recharge and crystal mush rejuvenation associated with early post-collapse Upper Basin Member rhyolites, Yellowstone caldera, Wyoming: Journal of Petrology, v. 50, no. 11, p. 2095–2125, https://doi.org/10.1093/petrology/egp070.

Girard, Guillaume, and Stix, John, 2010, Rapid extraction of discrete magma batches from a large differentiating magma chamber—The Central Plateau Member rhyolites, Yellowstone Caldera, Wyoming: Contributions to Mineralogy and Petrology, v. 160, no. 3, p. 441–465, https://doi.org/10.1007/s00410-009-0487-1.

Girard, Guillaume, and Stix, John, 2012, Future volcanism at Yellowstone caldera: Insights from geochemistry of young volcanic units and monitoring of volcanic unrest: GSA Today, v. 22, p. 4-10.

Graham, D.W., Reid, M.R., Jordan, B.T., Grunder, A.L., Leeman, W.P., and Lupton, J.E., 2009, Mantle source provinces beneath the northwestern USA delimited by helium isotopes in young basalts: Journal of Volcanology and Geothermal Research, v. 188, no. 1–3, p. 128–140, https://doi.org/10.1016/j.jvolgeores.2008.12.004.

Hamilton, Warren, 1965. Geology and petrogenesis of the Island Park caldera of rhyolite and basalt, eastern Idaho: U.S. Geological Survey Professional Paper 504-C, 37 p., https://pubs.er.usgs.gov/publication/pp504C.

Hawkes, L., 1945, The Gardiner River rhyolite-basalt complex: Geological Magazine, v. 82, no. 4, p. 182–184, https://doi.org/10.1017/S0016756800081899.

Hildreth, Wes, 1981, Gradients in silicic magma chambers—Implications for lithospheric magmatism: Journal of Geophysical Research—Solid Earth, v. 86, no. B11, p. 10153–10192, https://doi.org/10.1029/JB086iB11p10153.

Hildreth, Wes, Christiansen, R.L., and O'Neil, J.R., 1984, Catastrophic isotopic modification of rhyolitic magma at times of caldera subsidence, Yellowstone Plateau volcanic field: Journal of Geophysical Research—Solid Earth, v. 89, no. B10, p. 8339–8369, https://doi.org/10.1029/JB089iB10p08339.

Hildreth, Wes, Halliday, A.N., and Christiansen, R.L., 1991, Isotopic and chemical evidence concerning the genesis and contamination of basaltic and rhyolitic magma beneath the Yellowstone Plateau volcanic field: Journal of Petrology, v. 32, no. 1, p. 63–138, https://doi.org/10.1093/petrology/32.1.63.

Houseal, A.K., Fouke, B.W., Sanford, Robert, Fuhrmann, Robert, and Petrick, Ellen, 2010, Mammoth Hot Springs: Yellowstone Science, v. 18, no. 3, p. 7–14, http://repository.uwyo.edu/coe_facpub/23/.

Huang, H.-H., Lin, F.-C., Schmandt, Brandon, Farrell, Jamie, Smith, R.B., and Tsai, V.C., 2015, The Yellowstone magmatic system from the mantle plume to the upper crust: Science, v. 348, no. 6236, p. 773–776, https://doi.org/10.1126/science.aaa5648.

Huang, Ruifang, and Audétat, Andreas, 2012, The titanium-in-quartz (TitaniQ) thermobarometer—A critical examination and re-calibration: Geochimica et Cosmochimica Acta, v. 84, p. 75–89, https://doi.org/10.1016/j.gca.2012.01.009.

Humphreys, E.D., Dueker, K.G., Schutt, D.L., and Smith, R.B., 2000, Beneath Yellowstone—Evaluating plume and nonplume models using teleseismic images of the upper mantle: GSA Today, v. 10, no. 12, p. 1–7, http://pages.uoregon.edu/ghump/papers/yellowstone_gsatoday.pdf.

Hurwitz, Shaul, and Lowenstern, J.B., 2014, Dynamics of the Yellowstone hydrothermal system: Reviews of Geophysics, v. 52, no. 3, p. 375–411, https://doi.org/10.1002/2014RG000452.

Iddings, J.P., 1888, Obsidian Cliff, Yellowstone National Park: U.S. Geological Survey 7th Annual Report, p. 249–295.

Iddings, J.P., 1899, The rhyolites, *in* Hague, Arnold, Iddings, J.P. Weed, W.H., Walcott, C.D., Girty, G.H., Stanton, T.W., and Knowlton, F.H., Geology of the Yellowstone National Park: U.S. Geological Survey Monograph 32, Part 2, p. 356-432.

Izett, G.A., 1981, Volcanic ash beds—Recorders of upper Cenozoic silicic pyroclastic volcanism in the western United States: Journal of Geophysical Research—Solid Earth, v. 86, no. B11, p. 10200–10222, https://doi.org/10.1029/JB086iB11p10200.

Izett, G.A., and Wilcox, R.E., 1982, Map showing localities and inferred distributions of the Huckleberry Ridge, Mesa Falls, and Lava Creek ash beds (Pearlette family ash beds) of Pliocene and Pleistocene age in the western United States and southern Canada: U.S. Geological Survey Miscellaneous Investigations Series Map I-1325, 5 maps on 1 sheet, https://pubs.er.usgs.gov/publication/i1325.

Izett, G.A., Wilcox, R.E., Powers, H.A., and Desborough, G.A., 1970, The Bishop Ash Bed, a Pleistocene marker bed in the western United States: Quaternary Research, v. 1, no. 1, p. 121–132, https://doi.org/10.1016/0033-5894(70)90014-1.

James, D.E., Fouch, M.J., Carlson, R.W., and Roth, J.B., 2011, Slab fragmentation, edge flow and the origin of the Yellowstone hotspot track: Earth and Planetary Science Letters, v. 311, no. 1–2, p. 124–135, https://doi.org/10.1016/j.epsl.2011.09.007.

Jicha, B.R., Singer, B.S., and Sobol, P., 2016, Re-evaluation of the ages of $^{40}Ar/^{39}Ar$ sanidine standards and supereruptions in the western US using a Noblesse multi-collector mass spectrometer: Chemical Geology, v. 431, no. 1, p. 54–66, https://doi.org/10.1016/j.chemgeo.2016.03.024.

Kharaka, Y.K., Mariner, R.H., Bullen, T.D., Kennedy, B.M., and Sturchio, N.C., 1991, Geochemical investigations of hydraulic connections between the Corwin Springs known geothermal resources area and adjacent parts of Yellowstone National Park, *in* Sorey, M.L., ed., Effects of potential geothermal development in the Corwin Springs known geothermal resources area, Montana, on the thermal features of Yellowstone National Park: U.S. Geological Survey Water-Resources Investigations Report 91-4052, p. F1–F38, https://pubs.er.usgs.gov/publication/wri914052.

Konstantinou, Alexandros, and Miller, Elizabeth, 2015, Evidence for a long-lived accommodation/transfer zone beneath the Snake River Plain—A possible influence on Neogene magmatism?: Tectonics, v. 34, no. 12, p. 2387–2398, https://doi.org/10.1002/2015TC003863.

Kuiper, K.F., Deino, A., Hilgen, F.J., Krijgsman, W., Renne, P.R., and Wijbrans, J.R., 2008, Synchronizing rock clocks of Earth history: Science, v. 320, no. 5875, p. 500–504, https://doi.org/10.1126/science.1154339.

Lanphere, M.A., Champion, D.E., Christiansen, R.L., Izett, G.A., and Obradovich, J.D., 2002, Revised ages for tuffs of the Yellowstone Plateau volcanic field—Assignment of the Huckleberry Ridge Tuff to a new geomagnetic polarity event: Geological Society of America Bulletin, v. 114, no. 5, p. 559–568, https://doi.org/10.1130/0016-7606(2002)114<0559:RAFTOT>2.0.CO;2.

Lisiecki, L.E., and Raymo, M.E., 2005, A Pliocene-Pleistocene stack of 57 globally distributed benthic $\delta^{18}O$ records: Paleoceanography, v. 20, no. 1, PA1003, https://doi.org/10.1029/2004PA001071.

Loewen, M.W., and Bindeman, I.N., 2015, Oxygen isotope and trace element evidence for three-stage petrogenesis of the youngest episode (260–79 ka) of Yellowstone rhyolitic volcanism: Contributions to Mineralogy and Petrology, v. 170, no. 4, art. 39, https://doi.org/10.1007/s00410-015-1189-5.

Loewen, M.W., Bindeman, I.N., and Melnik, O.E., 2017, Eruption mechanisms and short duration of large rhyolitic lava flows of Yellowstone: Earth and Planetary Science Letters, v. 458, p. 80–91, https://doi.org/10.1016/j.epsl.2016.10.034.

MacLeod, N.S., Walker, G.W., and McKee, E.H., 1975, Geothermal significance of eastward increase in age of upper Cenozoic rhyolitic domes in southeastern Oregon: U.S. Geological Survey Open File Report 75-348, 22 p.

Mark, D.M., Renne, P.R., Dymock, R.C., Smith, V.C., Simon, J.I., Morgan, L.E., Staff, R.A., Ellis, B.S., and Pearce, N.J.G., 2017, High-precision $^{40}Ar/^{39}Ar$ dating of Pleistocene tuffs and temporal anchoring of the Matuyama-Bruhnes boundary: Quaternary Geochronology, v. 39, 1–23, https://doi.org/10.1016/j.quageo.2017.01.002.

Mastin, L.G., Van Eaton, A.R. and Lowenstern, J.B., 2014. Modeling ash fall distribution from a Yellowstone supereruption: Geochemistry, Geophysics, Geosystems, v. 15, p. 3459-3475.

Matthews, N.E., Vazquez, J.A., and Calvert, A.T., 2015, Age of the Lava Creek supereruption and magma chamber assembly at Yellowstone based on $^{40}Ar/^{39}Ar$ and U-Pb dating of sanidine and zircon crystals: Geochemistry, Geophysics, Geosystems, v. 16, no. 8, p. 2508–2528, https://doi.org/10.1002/2015GC005881.

McCurry, M., and Rodgers, D.W., 2009, Mass transfer along the Yellowstone hotspot track I—Petrologic constraints on the volume of mantle-derived magma: Journal of Volcanology and Geothermal Research, v. 188, no. 1–3, p. 86–98, https://doi.org/10.1016/j.jvolgeores.2009.04.001.

Myers, M.L., Wallace, P.J., Wilson, C.J., Morter, B.K., and Swallow, E.J., 2016, Prolonged ascent and episodic venting of discrete magma batches at the onset of the Huckleberry Ridge supereruption, Yellowstone: Earth and Planetary Science Letters, v. 451, p. 285-297.

Morgan, L.A., and Bonnichsen, B., 1989, Heise volcanic field: New Mexico Bureau of Mines and Mineral Resources Memoir 47, p. 153–160.

Morgan, L.A., and McIntosh, W.C., 2005, Timing and development of the Heise volcanic field, Snake River Plain, Idaho, western USA: Geological Society of America Bulletin, v. 117, no. 3–4, p. 288–306, https://doi.org/10.1130/B25519.1.

Morgan, L.A., Pierce, K.L., and Shanks, W.P., 2008, Track of the Yellowstone hotspot: Young and ongoing geologic processes from the Snake River Plain to the Yellowstone Plateau and Tetons, *in* Raynolds, R.G., ed., Roaming the Rocky Mountains and Environs—Geological Field Trips: Geological Society of America Field Guides, v. 10, p. 139–173, https://doi.org/10.1130/2008.fld010(08).

Morgan, L.A., Shanks, W.C.P., and Pierce, K.L., 2009, Hydrothermal processes above the Yellowstone magma chamber: Large hydrothermal systems and large hydrothermal explosions: Geological Society of America Special Paper 459, 95 p, https://doi.org/10.1130/2009.2459(01).

Naeser, C.W., Izett, G.A., and Wilcox, R.E., 1973, Zircon fission-track ages of Pearlette family ash beds in Meade County, Kansas: Geology, v. 1, no. 4, p. 187–189, https://doi.org/10.1130/0091-7613(1973)1<187:ZFAOPF>2.0.CO;2.

Nash, B.P., Perkins, M.E., Christensen, J.N., Lee, D.C., and Halliday, A.N., 2006, The Yellowstone hotspot in space and time—Nd and Hf isotopes in silicic magmas: Earth and Planetary Science Letters, v. 247, no. 1–2, p. 143–156, https://doi.org/10.1016/j.epsl.2006.04.030.

Nastanski, N.M., 2005, Petrogenesis of extracaldera rhyolites at Yellowstone volcanic field: Las Vegas, University of Nevada, M.S. thesis, 192 p.

Neace, T.F., Hackett, W.R., Davis, L.C., Johnson, R.J., and Link, P.K., 1986, Eruptive style, emplacement, and lateral variations of the Quaternary Mesa Falls Tuff, Island Park, Idaho, *in* Garrison, P.B., ed., Geology of the Beartooth Uplift and adjacent basins: Montana Geological Society and Yellowstone Bighorn Research Association Joint Field Conference and Symposium, p. 71–78, http://archives.datapages.com/data/mgs/mt/data/0040/0071/pdfs/0071.pdf.

Obradovich, J.D., 1992, Geochronology of the Late Cenozoic volcanism of Yellowstone National Park and adjoining areas, Wyoming and Idaho: U.S. Geological Survey Open-File Report 92-408, 45 p, https://pubs.er.usgs.gov/publication/ofr92408.

Pamukcu, A.S., Ghiorso, M.S., and Gualda, G.A., 2016, High-Ti, bright-CL rims in volcanic quartz–A result of very rapid growth: Contributions to Mineralogy and Petrology, v. 171, no. 12, article 105, https://doi.org/10.1007/s00410-016-1317-x.

Pierce, K.L., 2003, Pleistocene glaciations of the Rocky Mountains: Developments in Quaternary Sciences, v. 1, p. 63–76, https://doi.org/10.1016/S1571-0866(03)01004-2.

Pierce, K.L., and Morgan, L.A., 1992, The track of the Yellowstone hot spot—Volcanism, faulting, and uplift, *in* Link, P.K., Kuntz, M.A., and Platt, L.B., eds., Regional Geology of eastern Idaho and western Wyoming: Geological Society of America Memoirs 179, p. 1–54, https://doi.org/10.1130/MEM179-p1.

Pierce, K.L., Adams, K.D., and Sturchio, N.C., 1991, Geologic setting of the Corwin Springs known geothermal resources area-Mammoth Hot Springs area in and adjacent to Yellowstone National Park, *in* Sorey, M.L., ed., Effects of potential geothermal development in the Corwin Springs known geothermal resources area, Montana, on the thermal features of Yellowstone National Park: U.S. Geological Survey Water-Resources Investigations Report 91-4052, p. C1–C37, https://pubs.er.usgs.gov/publication/wri914052.

Pierce, K.L., Cannon, K.P., Meyer, G.A., Trebesch, M.J., and Watts, R.D., 2002, Post-glacial inflation-deflation cycles, tilting, and faulting in the Yellowstone caldera based on Yellowstone Lake shorelines: U.S. Geological Survey Open-file Report 2002-142, 63 p, https://pubs.er.usgs.gov/publication/ofr02142.

Pritchard, C.J., and Larson, P.B., 2012, Genesis of the post-caldera eastern Upper Basin Member rhyolites, Yellowstone, WY—From volcanic stratigraphy, geochemistry, and radiogenic isotope modeling: Contributions to Mineralogy and Petrology, v. 164, no. 2, p. 205–228, https://doi.org/10.1007/s00410-012-0733-9.

Pritchard, C.J., Larson, P.B., Spell, T.L., and Tarbert, K.D., 2013, Eruption-triggered mixing of extra-caldera basalt and rhyolite complexes along the East Gallatin–Washburn fault zone, Yellowstone National Park, WY, USA: Lithos, v. 175, p. 163–177, https://doi.org/10.1016/j.lithos.2013.04.022.

Renne, P.R., Mundil, R., Balco, G., Min, K., and Ludwig, K.R., 2010, Joint determination of ^{40}K decay constants and $^{40}Ar^*/^{40}K$ for the Fish Canyon sanidine standard, and improved accuracy for $^{40}Ar/^{39}Ar$ geochronology: Geochimica et Cosmochimica Acta, v. 74, no. 18, p. 5349–5367, https://doi.org/10.1016/j.gca.2010.06.017.

Rivera, T.A., Schmitz, M.D., Crowley, J.L., and Storey, M., 2014, Rapid magma evolution constrained by zircon petrochronology and $^{40}Ar/^{39}Ar$ sanidine ages for the Huckleberry Ridge Tuff, Yellowstone, USA: Geology, v. 42, no. 8, p. 643–646, https://doi.org/10.1130/G35808.1.

Rivera, T.A., Schmitz, M.D., Jicha, B.R., and Crowley, J.L., 2016, Zircon petrochronology and 40Ar/39Ar sanidine dates for the Mesa Falls Tuff—Crystal-scale records of magmatic evolution and the short lifespan of a large Yellowstone Magma Chamber: Journal of Petrology, v. 57, no. 9, p. 1677–1704, https://doi.org/10.1093/petrology/egw053.

Rivera, T.A., Darata, R., Lippert, P.C., Jicha, B.R., and Schmitz, M.D., 2017, The duration of a Yellowstone supereruption cycle and implications for the age of the Olduvai subchron: Earth and Planetary Science Letters, v. 479, p. 377-386, https://doi.org/10.1016/j.epsl.2017.08.027.

Sarna-Wojcicki, A.M., Bowman, H.R., Meyer, C.E., Russell, P.C., Woodward, M.J., McCoy, Gail, Rowe, J.J., Jr, Baedecker, P.A., Asaro, Frank, and Michael, Helen, 1984, Chemical analyses, correlations, and ages of upper Pliocene and Pleistocene ash layers of east-central and southern California: U.S. Geological Survey Professional Paper 1293, 40 p., https://pubs.er.usgs.gov/publication/pp1293.

Sarna-Wojcicki, A.M., Morrison, S.D., Meyer, C.E., and Hillhouse, J.W., 1987, Correlation of upper Cenozoic tephra layers between sediments of the western United States and eastern Pacific Ocean and comparison with biostratigraphic and magnetostratigraphic age data: Geological Society of America Bulletin, v. 98, no. 2, p. 207–223, https://doi.org/10.1130/0016-7606(1987)98<207:COUCTL>2.0.CO;2.

Seligman, A.N., Bindeman, I.N., McClaughry, J., Stern, R.A., and Fisher, Chris, 2014, The earliest low and high $\delta^{18}O$ caldera-forming eruptions of the Yellowstone plume—Implications for the 30–40 Ma Oregon calderas and speculations on plume-triggered delaminations: Frontiers in Earth Science, v. 2, Article 34, 9 p., https://doi.org/10.3389/feart.2014.00034.

Singer, B.S., Jicha, B.R., Condon, D.J., Macho, A.S., Hoffman, K.A., Dierkhising, J., Brown, M.C., Feinberg, J.M., and Kidane, T., 2014, Precise ages of the Réunion event and Huckleberry Ridge excursion—Episodic clustering of geomagnetic instabilities and the dynamics of flow within the outer core: Earth and Planetary Science Letters, v. 405, p. 25–38, https://doi.org/10.1016/j.epsl.2014.08.011.

Smith, R.B., Jordan, Michael, Steinberger, Bernhard, Puskas, C.M., Farrell, Jamie, Waite, G.P., Husen, Stephan, Chang, W.-L., and O'Connell, Richard, 2009, Geodynamics of the Yellowstone hotspot and mantle plume—Seismic and GPS imaging, kinematics, and mantle flow: Journal of Volcanology and Geothermal Research, v. 188, no. 1, p. 26–56, https://doi.org/10.1016/j.jvolgeores.2009.08.020.

Smith, R.L., 1979, Ash-flow magmatism: Geological Society of America Special Papers 180, p. 5–28, https://doi.org/10.1130/SPE180-p5.

Stelten, M.E., Cooper, K.M., Vazquez, J.A., Calvert, A.T., and Glessner, J.J., 2015, Mechanisms and timescales of generating eruptible rhyolitic magmas at Yellowstone caldera from zircon and sanidine geochronology and geochemistry: Journal of Petrology, v. 56, no. 8, p. 1607–1642, https://doi.org/10.1093/petrology/egv047.

Stelten, M.E., Cooper, K.M., Vazquez, J.A., Reid, M.R., Barfod, G.H., Wimpenny, Josh, and Yin, Q.-Z., 2013, Magma mixing and the generation of isotopically juvenile silicic magma at Yellowstone caldera inferred from coupling ^{238}U–^{230}Th ages with trace elements and Hf and O isotopes in zircon and Pb isotopes in sanidine: Contributions to Mineralogy and Petrology, v. 166, no. 2, p. 587–613, https://doi.org/10.1007/s00410-013-0893-2.

Stelten, M.E., Cooper, K.M., Wimpenny, J.B., Vazquez, J.A., and Yin, Q-Z, 2017, The role of mantle-derived magmas in the isotopic evolution of Yellowstone's magmatic system: Geochemistry, Geophysics, Geosystems, v. 18, p. 1350-1365.

Struhsacker, D.W., 1978, Mixed basalt-rhyolite assemblages in Yellowstone National Park—The petro-genetic significance of magma mixing: Missoula, Mont., University of Montana, M.S. thesis, 112 p., http://scholarworks.umt.edu/cgi/viewcontent.cgi?article=7153&context=etd.

Sturchio, N.C., Pierce, K.L., Murrell, M.T., and Sorey, M.L., 1994, Uranium-series ages of travertines and timing of the last glaciation in the northern Yellowstone area, Wyoming-Montana: Quaternary Research, v. 41, no. 3, p. 265–277, https://doi.org/10.1006/qres.1994.1030.

Szymanowski, D., Ellis, B.S., Bachmann, Olivier, Guillong, Marcel, and Phillips, W.M., 2015, Bridging basalts and rhyolites in the Yellowstone-Snake River Plain volcanic province—The elusive intermediate step: Earth and Planetary Science Letters, v. 415, p. 80–89, https://doi.org/10.1016/j.epsl.2015.01.041.

Szymanowski, D., Ellis, B.S., Wotzlaw, J.F., Buret, Y., von Quadt, A., Peytcheva, I., Bindeman, I.N., and Bachmann, O., 2016, Geochronological and isotopic records of crustal storage and assimilation in the Wolverine Creek–Conant Creek system, Heise eruptive centre, Snake River Plain: Contributions to Mineralogy and Petrology, v. 171, no. 12, p. 106–121, https://doi.org/10.1007/s00410-016-1314-0.

Thomas, J.B., and Watson, E.B., 2012, Application of the Ti-in-quartz thermobarometer to rutile-free systems. Reply to—a comment on—'TitaniQ under pressure—the effect of pressure and temperature on the solubility of Ti in quartz' by Thomas and others: Contributions to Mineralogy and Petrology, v. 164, no. 2, p. 369–374, https://doi.org/10.1007/s00410-012-0761-5.

Till, C., Vazquez, J.A., Boyce, J.W. and Stelten, M.E., 2013, Probing the source and timing of rejuvenation and hybridization in post-caldera rhyolite magmas at Yellowstone Caldera: American Geophysical Union, Fall Meeting 2013, abstract V53A-2763.

Till, C.B., Vazquez, J.A., and Boyce, J.W., 2015, Months between rejuvenation and volcanic eruption at Yellowstone caldera, Wyoming: Geology, v. 43, no. 8, p. 695–698, https://doi.org/10.1130/G36862.1.

Troch, J., Ellis, B.S., Mark, D.F., Bindeman, I.N., Kent, A.J.R., Guillong, M., and Bachmann, O., 2017, Rhyolite generation prior to a Yellowstone supereruption—Insights from the Island Park–Mount Jackson Rhyolite series: Journal of Petrology, v. 58, no. 1, p. 29–52, https://doi.org/10.1093/petrology/egw071.

Truesdell, A.H., Nathenson, Manuel and Rye, R.O., 1977, The effects of subsurface boiling and dilution on the isotopic compositions of Yellowstone thermal waters: Journal of Geophysical Research, v. 82, p. 3694–3704, https://doi.org/10.1029/JB082i026p03694.

Vazquez, J.A., and Reid, M.R., 2002, Time scales of magma storage and differentiation of voluminous high-silica rhyolites at Yellowstone caldera, Wyoming: Contributions to Mineralogy and Petrology, v. 144, no. 3, p. 274–285, https://doi.org/10.1007/s00410-002-0400-7.

Vazquez, J.A., Kyriazis, S.F., Reid, M.R., Sehler, R.C., and Ramos, F.C., 2009, Thermochemical evolution of young rhyolites at Yellowstone—Evidence for a cooling but periodically replenished postcaldera magma reservoir: Journal of Volcanology and Geothermal Research, v. 188, no. 1, p. 186–196, https://doi.org/10.1016/j.jvolgeores.2008.11.030.

Watts, K.E., Leeman, W.P., Bindeman, I.N., and Larson, P.B., 2010, Supereruptions of the Snake River Plain—Two-stage derivation of low-$\delta^{18}O$ rhyolites from normal-$\delta^{18}O$ crust as constrained by Archean xenoliths: Geology, v. 38, no. 6, p. 503–506, https://doi.org/10.1130/G30735.1.

Watts, K.E., Bindeman, I.N., and Schmitt, A.K., 2011, Large-volume rhyolite genesis in caldera complexes of the Snake River Plain—Insights from the Kilgore Tuff of the Heise Volcanic Field, Idaho, with comparison to Yellowstone and Bruneau–Jarbidge rhyolites: Journal of Petrology, v. 52, no. 5, p. 857–890, https://doi.org/10.1093/petrology/egr005.

Watts, K.E., Bindeman, I.N., and Schmitt, A.K., 2012, Crystal scale anatomy of a dying supervolcano—An isotope and geochronology study of individual phenocrysts from voluminous rhyolites of the Yellowstone caldera: Contributions to Mineralogy and Petrology, v. 164, no. 1, p. 45–67, https://doi.org/10.1007/s00410-012-0724-x.

Werner, C., and Brantley, S., 2003, CO2 emissions from the Yellowstone volcanic system: Geochemistry, Geophysics, Geosystems, v. 4, no. 7, 13 p., https://doi.org/10.1029/2002GC000473.

Westgate, J.A., Christiansen, E.A., and Boellstorff, J.D., 1977, Wascana Creek Ash (Middle Pleistocene) in southern Saskatchewan—Characterization, source, fission track age, palaeomagnetism and stratigraphic significance: Canadian Journal of Earth Sciences, v. 14, no. 3, p. 357–374, https://doi.org/10.1139/e77-037.

White, D.E., 1967, Some principles of geyser activity, mainly from Steamboat Springs, Nevada: American Journal of Science, v. 265, no. 8, p. 641–684, https://doi.org/10.2475/ajs.265.8.641.

White, D.E., Fournier, R.O., Muffler, L.J.P., and Truesdell, A.H., 1975, Physical results of research drilling in thermal areas of Yellowstone National Park, Wyoming: U.S. Geological Survey Professional Paper 892, p. 70, https://pubs.er.usgs.gov/publication/pp892.

White, D.E., Hutchinson, R.A., and Keith, T.E., 1988, Geology and remarkable thermal activity of Norris Geyser Basin, Yellowstone National Park, Wyoming: U.S. Geological Survey Professional Paper 1456, 94 p.

White, S.M., Crisp, J.A., and Spera, F.J., 2006, Long-term volumetric eruption rates and magma budgets: Geochemistry, Geophysics, Geosystems, v. 7, no. 3, art. Q03010, 20 p., https://doi.org/10.1029/2005GC001002.

Wilcox, R.E., 1944, Rhyolite-basalt complex on Gardiner River, Yellowstone Park, Wyoming: Geological Society of America Bulletin, v. 55, no. 9, p. 1047–1080, https://doi.org/10.1130/GSAB-55-1047.

Wooton, K.M., 2010, Age and petrogenesis of the Roaring Mountain rhyolites, Yellowstone Volcanic Field, Wyoming: Las Vegas, University of Nevada, M.S. thesis, 296 p.

Wotzlaw, J.F., Bindeman, I.N., Watts, K.E., Schmitt, A.K., Caricchi, Luca, and Schaltegger, Urs, 2014, Linking rapid magma reservoir assembly and eruption trigger mechanisms at evolved Yellowstone-type supervolcanoes: Geology, v. 42, no. 9, p. 807–810, https://doi.org/10.1130/G35979.1.

Wotzlaw, J.F., Bindeman, I.N., Stern, R.A., D'Abzac, F.-X., and Schaltegger, Urs, 2015, Rapid heterogeneous assembly of multiple magma reservoirs prior to Yellowstone super-eruptions: Nature Scientific Reports, v. 5, no 1, art. 14026, https://doi.org/10.1038/srep14026.

Menlo Park Publishing Service Center, California
Manuscript approved for publication, October 27, 2017
Edited by Scott D. Darling
Layout and design by Vivian Nguyen

ISSN 2328-0328 (online)
https://doi.org/10.3133/sir20175022q